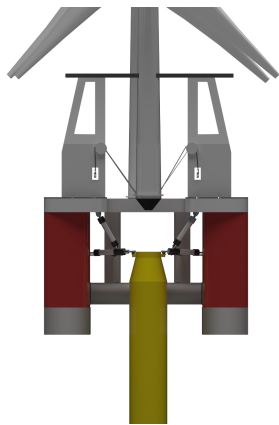Hans Marius Remmen

DYNAMIC RESPONSE ANALYSES OF A SEMI-SUB INSTALLATION VESSEL DURING THE INSTALLATION OF A WIND TURBINE ONTO A FLOATING SPAR BUOY

Master's thesis in Ship Design
Supervisor: Karl Henning Halse

June 2019

NTNU
Norwegian University of
Science and Technology

Hans Marius Remmen

DYNAMIC RESPONSE ANALYSES OF A SEMI-SUB INSTALLATION VESSEL DURING THE INSTALLATION OF A WIND TURBINE ONTO A FLOATING SPAR BUOY

Master's thesis in Ship Design
Supervisor: Karl Henning Halse
June 2019

Norwegian University of Science and Technology
Department of Ocean Operations and Civil Engineering

NTNU
Norwegian University of
Science and Technology

Preface

This Master thesis is written as the final project for the Master's degree program Ship Design at NTNU Ålesund. The project work was conducted during the spring semester of 2019. Karl Henning Halse provided the topic as part of the SFI MOVE project to look into the possibilities of using existing semi-submersible platforms as installation vessel for offshore wind turbines. Modelling and simulation were performed in Sintef's newly developed software SIMA, a simulation tool for multi-body marine operations. Parameters used in the study is either imported from models provided by the supervisor or relevant statistics and theory; the intention was to keep distance to real life as short as possible. To fully grasp the theory and methods used in this paper, a fundamental knowledge of marine construction, marine hydrodynamics, and simulation are recommended. The paper is therefore mostly intended for engineers with some marine knowledge.

Acknowledgment

Master agreement

MASTER THESIS 2019

FOR

HANS MARIUS REMMEN

Dynamic Response Analysis of a Semi-sub Installation Vessel During Installation of a Wind Turbine onto a Floating SPAR Buoy

The current installation cost of Offshore Wind Turbines (OWT) is high, and profit margins in the offshore wind energy sector are low. However, the offshore wind industry has gradually lowered their costs to a level where energy from offshore wind parks is competitive. So far offshore wind parks have been exclusively for turbines fixed to the sea bottom, but in 2017, Equinor installed the world's first floating wind park: *Hywind Scotland*. This wind park consists of five 6 MW wind turbines mounted on top of floating SPAR buoys. The turbines were installed on floating SPAR buoys in a sheltered area in a Norwegian fjord and then towed across the North Sea to its final destination. This was a time-consuming and costly installation process, and Equinor is searching for alternatives to reduce both time and costs associated with the installation process. In the SFI MOVE project, various alternatives for the offshore installation of floating wind turbines have been addressed. One alternative is to preinstall the floating SPAR buoy at its location by horizontal towing, upending and mooring, and then perform an offshore lifting/mating operation of the OWT onto the floating foundation.

The objective of this work is to investigate if a semi-submersible can be used as an offshore wind turbine installation vessel. The critical response is the relative motion between the lower end of the lifted OWT and the upper end of the floating SPAR. In the present work, this relative motion is studied and the need for motion compensation is investigated. The concept will be analyzed in SIMA, and the feasibility will be evaluated based on the results and relevant response criteria.

Research questions:

- Can an existing semi-sub platform technically be used as installation vessel for offshore wind turbines?
- How large will the relative motion between the semi-sub and the spar foundation become – if necessary, is a heave compensation system sufficient enough to reduce the motion?
- Is it possible to increase the weather window with this installation method?

The work can be broken down to the following tasks

- The literature of offshore installation projects, and in particular offshore heavy lifting projects

- Become familiar with the computer simulation system SIMA

- Establish a SIMA computer model of the lifting mechanism to be used in the installation

- Establish and tune a control model for heave compensation of the lifted object in SIMA

- Simulate the multibody system (OWT, SPAR and semi-submersible) in SIMA

- Analyze the multibody system for varying wave conditions

- Evaluate the feasibility of performing offshore installation of OWT from a semi-submersible.
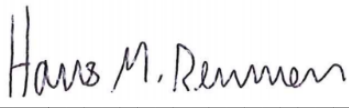
The scope of work may prove to be larger than initially anticipated. Subject to approval from the advisor, topics from the list above may be deleted or reduced in extent.

The thesis should be written as a research report with summary, conclusion, literature references, table of contents, etc. During preparation of the text, the candidate should make efforts to create a well arranged and well written report. To ease the evaluation of the thesis, it is important to cross-reference text, tables and figures. For evaluation of the work a thorough discussion of results is needed. Discussion of research method, validation and generalization of results is also appreciated.

The thesis shall be submitted in electronic version according to standard procedures. Instructions are found on the NTNU website (Inspera) and on Blackboard. In addition one paper copy of the full thesis together with an electronic device carrying all relevant documents and files shall be submitted to your supervisor.

Karl H. Halse

Supervisor

Delivery: 11.06.2019   Signature candidate: _____

Summary

The paper starts with a brief introduction to the topic of marine operations, with focus on SSP technology and lifting operations. There are a lot of information regarding the use of a SSP in the oil and gas industry, but not so extensive information regarding the installation of floating offshore wind turbines.

One of the main research questions is if a typical SSP platform can be used as installation platform technically and if the motion characteristics suit the purpose. Simulation research method was chosen for this study to analyze the installation concept.

To conduct the response analyses of the floating objects SIMA was used. SIMA is a simulation tool for marine operations with a superior hydrodynamic model in time-domain. Both the SSP model and spar buoy model was imported into SIMA. Hydrodynamical coefficients and model characteristics were included in the provided SIMA models, further the models were imported into the simulation environment and physics were applied.

The concept model was simulated in multiple environmental conditions - the North Sea was chosen as installation site. A combination of natural frequencies and scatter diagram with the most probable wave heights/periods was used to determine simulation environments. SSP and spar total motion with and without couplings was analyzed to see the effect of different couplings. One of the major goals with the concept was to reduce relative motion at mating point with the intention to have minimal contact forces between spar and OWT. Multiple simulations were performed in initial position to analyze the improvement with different coupling parameters. Analyses of docking cone contact forces in lowered position was also conducted in different env. conditions. For result validation a sensitivity analyses with environmental heading 30 degrees was conducted.

Total motion result from the SSP and spar shows that damper DX/DY, damper between SSP and spar, have positive effect on the response. Surge motion gets synchronized and spar pitch motion is reduced to a minimum. Vertical relative motion is largely reduced with the combinations of the active heave compensator (AHC) and the passive dampers. A separate tuning of the heave compensator controller parameters was conducted – two different controllers where addressed: PID and PD + FF. After mating of the OWT and no tension in the lifting wires the SSP is introduced to a 15 degree aft trim with initial ballast. Small waterplane area causes high load sensitivity which limits the possibilities. Suggestions to this problem is to add buoyant volumes between pontoons and top deck to increase w.p. area, and a sliding mass underneath the top deck would shorten the ballasting time.

Analyses including wind induced forces should be performed and integration of a controller for OWT motion control in horizontal plane to further develop the concept.

Sammendrag

Studien starter med en kort introduksjon til temaet marine operasjoner, med fokus på SSP teknologi og løfteoperasjoner. Det er mye informasjon om bruken av nedsenkbare plattformer i olje- og gassindustrien, men ikke så mye mot installasjon av flytende havvindmøller.

Et av forskningsspørsmålene er om en typisk SSP-plattform kan brukes som installasjonsplattform teknisk, og om bevegelsesegenskapene passer til formålet. Simulering ble valgt som forskningsmetode for denne studien for å analysere installasjonskonseptet.

For å utføre responsanalysene av de flytende objektene ble SIMA brukt. SIMA er et simuleringsverktøy for marine operasjoner med en overlegen hydrodynamisk modell i tidsdomene. Både SSP-modellen og sparmodellen ble importert til SIMA. Hydrodynamiske koeffisienter og modellegenskaper ble inkludert i de tilveiebragte SIMA-modellene, videre ble modellene importert til simuleringsmiljøet og koblinger/grensebetingelser ble definert.

Konseptmodellen ble simulert i flere miljøforhold - Nordsjøen ble valgt som installasjonssted. En kombinasjon av egenfrekvenser og scatter-diagram med de mest sannsynlige bølgehøyder / perioder ble brukt til å bestemme aktuelle bølgekondisjoner. SSP og spar total bevegelse med og uten koblinger ble analysert for å se effekten av forskjellige fysiske koblinger. Et av hovedmålene med konseptet var å redusere relativ bevegelse ved referansepunktet med sikte på å ha minimale kontaktkrefter mellom spar og OWT. Flere simuleringer ble utført i opprinnelig posisjon for å analysere forbedringen med forskjellige koblingsparametere. Analyser av kontaktkrefter i «docking cone» i senket posisjon ble også utført i forskjellige bølgekondisjoner. For å validere resultat ble det gjennomført sensitivitetsanalyser med bølgeretning 30 grader.

Totalt bevegelsesresultat fra SSP og spar viser at passive dempere, dempere mellom SSP og spar, har positiv effekt på responsen. «Surge» blir synkronisert, og spar «pitch» reduseres til et minimum. Vertikal relativ bevegelse reduseres i stor grad med kombinasjonene av den aktive «heave» kompensatoren (AHC) og de passive demperne. Det ble utført en separat parameteranalyse av parameterne for kompensatorkontrolleren - to forskjellige kontrollere ble adressert: PID og PD + FF. Etter installasjon av OWT og ingen spenning i løfte-wire, blir SSP introdusert for en 15 graders akterlig trim med inneværende ballastkondisjon. Et lite vannlinjeareal forårsaker høy lastfølsomhet som begrenser mulighetene. Forslag til dette problemet er å legge til store volumer mellom pongtonger og toppdekk for å øke vannlinjeareal, og en glidende masse under toppdekket ville forkorte total ballasteringstid.

Analyser, inkludert vindinduserte krefter, bør utføres og integrering av en kontroller for bevegelseskontroll for SSP i horisontalplan for å videreutvikle konseptet.

Table of Contents

List of figures

List of tables

Nomenclature

Roman letters

Tp = Peak period

Hs = Significant wave height

n = Radial reference error (radial distance at reference point)

(XG,YG,ZG) = Global coordinate system

(XB,YB,ZB) = Local coordinate system

Greek letters

β = environmental heading

σ = Standard deviation

Abbreviations

OWT = Offshore Wind Turbine (Turbine tower with nacelle and blades, not spar fundament)

SSP = Semi-submersible platform

DOF = Degree of freedom

PHC = Passive heave compensator

AHC = Active heave compensator

STD = Standard deviation

DX = Passive damper X-component between SSP and spar

DY = Passive damper Y-component between SSP and spar

1 Introduction

1.1 Problem definition

The current installation cost of offshore wind turbines is high, and increasing exponentially with water depths. Profit margins in the offshore wind energy sector are low. According to DNV GL, the operational forecast for the European offshore wind sector predicts an increase in megawatt output of more than 50% in year 2020. As with almost everything, the wind turbines increase in size, and the installation vessels need to follow suit [1].
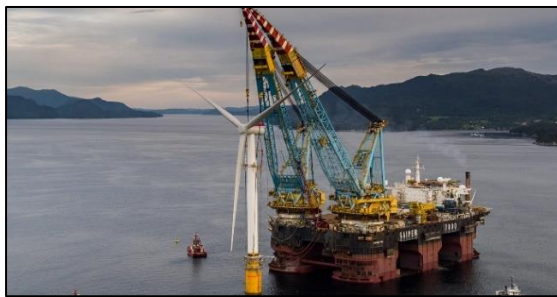
Figure 1.1: Left: Installation of OWT on spar fundament. Right: Towing of the complete assembly to mooring site.

Equinor installed in 2017 five wind turbines on SPAR buoys, part of the developing program Hywind Scotland project. **Figure 1.1** present both mating of OWT and towing of the complete assembly to installation site. They installed the wind turbines onto the spar foundations in calm waters inside a Norwegian fjord; this method is not preferred for offshore installation where the environmental forces are severe. The extreme height of the turbine amplifies wind and wave induced motion, which makes it harder to install [2]. The industry needs efficient installation methods for installation bad weather. Preferably existing offshore equipment such as SSP oil platforms shall be used to maximize profit margin.

1.2 Scope of view

The scope of the thesis will be to investigate if a SSP can be used as an offshore wind turbine installation vessel. In other words: analyze the relative motion between the spar buoy and the SSP with relating coupling forces. The analyses will reveal if it is necessary to heave compensate the turbine when mounting and if the forces acting on the structure is within satisfying levels. Part of the study will be to address heave compensation technology and tuning of the control system. The installation concept model will be simulated in SIMA and the feasibility will be evaluated based on the result and relevant limitations.
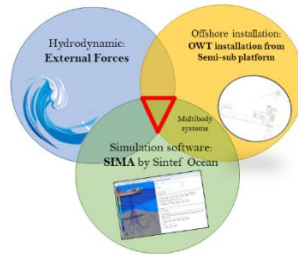
Figure 1.2: Scope of the thesis.

1.3 Motivation/Background

The demand for electricity throughout the world is increasing rapidly, simultaneously as the oil and gas reservoirs are decreasing, and the global emissions are in need to be reduced due to its impact on global warming. This makes it necessary to develop innovative and sustainable technology and methodologies. Wind energy as an energy resource is underutilized globally. The sea surface is covering in total 71% of the world, that means hypothetically that the offshore wind turbines could replace all other pollutive power plants in the world. In addition, offshore wind parks can be placed with optimally environmental conditions. Offshore wind energy is one of the fields with great potential. To be a part of this challenging development, even in a minor matter, is highly motivating. The results from this project will presumably and hopefully take the development one little step further to the main goal of clean energy production.

1.4 Research questions

- Can an existing semi-sub platform technically be used as installation vessel for offshore wind turbines?
- How large will the relative motion between the semi-sub and the spar foundation become – if necessary, is an AHC-system enough to dampen the motion?
- Is it possible to increase the weather window with this installation method?

1.5 Research approach

For this research, the obvious approach is quantitative since the research method is numerical simulation of offshore wind turbine installation. Methods which identifies a quantitative approach: assumed fixed and measurable reality, data are collected through measuring elements, data are analyzed through numerical comparisons and statistical inferences and data are reported through statistical analyses. Part of the approach will be qualitative as solving the computational errors will need human intuition. Results from the different phases of the installation, both with and without motion compensators, will be compared. In addition to comparing data to other studies to evaluate the feasibility of the concept.

2 Literature study: OWT installation

2.1 The evolution of offshore wind turbine installation methods

In general, maritime operations offshore have been widely studied. Installation of OWT's is in contrast not very widespread. There has not been possible to perform usable simulations, but with maturity and development, the state-of-the-art numerical simulation tools have gained momentum [3].

One primary challenge with OWT installations is the weather window and to avoid unexpected delays. Considering there is now developed numerical methods and models to estimate systems dynamic response during installation, there are possibilities to predict the operability [3]. Designers all over the world have moved on to develop new and applicable simulation methods. [4]

Figure 2.1: Three-column semisubmersible test platform.

Prof. Habib Daghe, University of Maine, lead the work on a test turbine in 2013 named: The VolturnUS 1:8 Floating Wind Turbine, see **Figure 2.1** [5]. He is saying that the problem is to couple wave loads, hydrodynamics and aerodynamic forces. He is also stating that all engineers should verify and validate the work put into the subject to ensure technology is moving forward [4].

2.2 Installation of a wind turbine from a floating platform

There are some projects and studies done on the subject of OWT installations on floating platforms. Some experimental work has been done in the past few years, e.g. the VolturnUS and Hywind wind farm project by Equinor [5] [6]. Equinor installed five wind turbines on floating spar buoys late 2017 at Hywind wind farm, but they used an unpractical and expensive installation method [2]. Practical testing of possible installation concepts is expensive in the necessary scale, but it is thus possible to reduce the scale and partly test mechanisms such as locks, gripping arms and heave compensating technology. The wind farm technology itself is innovative and has a lot of potentials. The result for the first year has been

published; Operation manager Halvor Hersleth says that the project is a success and has delivered a capacity factor of 56%, which is well above the average of about 40%. The reason is the good wind conditions in this area. The main advantage of floating wind farms is the flexibility of locating the turbines where the best efficiency can be obtained. He also says that they had some start-up

Figure 2.2: Illustration: Motion compensated gangway for safe transfer from vessel to platform.

problems regarding the electronics and cooling systems. The main problem was the small weather window since it is problematic to transfer people from the vessel to the turbine-platform, ironic since the weather condition ensures the profitability [7]. Ulstein delivered a service vessel named "*Acta Auriga"* intended for wind turbines in 2018 which has a 3D motion compensated crane and the innovative X-bow and X-stern. This vessel has a motion compensated gangway, as presented in **Figure 2.2**, and provide a much safer transfer of people from the vessel to the platform and increase the weather window for maintenance. Ulstein participated in Statoil's Hywind installation challenge in 2015 and presented a solution which is probably too structurally weak [8]. A more interesting participant in the challenge was Atkins. They presented a SSP reusable frame to carry pre-assembled wind turbines from the quay to the installation location. Their idea is to tow multiple turbines at reduced draughts to respectively reduce the transportation cost and deal with shallow inshore locations. The SSP has excellent motion characteristics, reduce weather restrictions on towing, and allow an increase in tow speed [9]. The article is not presenting any solution on how they are going to install the wind turbines at sea; the rig is only a transportation device. The idea is efficient and cost-effective.

A part of the VolturnUS project was the decommissioning and recovery. After 18-months out on the ocean, the rig was towed back to shore. The turbines were exposed to a 50-year return period wave environment. Some of the main data recorded in the period were wind speed in relative to wave properties, wire tension to anchors, and towing speed. The decommissioning gave valuable information about marine growth, corrosion, and structural health were also completed to assess the robustness of the hull system's materials and design [5]. In 2017 Lars Ivar Hatledal presented a novel gripper mechanism between catamaran and turbine foundation for offshore wind installation. During installation, the sliding grippers are mounted such that they will
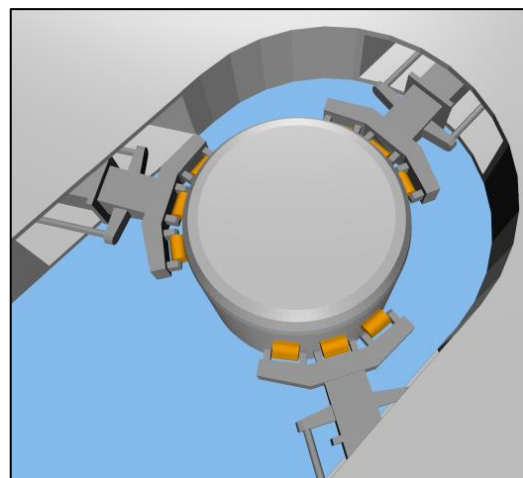
Figure 2.3: Sliding grippers between catamaran and spar fundament **[10]**.

grasp the spar, as shown in **Figure 2.3**. The grippers consist of hydraulically actuated sliding mechanisms. The result presents that the grippers have a large effect on the relative motion in the horizontal plane between the spar and turbine tower, but the contact forces may cause some concerns [10]. Z. Jiang presented in 2018 a similar gripper arrangement [3]. Coupling forces between SSP and spar should be specially considered and evaluated.

2.2.1 Semi-submersible technology

Dr. Habib Dagher and his team at University of Maine's Advanced Structure and Composite Center began extensive testing of SSP structures. They had the goal: "*Get the cost of this technology to compete on the grid without subsidies*". His team spent years figuring out how to drive costs down. They tested spars and tension line platforms as well as the VolturnUS design – the conclusion: submersible made more sense. The university maintains a wave-wind basin, featuring a movable wind tunnel over wave basin that allows physical model testing.

The VolturnUS is designed with concrete as material. They developed a whole different supply chain to drive costs down. With this design, it is feasible to drive hull costs down by 50%, at least in the U.S. The main advantage with concrete hull design instead of a steel hull is that it drives natural hull motion periods higher than the extreme wave periods. Also, the design provides a good amount of added mass, further elongating the natural periods while increasing motion damping. When the VolturnUS was deployed at sea it collected some valuable data: Maximum nacelle acceleration < 0.2g, maximum heel angle was less than 7° in a relative 500-year storm. That is data of the kind helping to build confidence with turbine suppliers and sponsors. Their next project is two full scale 6-MW turbines – will be completed in 2019 [11] [5].

TetraSpar is a tension leg platform concept, presented in **Figure 2.4**. The advantage with this design is a low weight - can be installed quayside and towed to site. Which means no need for installation vessels, but the anchoring requires assistance from a purpose built vessel. In addition, the tether arrangements are demanding and expensive, and it requires a complex

Figure 2.4: TetraSpar concept **[11].**

steel structure. Henrik Stiesdal, formerly Siemens, suggests combining the best from all three technologies. The spar's dynamic behavior is solid as a rock, the SSP allows quayside turbine installation and is easy to tow, and the TLP technology allows relatively light structure to obtain necessary strength. He also suggests using already working methods onshore and apply it to offshore designs, so the structure is built with components that have the same familiar dimensions and

weights – costs are driven down by mass production and assembling onshore. Further, he predicts that offshore wind will be competitive in short time [11].

2.3 Modeling challenges

Some challenges regarding dynamic modelling are listed below [3]:

- *Structural dynamics:* The model exists of multiple bodies which are connected via mechanical couplings. It is important to model the coupling and understand their effect on the dynamic characteristic of the system.
- *Hydrodynamics:* Hydrodynamic properties of two rigid bodies are involved in the SSP-spar system, and the hydrodynamic interaction must be considered during the hydrodynamic load calculation. Sloshing between the two hulls could is a problem that should be addressed. More problems can occur with the spar foundation; second-order hydrodynamic effects could play a bigger role in shallow waters. For both bodies, viscous effects should be considered. The added mass and potential damping should be calculated in the frequency domain, and then applied in the time domain for the coupled motion analysis of two bodies through retardation functions [3].
- *Automatic control:* There are different stages of the installation process which demands automatic control. For example, the dynamic positioning system (DPS) of the semi-sub when aligning the turbine on to the buoy and a heave compensation system of the OWT with associated control system.

3 Methodology and applied theory

3.1 Dynamic analyses of floating objects

For larger water depths, the floating structures such as spar and SSP are more suitable, but it induces other challenges to the operation. During the installation of an offshore wind turbine onto a spar fundament there are several types of environmental loads; wave, wind and current. To determine the water particle kinematics, it is necessary to use the appropriate wave theory – for example linear wave theory, Stokes theory or Cnoidal theory. In SIMA Stokes' 5th order wave theory is used to model regular waves. Using regular wave models, wave-induced velocities and acceleration are calculated at every node at every time step during the time integration. The current is normally constant with time and is described at a given position by speed and direction. This is obtained by interpolation and input of discrete values. For calculation of wind forces there exist different models, which has different related assumptions. In SIMA the aerodynamical loads are based on either interpolation from static lift, drag and moment curves, or Morison-type quadratic drag loads [12].

3.2 Methodology

A recent and more commonly used research method is the use of computer simulation. The main advantage with simulation research methods is that you do not need to take assumptions about the cause and effect of the system under study and it enables studies of more complex systems because of the "moving forward" philosophy. Other methods primarily look backwards to find what happened and how. With numerical methods we want to find quantitative answers, but qualitative results may be useful to compare relative merits [13] [14].

3.2.1 Flow chart

Figure 3.1 presents the flow chart of the conceptual methodology of the development of an installation procedure of offshore wind turbines applied in this study.
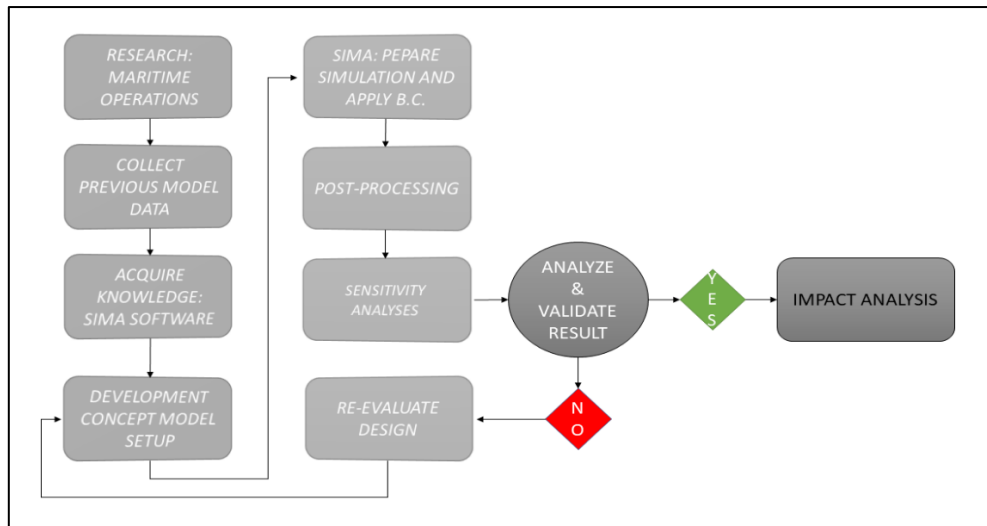
Figure 3.1: Flow chart of the methodology applied in this study.

3.3 Simulation software: SIMA ver. 3.6

SIMA is continuously being developed as a joint industry project by SINTEF Ocean and Equinor. SIMA is a powerful tool for modelling and analysis of tasks within the field of marine technology, it is a graphical presentation of different physics engines. The main goals when creating SIMA was [12]:

- Creating a tool for beginners to easily be proficient within the field
- Creating a tool for experts to shorten the time from concept to conclusion

With SIMA you get a 3D graphical representation of the objects you are modelling, and instant validation of all changes done. The physics engines get fed from the input files SIMA writes under the hood. SIMA supports multiple physics engines – engines worth mentioning [12]:

- SIMO – Used to model marine operations
- RIFLEX – Used to model a system consisting of slender elements
- RIFLEX Coupled – SIMO and RIFLEX coupled. E.g. used to model slender elements in a marine operation

SIMO is an equation solver. It solves the equations of motions for an arbitrary number of bodies, with and without couplings between them. The big challenge is to know how to make a numerical model of a real physical system and which values to give as input [15].

3.3.1 Procedure

The SIMO physics engine is the most suited for simulating motions and station keeping of multi-body systems. Modelling of large bodies in SIMO is based on hydrodynamic data calculated from different diffraction programs, such as WAMIT, WADAM or HydroD. For cases where couplings between bodies are expected to have any influence on first order wave induced motion a 6DOF - time

10

domain simulation is necessary. For less complex cases it is recommended with a less time consuming 6DOF – separated analysis body. For an SSP viscous damping in heave, roll and pitch can be significant, especially when mooring lines is applied – can be taken care of with a specific upward force.

3.3.2 Physical coupling elements

In the next sub-sections different physical couplings in SIMA applied for this study is defined with its limitations and definitions.

Bumper

The bumper elements are ideal to model contact force between either a globally fixed bumper or contact forces between bodies. In SIMA two different types of bumpers can be defined [12]:

- Positioning element: Bumper data
- Coupling element: Bumper or bumper group
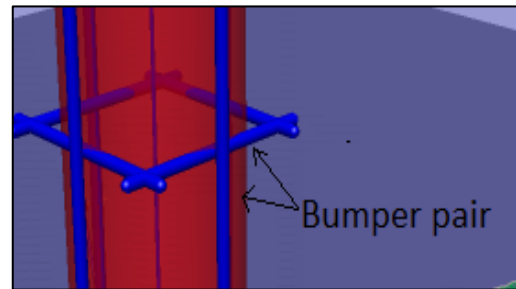
Figure 3.2: Bumper coupling illustrated.

The bumper elements represent a defined pair of lines (vectors) – the user can specify length, radius and location. **Figure 3.2** presents visually a bumper pair. The element radius and a force /distance relation can be defined, which can be non-linear and include damping. Same physical model as for fixed-elongation couplings apply for bumper couplings, presented in equation (3.7). Sliding friction between bumpers is neglected. The vectors is defined as expressed in equation (3.1) and the distance between is found by solving equation (3.2). The contact point can be found as equation (3.3) expresses. **Figure 3.3** presents the denotations.
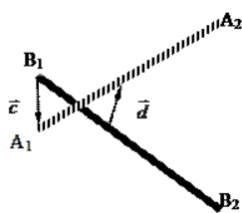
Figure 3.3: [12]

$$a = \{A_2\} - \{A_1\}$$
$$b = \{B_2\} - \{B_1\} \tag{3.1}$$

$$d = c \cdot e_n$$
$$e_n = \frac{a \times b}{|a \times b|} \tag{3.2}$$
$$d = d e_n$$

d   Distance between lines

d_0 Distance at contact

$${P} = \{A_1\} - d + pa = \{B_1\} + rb \tag{3.3}$$

Simple Lifting wire

A simple lifting wire coupling is a simplified bi-linear wire model without mass and drag. Special care should be taken when light weight modules is subject to high dynamic loads, the damping could cause unphysical load distribution because of numerical instability. Damping should normally be between 1-2% of Ea (cross section stiffness). The simple wire coupling is modelled as a linear spring according to equation (3.4) where the axial stiffness is given by equation (3.5). Material damping is expressed by equation (3.6) [12].

$$\Delta l = \frac{T}{k} \qquad (3.4)$$

Δl   Elongation

T   Wire tension

K   Effective axial stiffness

$$\frac{1}{k} = \frac{1}{EA} + \frac{1}{k_0} \qquad (3.5)$$

E   Modulus of elasticity

A   Cross-section area

$1/k_0$ Connection flexibility

$$F = \frac{C_w \Delta l}{l \Delta t} \qquad (3.6)$$

Fixed-elongation / Force-elongation

A fixed elongation coupling is an element for positioning of bodies globally and for coupling between bodies. As for the bumper it can be defined as a positioning element or a linear or non-linear relation between length and elastic force and damping, which is also suitable for PHC modelling. The purpose of the mathematical model in SIMA is to describe axial forces and shear forces in a general way. The axial force is given by equation (3.7):

$$F_a = F_{as}(d) + C_a(d)|\dot{d}|^p sign(\dot{d}) \qquad (3.7)$$

$F_{as}(d)$ Axial stiffness force

$C_a(d)$ Damping coefficient

This is just a general model that may integrate a wide range of restoring force and damping models. In this study only the damping coefficient is considered and

analysed. The fixed-elongation coupling is also used as position measurement tool for relative distance between body points, where force equals distance.

General damping

Damping is a result of stored energy dissipations of oscillations in a dynamic system. Damping becomes highly relevant when the system resonance is close to resonance. As it is very hard to calculate exact damping of a system approximations based on theoretical and empirical knowledge is necessary. One way to model the damping C is to assume it may be expressed as a percentage of the critical damping [16].

$$\omega_0 = \sqrt{\frac{K}{M}}$$

(3.8)

$$C_{crit} = 2M\omega_0 = 2\sqrt{MK}$$

$$C = x \cdot C_{crit}$$

(3.9)

The percentage x is selected based on experience. A mass M suspended by a spring K is considered, the eigen frequency of the system can then be expressed by equation (3.8) and (3.9). More about how the damping affects the eigen frequencies on the coupled rigid body system *6.2.4 Passive horizontal* spar dampers.
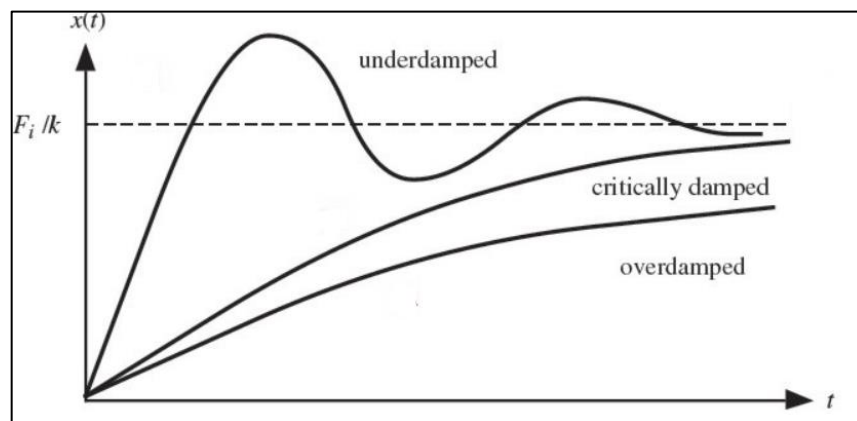
Figure 3.4: Illustration of underdamping, overdamping and critical damping **[17]**.

There exist many different mathematical models of damping systems. Generally, the responses presented in **Figure 3.4** illustrates the effect of overdamping, underdamping and critical damping. Main differences lie in their rise time and settling time and steady state value. The three different time responses are defined by the damper parameters, and the main goal is to reach the dotted line which represents steady state value. The choice of path should be chosen based on wanted system response and critical eigen frequencies [17].

3.4 Environmental modelling & positioning

The next sub-sections will cover the environmental force components a floating coupled multi-body system will encounter. Primarily focus on the phenomena which induce loads on the bodies – wind, waves and current.

3.4.1 Hydrodynamics

Equation of motion

The equation of motion for all bodies with 6DOF in sinusoidal motion is presented below in equation (3.10). This equation describes the behaviour of the physical system in terms of its motion as a function of time, or mathematical functions in terms of dynamic variable where the variable is either spatial coordinates or time. To account for frequency dependent added mass and damping in the time domain retardation functions is added, which is the body response received by an impulse from the system [15].

$$M\ddot{x} + C\dot{x} + D_1\dot{x} + D_2\dot{x}|\dot{x}| + K(x)x = q(t,x,\dot{x}) \qquad (3.10)$$

M	mass matrix, incl. frequency-dependent added mass (from WAMIT)
x	Position vector
C	Frequency-dependent (expressed by retardation functions) potential damping matrix (from WAMIT/HydroD)
D1	Linear damping matrix
D2	Quadratic damping matrix
q	Exciting force vector
K	Hydrostatic stiffness matrix (from WAMIT)

On the right hand of the equation of motion we have the excitation force, which is given by equation (3.11). It represents different force components, such as wind, waves and current [15].

$$q(t,x,\dot{x}) = q_{WA}^1 + q_{WA}^2 + q_{WI} + q_{CU} + q_{ICE} + q_{EXT} \qquad (3.11)$$

qWA	order wave excitation force (from WAMIT)
qwa	order wave excitation force (from WAMIT)
qWI	wind drag force

q_{CU} current drag force

q_{ICE} ice force (presently being implemented)

q_{EXT} any other forces (wave drift damping, specified forces, forces from wires, fenders, bumpers, docking/cones and forces from station-keeping, etc.) This also represents potential coupling forces

Short term wave statistics

If assumed that the sea state is stationary for 3-6 hours it can be described by a set of constant environmental parameters. The main parameters considered further is *Hs* and *Tp*. *Hs* is the significant wave height and is defined as the average height of the one-third highest wave heights in a given time period. *Tp* is the inverse frequency at which the wave energy spectrum has its maximum value.

Long term wave statistics

To determine the integrity assessment long term wave statistics are important to address. Long term statistics are usually determined based on return periods of 1, 10, 100, 1 000 or 10 000 years. The results in this study will be evaluated against the scatter diagram presented in appendix A - **Table A.0.1**. The point of interest is to determine if the natural periods occur in the most probable wave period. An operability analyses is normally performed, and should be done, but is not considered in this study.

Wave spectrum

A wave spectrum is a definition of the power spectral density function of a defined sea surface elevation. It describes the distribution of energy from the wave as a function of the angular spectral wave frequency ω. For a stationary irregular sea state the wave spectra are commonly used, it can and should be chosen based on geographical area studied sea states.

There exists multiple different wave spectrum, as for this study the Torsethaugen is well suited. The Torsethaugen double peak spectral model has frequently been used for design purposes on the Norwegian continental shelf. Originally the model was established fitting two JONSWAP shaped models, and the observed sea states where grouped with respect to *Hs* and *Tp*. Furthemrore, the JONSWAP spectrum was created based on the Pierson-Moskowitz (PM) spectrum with a peak enhancement function; see equation (3.12) for PM definition. The PM-spectrum assume equilibrium between wind and waves after some time – which is called a fully developed sea state. The peak shape factor can either be established by observed data or it can be established by equation (3.13). The modified PM spectrum is expressed in equation (3.14) [18].

$$S_{PM}(\omega) = \frac{5}{16} \cdot H_s^2 \omega_p^4 \cdot \omega^{-5} exp(-\frac{4}{5}\left(\frac{\omega}{\omega_p}\right)^{-4}) \tag{3.12}$$

ω_p is the angular spectral frequency

$$\gamma = \begin{cases} 5, & \left(\dfrac{T_p}{sqrt(H_s)}\right) \leq 3{,}6 \\[2mm] exp\left(5{,}75 - 1{,}15\left(\dfrac{T_P}{sqrt(H_S)}\right)\right), & 3{,}6 < \left(\dfrac{T_p}{sqrt(H_s)}\right) < 5 \\[2mm] 1, & 5 \leq \left(\dfrac{T_p}{sqrt(H_s)}\right) \end{cases}$$

(3.13)

$$SJ(\omega) = A_\gamma S_{PM}(\omega)\gamma^{exp\left(-0{,}5\left(\frac{\omega - \omega_p}{\sigma \omega p}\right)^2\right)}$$

(3.14)

Aγ is the normalizing factor

$S_{PM}(\omega)$ is the Pierson-Moskowitz spectrum

γ is the peak shape factor

σ is the spectral width parameter

Generally, the JONSWAP spectrum is best suited for environmental conditions where $3{,}6 > T_P \ / \sqrt{H_S} < 5$. Special care should be taken outside this range [16].

Wave elevation

In SIMA linear wave potential theory is used to define the incoming undisturbed wave field. The wave elevation is expressed below in equation (3.15). Equation (3.16) presents the expression of multiple wave elevations with different frequencies and directions [16].

$$\zeta(x,y,t) = \zeta_A \cos(\omega t - kx \cdot \cos(\theta) - ky \cdot \sin(\theta) + \epsilon)$$

(3.15)

k   Wave number

θ angle between X-axis and the wave propagation direction

ε the phase angle

$$\zeta(x,y,t) = \sum_{i=1}^{I} \sum_{j=1}^{J} \zeta_{Aij} \cos\left(\omega_i t - k_i x \cdot \cos(\theta_j) - k_i y \cdot \sin(\theta_j) + \epsilon_{ij}\right)$$

(3.16)

$$\zeta_{Aij} = \sqrt{2S(\omega_i,\theta_j)\Delta\omega\Delta\theta}$$

(3.17)

By inserting equation (3.17) into equation (3.18) we can express the final wave elevation based on a wave spectrum.

$$\zeta(x,y,t) = \sum_{i=1}^{I}\sum_{j=1}^{J}\sqrt{2S(\omega_i,\omega_j)\Delta\omega\Delta\theta}\,\cos\big(\omega_i t - k_i x \cdot \cos(\theta_j) - k_i y \cdot \sin(\theta_j) + \epsilon_{ij}\big)$$

(3.18)

Significant wave elevation (Hs) is usually defined as four times the standard deviation (σ) of the surface elevation. As **Figure 3.5** implies, Hs will not very often be encountered, but statistically it is possible to encounter waves much higher than Hs. Normally distributed by a Rayleigh distribution.
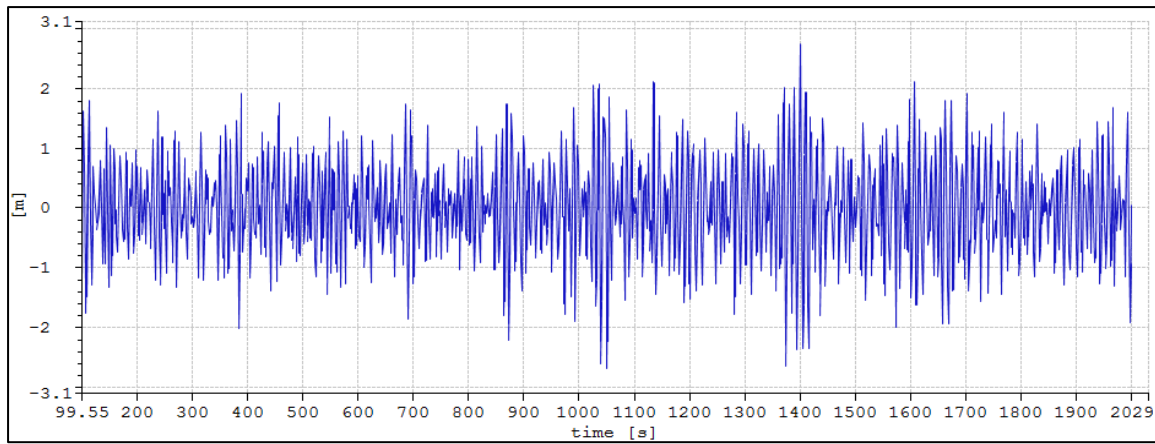
Figure 3.5: Plot of total wave elevation at global origo in SIMA. Hs = 3m, Tp = 10s.

Coupling

There is a possibility to model the interaction between two floating bodies, as for this study there will not be any hydrodynamical coupling. It was recommended early in the study by F. Solaas in SINTEF Ocean to focus on the uncoupled model, as the coupling may cause some problems which would have taken a lot of valuable time. A separate analysis from e.g. WAMIT must be conducted and coefficients further imported into SIMA.

Current

The current is in SIMA defined by the DNV profile and is expressed in equation (3.19) where d is water depth and z is distance above bottom.

$$u(z) = u_t\left(\frac{z}{d}\right)^{\frac{1}{7}} + u_w\left(\frac{z}{d}\right)$$

(3.19)

3.4.2 Aerodynamic

As there is not conducted any aerodynamic analyses on the model, wind forces will not be included in this study. Wind testing has been performed on the

provided SSP model, but as the total projected area has increased the wind matrix is invalid. Wind testing/simulation with the complete model assembly should be performed to provide valid data. As Z. Jiang presented in his paper, the turbine assembly on deck has effect on the stability and dynamic response of the lifting vessel (catamaran in the mentioned study), also the turbine blade angle has effect on the wind induced forces [3].

3.4.3 Motion compensator and control systems

A motion compensator can maintain constant line tension or use a mechanical feedback system to adjust for the body motion amplitude, divided into two main categories; passive and active, respectively. The most common is heave compensation – hanging load from ship side must be compensated for ship heave motion and lowered gently on the sea bed. There also exist hybrid active-passive systems which combine features of both systems. The same principals exist for compensating e.g. surge and sway, which will be mentioned in this study. Both passive and active motion compensators will be utilized in the model development but in simplified versions [19].

PHC at their simplest are just vibration isolators in open-loop; input is ship motion and output is reduced amplitude motion of the attached object. The advantage is that the PHC does not require any input energy to function – it is as simple as a spring-damper system as illustrated in **Figure 3.6**. Dependent on the spring-constant k and the damping c the spring-damper system acts as a

Figure 3.6: PHC illustrated **[19]**.

mechanical low-pass filter for different frequencies. Differential equation (3.20) describes the load motion [19].

$$m_L \ddot{x}_L = -k(x_L - x_H) - c(\dot{x}_L - \dot{x}_H)$$ (3.20)

x_H Heave of SSP

x_L Load displacement

m_L Load mass

After rearranging and taking the Laplace transform of equation (3.20) it can be expressed as equation (3.21) [19]:

$$\left(\frac{x_L}{x_H}\right) = \frac{cs + k}{m_L S^2 + cs + k}$$ (3.21)

A PHS is very sensitive to the frequencies of the SSP and the ocean waves, the goal should be to design a compensator such that ω_d occurs below the expected frequency range of the ocean waves. The spring-constant should be tuned so that

ω_d occurs outside the natural frequency. ω_d is expressed by equation (3.22) and ω_n is expressed by equation (3.23), which represents the corner frequency respectively. Corner frequency can be explained as where the maximum response from the system occur, or also called natural frequency [19].

$$\omega_d = \omega_n \sqrt{1 - \left(\frac{c}{2\omega_n}\right)^2}$$

(3.22)

$$\omega_n = \sqrt{\frac{k}{m_L}}$$

(3.23)

As a contrast to the PHC, the AHC systems involve control and require energy input. In a common ship related system, the heave motion is measured and relayed to a controller, which then moves an actuator to compensate the motion. The advantage with the AHC is that the feedback variable is not limited to heave motion, it can be used on a variety of cases. It mainly depends on the intelligence level of the control system. For this study a very simple control system which only compensates in regard of accelerations, e.g. between the OWT and spar. It does not counteract for external forces acting on the OWT. A modern control system like a motion reference unit (MRU) uses 3-axis accelerometers and gyroscopes to determine the ship motion, which tend to be very expensive.

To choose the right compensator technology for the correct purpose is a delicate and important aspect to address. Modern AHC often includes a lot of electronics, sensors and controlled actuators which can, or often does, increase the production cost. As for the PHC, production cost is relatively low.

In this study two different controllers will be tested and tuned; PD+FF and PID. The tuning procedure is presented in sub-section *4.5.1 Motion compensators*, and the result and discussion in section *6.1*. In the next sections is the theory for the two controllers expressed.

PID controller

Below is the control law for the PID controller expressed in equation (3.24). The PID controller controls loop feedback mechanism and is found in almost every industrial control system. The controller continuously calculates an error value which is corrected based on proportional, integral and derivative terms (PID).

$$F_{T0}(t) = K_D \dot{\epsilon}(t) + K_p \epsilon(t) + K_I \int_0^t \epsilon(\tau)d\tau$$
$$\epsilon(t) = x_0 - x(t)$$
$$\dot{\epsilon}(t) = \dot{x}_0(t) - \dot{x}(t)$$

(3.24)

$x(t)$ Filtered position

$x_0(t)$ Desired position

$\epsilon(t)$ Velocity error

F_{T0} Desired control force from thusters

K_P Position feedback gain

K_l Integral feedback gain

K_D Velocity feedback gain

PD + Feedforward controller

The feedforward controller quickly and directly demolishes the disturbance, and is almost always used as an add-on for feedback control. To fulfill the PD controller a feedforward part is added.

Positioning system

In SIMA the thruster's thrust, T, and the torque, Q, are given by equation (3.25). K_T and K_Q are dimensionless coefficients of thrust and torque, respectively.

$$T = n^2 \rho D^4 K_T(J)$$
$$Q = n^2 \rho D^5 K_Q(J)$$
$$J = \frac{v_a}{nD}$$

(3.25)

D Screw diameter

ρ Water density

$J \cdot v_a$ Axial component of relative velocity

The dynamic position for the SSP is achieved by regulating six thrusters with a Kalman filter-based control system. Thruster specifications; maximum thrust force is F = 7.9e+05N with minimum time change of 25s. The control systems mathematical model can be divided into high frequency mode, low frequency mode and a model for slowly varying wind and current forces. SSP motions and environmental forces are estimated, for this study current and waves. The input variables are updated every time step, which is why the choice of time step is so decisive. Control parameters was included in the provided SSP model. More details about the Kalman filter model can be found in ref. [20]. The control system follows a global reference point (0,0,0). A body relative reference point is optional in SIMA, but the control system input got disturbed by the coupling forces. The STD in (X,Y) increased when body relative reference point was applied.

4 Installation procedure development

In the next sections are three objects presented – the SSP, OWT and spar buoy, respectively. Selected properties for the OWT and spar are copied from Zhiyu Jiang's paper for comparability reasons [3]. In this chapter is the idea of the installation procedure presented with the choice of couplings, and related real life proposals on what the couplings represents. Elements as modelled in SIMA can be inspected in **Figure 5.1**. Some suggestions on improvements is also included, further explained in chapter 6.
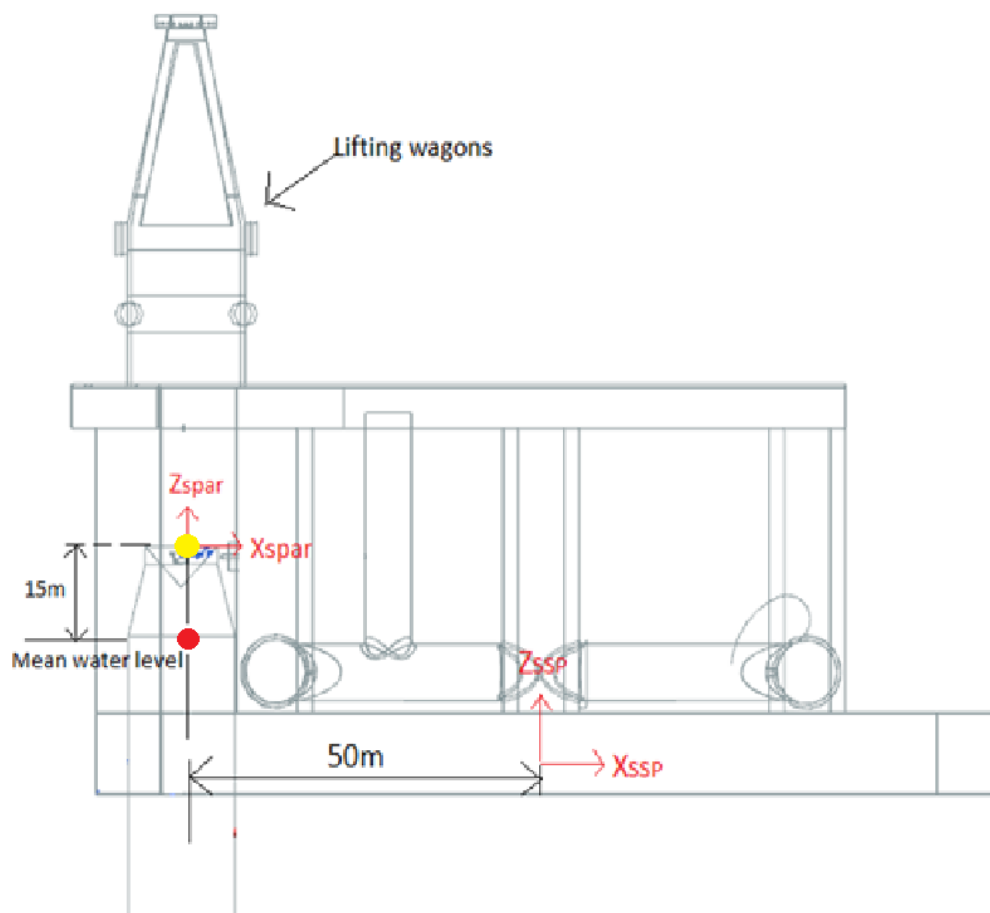
Figure 4.1: Installation concept main dimensions. Global zero at red dot, spar reference point at yellow dot. Local body axis' as presented.

In **Figure 4.1** the installation vessel main dimensions can be inspected. The spar buoy is placed 50m from centre SSP because of practical reasons but should have, optimally, been placed at SSP centre in regard of motion response and load sensitivity. Global zero is located at mean water level (red dot), and spar reference point 15m above mwl. (yellow dot). OWT reference point is located at bottom of structure.

4.1 Semi-submersible (SSP) with lifting wagons

An SSP is chosen as installation vessel for OWTs as the industry primarily wants to re-use old platforms from the oil industry. For motion reduction, the bigger the better is the philosophy [14]. One typical platform with dimensions in the high-range is considered in this study. Visually a six-legged platform is presented in this paper, but for the simulation in SIMA, a four-legged platform provided by supervisor was used. Dimensions for the four-legged SIMA SSP model is presented in **Table 4.1** with correlating description in **Figure 4.4**. The analyses are done with SSP at survival draft, T=19m. In this position, maximum added mass is present which reduces low frequency motions, but high load sensitivity is the consequence. Added buoyant volume as presented in **Figure 4.2** is not accounted for in the calculations, only part of the proposed design solution.

The idea is to transport pre-assembled OWTs on the SSP. The OWTs is lifted on the SSP deck from quay and secured for transportation out to the installation field. Some kind of clever transportation locking device should be provided to assure easy and secure lifting of the OWTs when offshore. **Figure 4.3** presents a crane wagon type which can provide secure and

Figure 4.2: Illustration: SSP with wagon rails and extra buoyancy volume at lifting long. position.

easy on board lifting of the OWT as well as it has sufficient space for winch arrangement inside. Two wagons are placed on the top deck of the SSP and rail type system for the wagons to slide in longitudinal direction (global x). The wagons are lifting the OWT tower and move it to the end of the SSP. Winch lifting points are modeled in SIMA with body points, see **Figure 5.1** for full SIMA model presentation.

Figure 4.3: Left: Front view of the crane wagon with explanations. Right: Side view of the wagon. Dimensions in meters.

Table 4.1: Selected main dimensions SSP used in this study **[21]**.

Parameter	Symbol	Value
Length overall [m]	L_{OA}	114.4
Breadth overall [m]	B_{OA}	76.7
Spacing between pontoons (centre to centre) [m]	L_{CCPT}	57.9
Height top deck [m]	H_{PL}	50
Length pontoons [m]	L_{PT}	114.4
Breadth pontoons [m]	B_{PT}	18.9
Height pontoons [m]	H_{PT}	16.25
Displacement in operational mode [t]	Δ	54 770
Waterplane area [m²]	W.p.a	1202
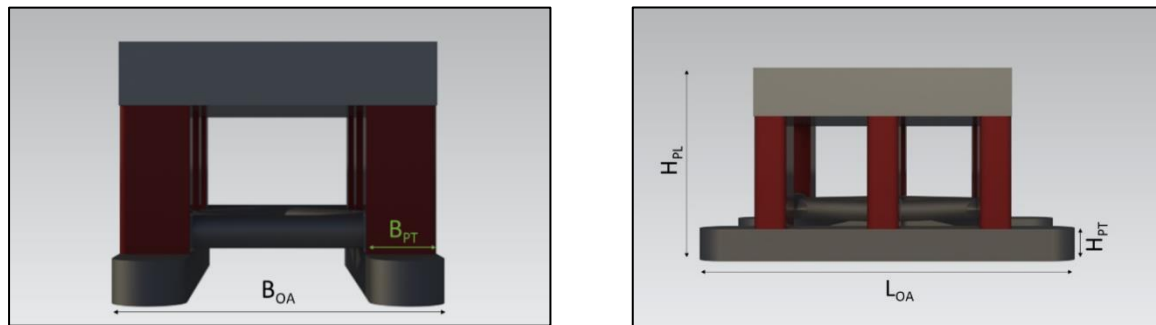
Figure 4.4: Six-legged SSP (dimensions applies for the four-legged SIMA SSP). Left: Front view, Right: Side view.

4.2 Offshore wind turbine

The OWT dimensions used by Z. Jiang in his study is probably a bit excessive, but forward-looking. For comparability, the same dimensions will be used in this study. It is realistic to think that the concept needs to be dimensioned and development with larger turbines in mind because the turbines are increasing rapidly in size.

Table 4.2: OWT dimensions **[3]**.

Parameter	Symbol	Value
Wind Turbine		
Rated power [MW]	RP	10
Rotor mass [ton]	M_{rotor}	200
Nacelle mass [ton]	$M_{nacelle}$	400
Tower mass [ton]	M_{tower}	600

4.3 Spar fundament

The selected spar properties are presented in **Table 4.3**.
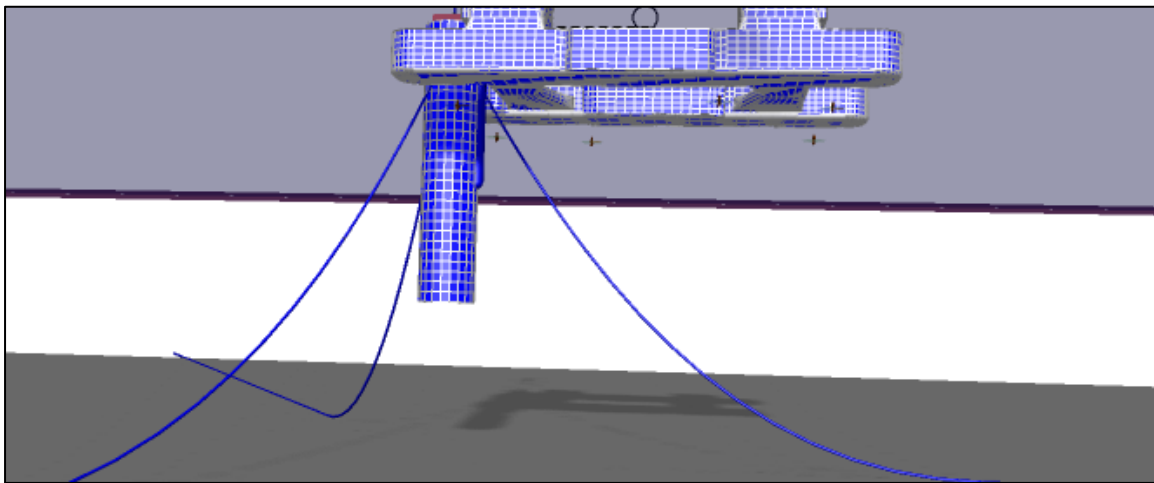
Figure 4.5: Spar fundament with selected mooring line system in SIMA.

The spar fundament needs some special attention when modelled in SIMA to get the correct response. Most of the hydrodynamic coefficients are imported from WAMIT, like the first order wave force transfer functions and the retardation functions. For calculation of linear and quadratic viscous damping, a slender element needs to be added to the body. It is important to select properties of the slender element with care, as it is easy to add "double" added mass and wave forces.

Table 4.3: Selected properties for the SPAR foundation **[3]**.

Parameter	Symbol	Value
SPAR foundation before mating (LC1)		
Diameter at top [m]	L_{LC1}	9,5
Diameter at waterline [m]	M_{LC1}	14
Draft [m]	T_{LC1}	70
Ver. position of centre of buoyancy [m]	Z_{COBLC1}	-35
Ver. position of COG [m]	Z_{COGLC1}	-51.8
Displacement mass [ton]	Δ_{LC1}	11045
Vertical position of fairlead [m]	Z_{FLC1}	-15
SPAR foundation with wind turbine (LC2)		
Diameter at top [m]	L_{LC2}	9,5
Diameter at waterline [m]	M_{LC2}	9,5
Draft [m]	T_{LC2}	80
Ver. position of centre of buoyancy [m]	Z_{COBLC2}	-41.5
Ver. position of COG [m]	Z_{COGLC2}	-50
Displacement mass [ton]	Δ_{LC2}	12160
Vertical position of fairlead [m]	Z_{FLC1}	-25

4.3.1 Installation of the fundament

Part of the installation procedure is to transport and install the spar buoy. Today's installation method involves large heavy lifting equipment and AHTS vessels, which is high cost. But unlike the OWT, the spar buoy can be installed for a long time, and OWT's can be swapped. In this study, it is assumed that the spar is pre-installed offshore and ready for mating with the OWT. The spar shall be towed from the production site and out to the installation field. After ballasting the fundament bottom, to rise it vertically, it shall be moored by three catenary lines.

4.3.2 Mooring lines

In general a catenary line is defined as a hanging line subjected to its own weight hanging between two points. For an anchor line in this study the two connection points are on the floating body (spar) and on the seafloor [16]. The spar buoy is moored to the sea bottom with three catenary lines. Mooring line specifications are imported from Z. Jiangs model and is presented below in **Table 4.4** with correlating explanation in **Figure 4.6**. **Figure 4.5** presents the spar fundament with mooring system as modelled in SIMA [3]. It is for this concept model relevant to analyse how the coupling forces between the SSP and the spar will affect the mooring line system, more detailed discussion and results in sub-section *6.2.6 Mooring lines*.
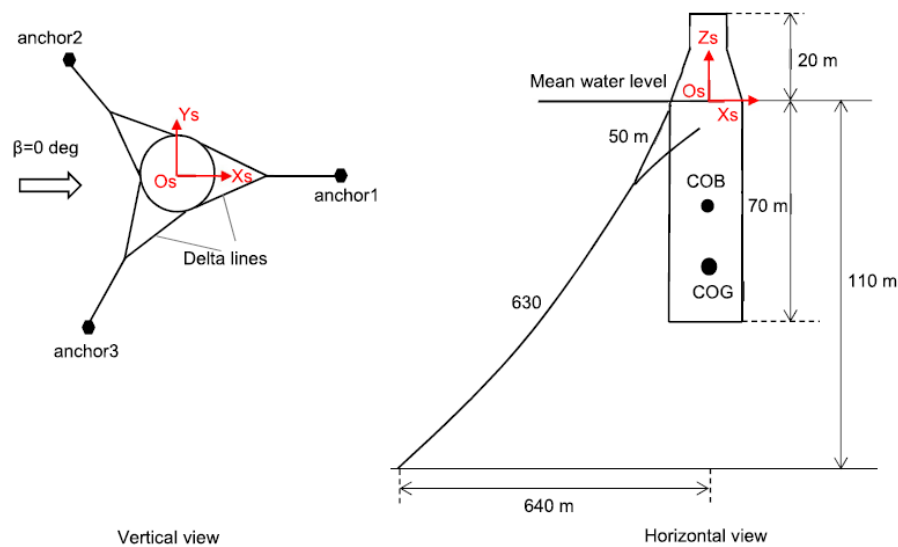
Figure 4.6: Layout of the mooring system for the spar buoy **[3]**.

Table 4.4: Selected properties of the mooring system with no environmental loads **[3]**.

Parameter	Symbol	Value
Total length of mooring line[m]	L_{moor}	680
Length of upper line[m]	L_{upper}	50
Length of lower line [m]	L_{lower}	630
Diameter of upper chain [mm]	D_{upper}	132
Diameter of lower chain [mm]	D_{lower}	147
Unit submerged weight of upper chain [kN/m]	W_{upper}	3.686
Unit submerged weight of lower chain [kN/m]	W_{lower}	4.240
Product of elastic modulus and cross sectional area of upper chain [kN]	EA_{upper}	1.373*E6
Product of elastic modulus and cross sectional area of lower chain [kN]	EA_{lower}	1.682*E6
Breaking strength of upper chain[kN]	$T_{b,\ upper}$	1.299*E4
Breaking strength of upper chain[kN]	$T_{b,\ lower}$	1.553*E4
Pretension in the top segment [kN]	T_0	674

4.4 Proposed installation vessel design preview

Complete CAD-model of the proposed concept is presented below in **Figure 4.7**. Note that this is only for visualization and suggestions on what the different elements in the model represent. SIMA-model main dimensions are correlating to the CAD-model except for the added buoyancy. Siemens NX was used as CAD-tool and for photo rendering. **Figure 4.8** presents the installation vessel in action when installing OWT's offshore.
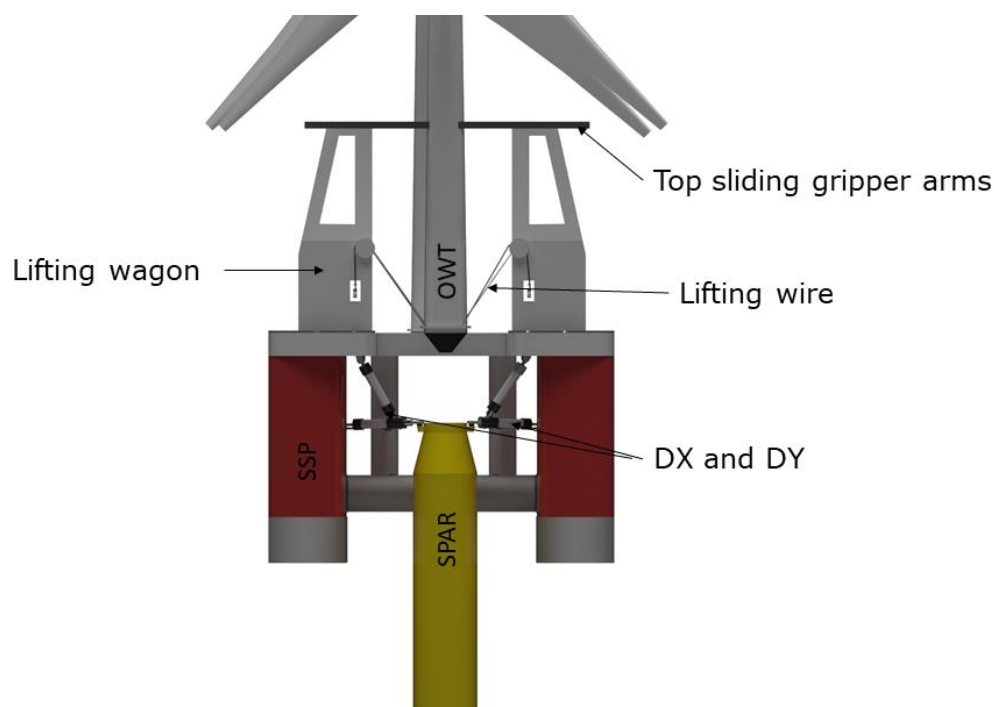
Figure 4.7: Presentation of the concept model as intended.

Figure 4.8: Illustration of the installation vessel with pre-assembled OWT's in action.

4.5 Coupling of objects

4.5.1 Motion compensators

For relative motion reduction between two bodies or between a body and a fixed reference point a motion compensator is needed. The compensator can either be added to winches or hydraulic cylinders, and the limitations are often the control system. One of the intentions with this concept is that it allows some motion in the horizontal plane, either compensated by a control system or/and a docking pin, and some dampers between the spar and SSP. The docking cone and the passive motion compensator system for the OWT and spar will be explained detailed in sub-section *4.5.2,* respectively. A compensator control system for the four lifting wires which compensate for motion in the vertical and horizontal plane is complex and is something that needs to be programmed externally. The compensator in SIMA is limited to compensation between a lifting point and a fixed global point - not evaluated any further. For heave compensation between the OWT and spar an external control system was applied to the four lifting wires – limitations presented in **Figure 4.9**. The javascript for the external controller was given by Thiago G. Monteiro (TGM). The script offers two different controllers, PD + FF or PID. As mentioned in section *3.4.3 Motion compensator and control system* the parameters
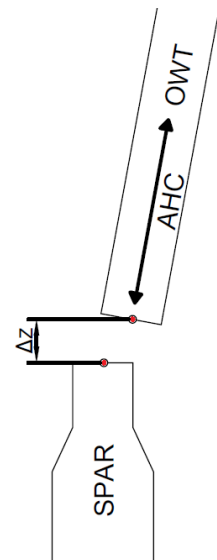
Figure 4.9: Limitations of the AHC - only compensating for vertical error (ΔZ).

for the controllers need tuning. Parameters which will be tuned for the respective controllers are presented in **Table 4.5** and **Table 4.6**.

Table 4.5: PID controller. Variable parameters.

PID controller	
zSet	Distance between OWT and spar
Kp	Proportional gain
Ki	Integral gain
Kd	Derivative gain
uMax	Max winch velocity
(x0,y0,z0)	Reference point on OWT
(x0spar,y0spar,z0spar)	Reference point on spar

Table 4.6: PD + FF controller. Variable parameters.

PD+FF controller	
zSet	Distance between OWT and spar
Kp	Feedback gain
Td	Feedback derivative time
Kf	Feedforward gain
Tfd	Feedforward derivative time
Tf	Time constant for low-pass filter
uMax	Max winch velocity
(x0,y0,z0)	Reference point on OWT
(x0spar,y0spar,z0spar)	Reference point on spar

The highlighted parameters are the ones that will be tuned, the others are only part of the model configuration and stays fixed. The fixed parameter values are presented in **Table 4.7**. The logic would be to choose reference point for each of the four winches individually, but the controller would not work properly with different reference points - SIMA responds with error message. Also, when only vertical ref. error is considered in the controller the radial error would increase. The parameter tuning procedure is done with four lifting wires attached as presented in sub-section *4.5.2,* and four independent controllers to each winch with equal parameters.

Table 4.7: Controller parametrization, fixed parameters.

PD+FF / PID controller fixed parameters		
zSet	Distance between OWT and spar	15 meters
uMax	Max winch velocity	3 m/s
(x0,y0,z0)	Reference point on OWT	(0,0,0)
(x0spar,y0spar,z0spar)	Reference point on spar	(0,0,0)

The parameter tuning procedure was done with advice from TGM. There is not a given science how to tune the parameters, but there exists some documentation on how it can be performed to save some time. The raw data from the parametrization procedure is presented in Appendix B (**Table B.0.2** to **Table B.0.11**). See section *6.1.1* for parametrization procedure. The method, or philosophy, with the procedure was to narrow it down to the correct parameter value to obtain least possible vertical STD between OWT bottom and spar top – reference points are located at red dot as presented in **Figure 4.10**.
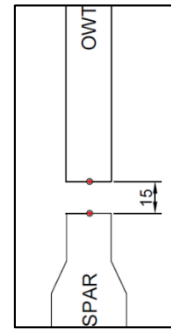
Figure 4.10: Reference point.

4.5.2 Relative motion dampers

In the next sub-sections are the object couplings used in SIMA with correlating proposal on what the couplings could physically represent.

Lifting wire arrangement

The idea for the lifting arrangement is to use four lifting wires. The lifting arrangement is presented in **Figure 4.11.** The red circles locate the lifting points, or body points, fixed to the SSP, at each point a winch with a controller is added. The yellow circles locate where the
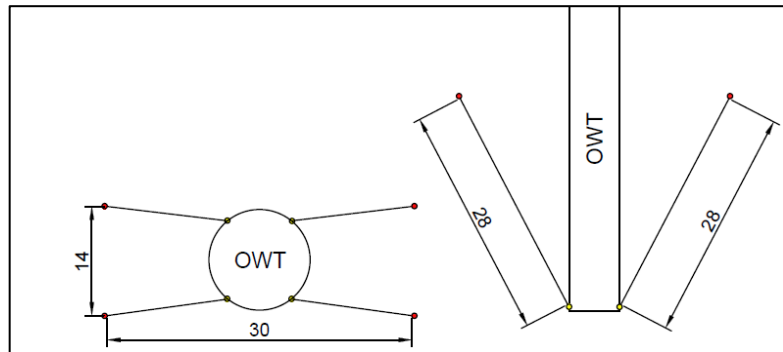
Figure 4.11: Four lifting wires as modelled in SIMA, attached to body points associated to the respective bodies. Global coordinate system. Dimensions in meters.

attachment point on the OWT is defined. The heave compensator for the four winches is limited to only compensation in Z-direction, but the idea with the four wires configured as presented in **Figure 4.11** is that it allows for some displacement in X and Y direction, also the reason of the wire length.

Selected parameters for the simple lifting wire are presented in **Table 4.8**. With these specifications, the static stretch can easily be calculated with the expression presented in equation (4.26) [12].

$$dl = \frac{F_n l_0}{AE} \qquad (4.26)$$

dl   Stretched length

Fn   Static load

A   Cross-section area

l_0 Length of wire

Table 4.8: Material data for the steel lifting wire

Material data	Stainless steel AISI 302
Length [m]	28.018
Damping [Ns]	2% of Ea
Ea [N]	9.45e+09
Modulus of elasticity [GPa]	180
Cross section area [mm^2]	5281
Wire diameter [mm]	82

With the presented material data the total wire stretch is *dl = 88mm* in static condition, result is confirmed in the static calc. in SIMA. The winch performance is defined by the external controller that only takes into account the winch velocity.

Top bumpers

Four bumper elements, modelled in SIMA as shown in **Figure 4.12**, are used to model top sliding gripper arms with rollers. Proposed design in **Figure 4.13** of the sliding gripper arms. The purpose is to hold the OWT firm in the horizontal plane (X,Y translation), and the rollers shall allow sliding in vertical direction (Z-translation) as well as some small rotation about (X,Y) axis. Z-rotation(yaw) is prevented by the four lifting wires and the top gripper arm rollers but is fixed in SIMA

Figure 4.12: Horizontal bumper elements is fixed to SSP body and vertical bumper elements are fixed to OWT body.

for simplicity. Damping in Y-direction should be provided by active/passive hydraulic cylinders to control the gripper arms. The motion induced forces in X-direction from the OWT would probably cause the installation wagons to rotate – more details governing this concern in chapter *6 Results and discussion.*
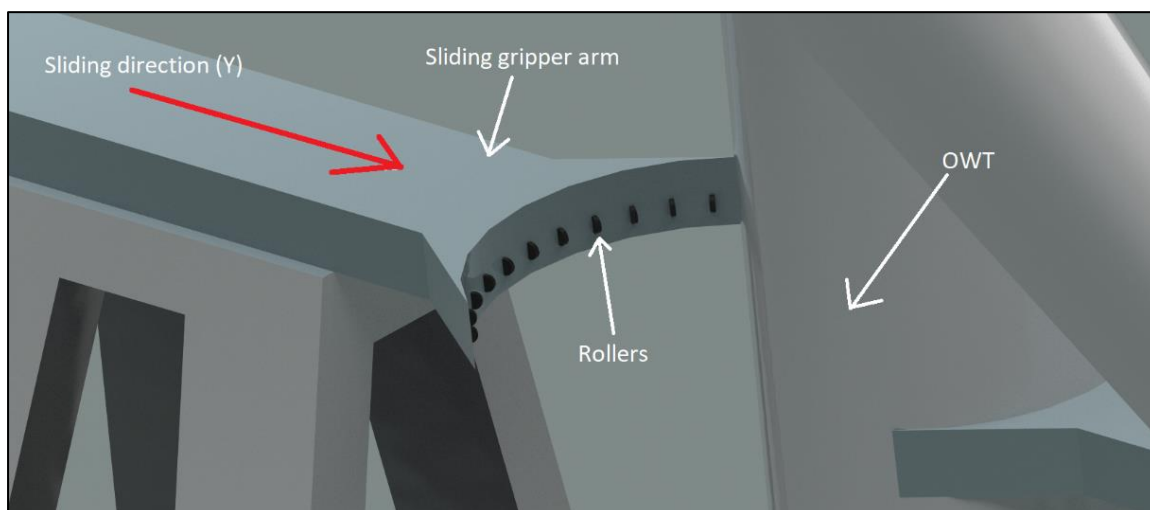
Figure 4.13: Top sliding gripper arms details

The bumper elements can be defined with length/force relation as wanted. To model the gripper arms the relation presented in **Table 4.10** was considered.

Distance *d,* see **Figure 3.2**, between the elements is 0.5m. This means that there will be no force present in the couplings when OWT is completely in equilibrium. When the OWT starts tilting and d decreases force is increasing linearly, max force is obtained when d = -0.5m. This represents something like a soft cushion to dampen the high frequency motion – the OWT tends to oscillate in high frequency when the bumpers are not modelled correctly. Further, the bumper couplings are modeled to withstand a maximum force of F_{max} = 5.0e+08N, which means max force before slip through. A damping coefficient of 1.0e+06Ns/m is selected at d = -0.5m and 5000Ns/m at d = 0.45m.

Table 4.9: Bumper element dimensions.

Top bumper elements	SSP
Length [m]	10
Global height (Z) [m]	50
	OWT
Length [m]	20
Global height (Z) [m]	40-60

Table 4.10: Bumper characteristics.

No	Distance[n]	Force[N]	Damping[Ns/m]
1	-5.5	5.0e+08	1.0e+06
2	-0.5	5.0e+08	1.0e+06
3	0.45	0.0	5000.0

OWT mating - docking cone

One of the most crucial phases of the installation procedure is the contact force between OWT and spar. A solution to this is in this study solved as a docking cone. The OWT bottom is modelled as the docking pin and the top spar is shaped as the docking cone. For maximum impact force damping the docking pin core can be made of steel and wrapped with some kind of rubber or plastic layer, and the docking cone can also be made of some similar material - the friction force has to be evaluated.

The main reason for the choice of a docking cone was to increase the installation limitation in the horizontal plane. OWT axial rotation is considered to be damped/fixed by the lifting wires and top sliding arms. Below are scenarios of the relative position between spar top and OWT bottom presented in **Figure 4.14**. Where *n* represents relative radial motion radius and O_{cr} is the outcrossing rate. It is favourable to have as low as possible outcrossing rate - how many times the tower crosses the safety boundary. For this study radius of safety boundary is considered R_{sb} = 1m. The max allowable outcrossing rate is considered less than presented below in equation (4.27) [3]:

$$O_{cr} = 5.26 \cdot 10^{-3} Hz \qquad (4.27)$$
$$n \leq R_{sb}$$

O_{cr} Outcrossing rate

n   Critical radial relative distance

R_{sb} Radius of safety boundary

The mating face will be initiated when the outcrossing rate is below limit.

The contact force between the docking pin and the docking cone will hypothetically provide enough force such that the OWT will centre itself when lowered, if inside of boundary limit. This is where the OWT bottom translation flexibility in horizontal plane caused by the lifting wires serves its purpose - they will intentionally provide enough flexibility in (X, Y) direction.
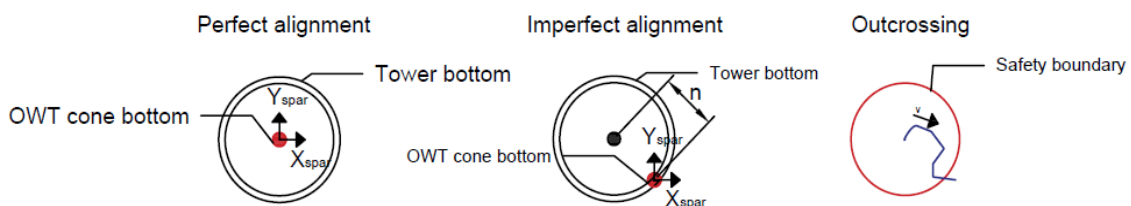
Figure 4.14: Scenarios of different relative positions between spar and OWT.

When the lowering phase is successfully completed the intention is to have a automatically controlled locking mechanism. A pin located in the cone can be pushed horizontally and lock the OWT bottom to spar top temporary until permanently bolted together. **Figure 4.15** presents a drawing of the suggested mating mechanism. The docking cone is modelled with bumper group elements in SIMA. The bumper elements feature good visual feedback and the physics are easy to understand, the SIMA-model is presented in **Figure 4.15** and selected parameters for the elements in **Table 4.11**.
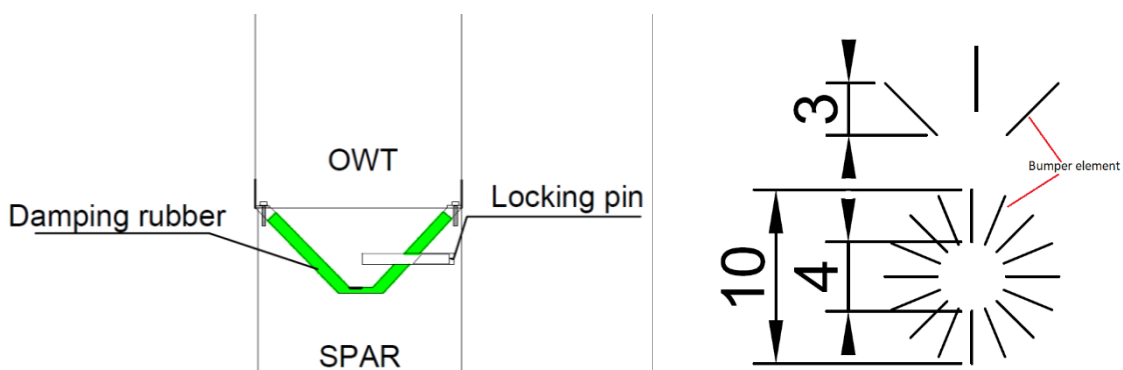
Figure 4.15: Left: Docking cone with suggested locking pin. Rubber wrapping to dampen impact forces between OWT and spar. Right: Horizontal(bottom) and vertical (top) projection of the docking cone elements in SIMA. Dimensions in meters.

Table 4.11: Selected parameters for the modelled docking cone.

Selected bumper parameters	Docking cone elements
Length [m]	4.24
Radius[m]	0.5
Stiffness [N/m]	1.0e+06
Damping [Ns/m]	1.0e+05
	Docking pin element
Length [m]	3.0
Radius [m]	1.0
Stiffness [N/m]	1.0e+06
Damping [Ns/m]	1.0e+05

Passive horizontal spar dampers

One of the major concerns when installing OWT is the relative motion in horizontal plane between OWT and spar, and as mentioned the possible impact forces. This problem can be partly solved with passive hydraulic dampers between SSP and spar. The dampers is arranged to dampen relative motion between SSP and spar in (X,Y) direction – damper arrangement can be inspected in **Figure 4.16**. More detailed about how the dampers affect the STD in relative (X,Y,Z) between the objects and element forces in sub-section *6.2.4 Passive horizontal spar dampers.*
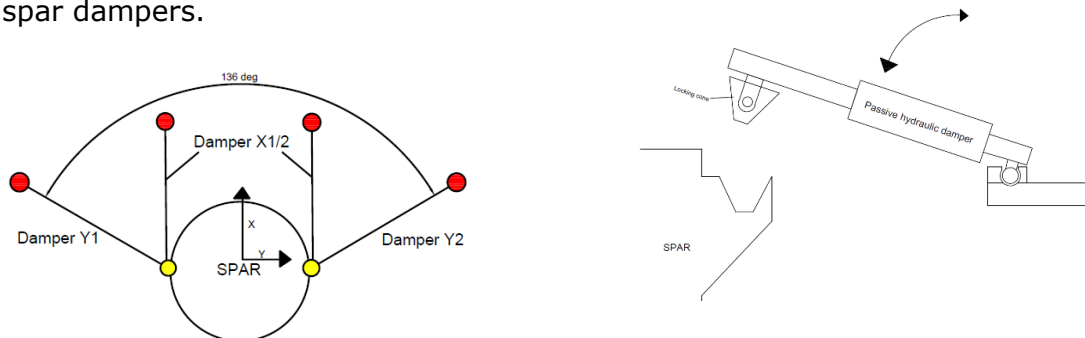
Figure 4.16: Left: Presents the damper arrangement, global coordinates. Yellow circles represent spar connection point and red circles represents SSP connection points. Right: Connection cone proposal between damper and spar. Damper arm is lifted into position by hydraulic cylinders.

DX1/2 (damper) is connected to DY1/2 (damper), respectively. Only one connection cone between spar and damper pair is needed. A simple sketch of the proposed damper connection cone is presented in **Figure 4.16**. To assure firm connection the cone shall be equipped with a controlled magnet or some kind of suction technology. The dampers are lowered into position when the spar is inside the boundary limit of the SSP, and the relative motion is at a possible mating level. The connection cones/arms should be designed to withstand some impact force, as there is expected some relative motion between the objects before dampers are activated. To prevent impact forces between spar and SSP's transverse stiffener, a cushion of some sort should be mounted on the stiffener, e.g. a fender roller. Hydraulic lifting cylinders are used to lower and lift the damper arrangement into position, as presented in **Figure 4.16**. Damper connection to the SSP shall be a

ball joint which allow lowering/lifting and rotation. Modelled as fixed connection (body points) in SIMA – free rotation in all axis.

5 SIMA simulation

The installation concept is presented below in **Figure 5.1**, screenshot of SIMA-model. Selected dimensions are as presented in the previous chapter. Simulations with DY1/2, DX1/2 and heave compensator active is identified as coupled and uncoupled if inactive – accounts for the whole study.
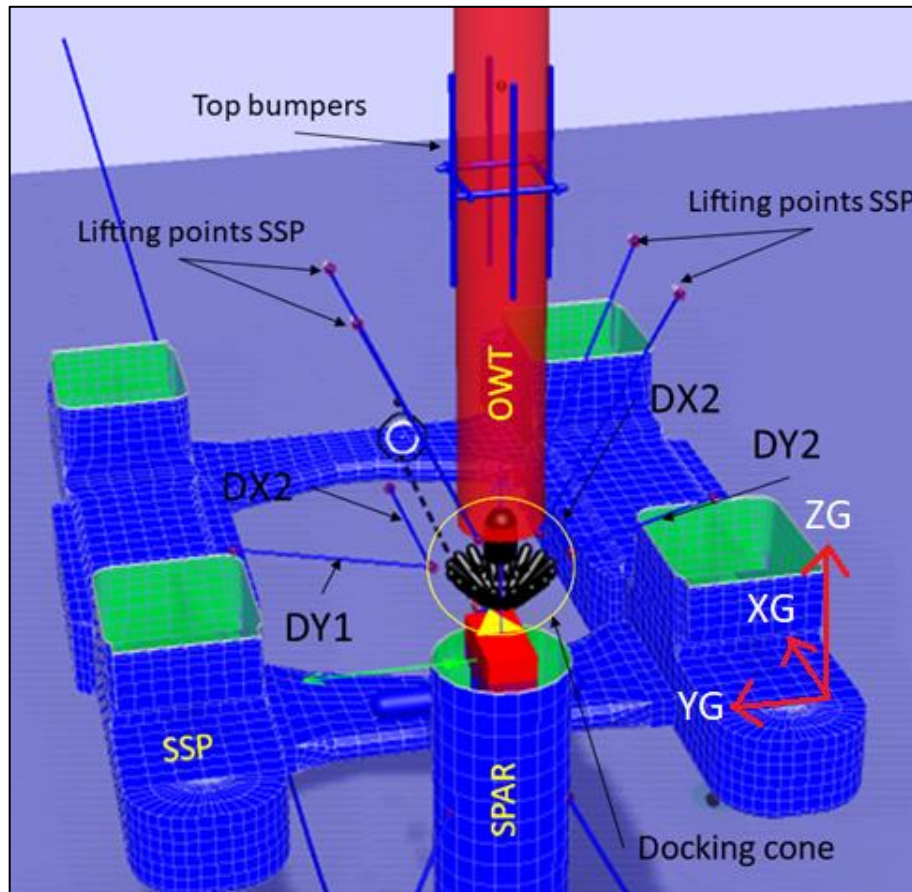
Figure 5.1: SIMA-model presented with description of elements. Global centre at mean water level, spar centre.

5.1 Simulation configuration

Dynamic calculation parameters

To obtain a stable simulation, it was necessary to "tune" the time step. Especially the heave compensator would be unstable if a larger time step was applied, small high-frequency oscillations could occur. If too large time step, an error message will occur which states that the simulation is terminated due to large accelerations. Too small time step is unwanted as the computational time increase rapidly, but time step of 0.005 had to be selected where inconsistent results occurred. The goal with numerical simulations is always to find the compromise.

To get valuable and comparable data for standard deviation analyses, a simulation length between 1000-4000 seconds should be considered – 1900 seconds for all conditions in this study. First 100 seconds of the simulation is not accounted for in the results as the transients need stabilization time, time history presented in **Figure 6.2** confirms this statement. Selected dynamic simulation parameters are presented in **Table 5.1**.

Table 5.1: Dynamic calculation parameters

Integration method	3rd order Runge-Kutta
Time step	0.005 - 0.01s
Simulation length	2000s
Requested time series length	2000s
Time increment	0.01s

Coordinate system

In SIMA it can be chosen between different DOF for each of the bodies. The choices are [15]:

- Prescribed: fixed or prescribed body position
- 6 DOF time domain: total motion is simulated in the time domain; retardation functions + wave forces
- 6 DOF separated analysis: wave frequency motion in the frequency domain; RAO
- 3 DOF: time domain: motion simulated in the time domain (no rotations)

For this study, the model is simulated in 6 DOF time domain to capture all the forces and motions affected by the hanging load. Computational time could have been reduced by using a 6 DOF separated analysis. A separated analyses will cause the body to move according to the transfer function and not get affected by a heavy load hanging from the ship side – not preferable for this study.

The rigid bodies in SIMA are globally following the same coordinate system, identified by XG. For each of the bodies, a local coordinate system is defined - XB. It is used to describe the coordinates of positioning elements and coupling elements. XR is the local coordinate system that follows the body's horizontal motion for floating vessels. The XY-plane is parallel to the calm water with the Z-axis pointing upwards, global zero at calm water level.

Simulation setting

Table 5.2: Environmental conditions analysed in this study.

EC	Hs[m]	Tp[s]	β[deg]	C_v[m/s]
1	0.5	6, 8, 10, 12, 14, 16, 17	0, 30	0.35
2	1.0	6, 8, 10, 12, 14, 16, 17	0, 30	0.35
3	1.5	6, 8, 10, 12, 14, 16, 17	0, 30	0.35
4	2.0	6, 8, 10, 12, 14, 16, 17	0, 30	0.35
5	2.5	6, 8, 10, 12, 14, 16, 17	0, 30	0.35
6	3	6, 8, 10, 12, 14, 16, 17	0, 30	0.35
7	4	6, 8, 10, 12, 14, 16, 17	0, 30	0.35
8	5	6, 8, 10, 12, 14, 16, 17	0, 30	0.35

The intent of different environmental conditions is to test the feasibility of the installation concept model. As this vessel is thought to operate in the North Sea, the "Norway 5" site was selected. Water depths on the selected site is between 100-200m, A water depth of 110m was assumed. Both the SSP and spar hydrodynamical coefficients are calculated based on deep water theory – the
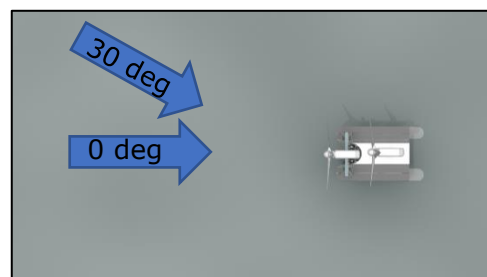
Figure 5.2: Environment headings.

SSP was initially modelled in 340m water depth and the spar 110m. **Table 5.2** presents the analysed env. conditions in this study, directions shown in **Figure 5.2**. The only deviation is uncoupled analyses in β=30, different wave heading applies for the coupled model. The different phases of the installation are interpreted in section *5.2 Installation proc*. EC stands for environmental condition, *Hs* stands for the significant wave height, *Tp* stands for the wave peak period, C_v stands for the current velocity. β is the wave heading, where alignment to the X-axis represents 0 degrees. Current and waves are collinear. Irregular waves were created using the Torsethaugen wave spectrum with a unidirectional spreading, 11 number of directions were considered. Only one simulation per condition was performed with random wave seeds. Wave seed is a random number where every seed number represents different phases for waves, wind and current. Random wave seed 1 was selected for every simulation. [22] [23] [3].

5.1.1 Static calculation

Before SIMA initialize the dynamic simulation in time domain, it calculates the static stability of the model. This reveals if the model is stable or not. If not, the dynamic calculation is terminated. But the user has the choice to skip right to the dynamic, a method to easily disclose wrong input with e.g. incorrect boundary

conditions and large body accelerations. The eigenvalues can by choice be calculated in the static calculation.

Eigenvalues

Eigen properties of the rigid body motions of the coupled system were calculated in the frequency domain, without interaction from the DP-system. The eigenvalues were obtained by solving equation (5.28) with 6DOF for both SSP and spar [3].

$$[-\omega^2(M + A) + C] \cdot X = 0 \qquad (5.28)$$

M   Mass matrix of the SSP, spar and OWT

A   Added mass matrix

C   Total restoring stiffness matrix

X   Eigenvector which represents rigid body motions, with 6 DOF for all three objects

The natural periods (T_n) and eigen vectors are presented in **Table 5.3** for the coupled model. The sensitive periods for the system are revealed in the calculated eigen vectors of the system – periods which needs to be prioritized when analyzing the system response in different environmental conditions. The spar has three nat. periods in pitch, the lower period is due to the SSP coupling and the two other wave periods are around 12s and 80s. The more interesting is the spar heave T_n which is around 17 seconds. The natural periods of the SSP in heave, roll and pitch is all below 9s, natural period in pitch is caused by the coupling stiffness. The SSP natural roll response is dominant at $T_n = 8.6$s which is the natural heave period for the SSP, pitch is also dominating at this period. Some modes have multiple natural periods which can be explained by the coupling effect.

Table 5.3: Eigenvectors of the rigid body motions of the coupled system. Natural periods (T_n) in top row with corresponding eigen vectors below.

Body	Mode	T_n	1.25	3.36	3.96	6.11	8.59	8.87	11.51	17.26	29.91	79.16	81.18	160.14
SSP	Surge	m	-0.08	0.04	-0.12	0.01	0.27	0.00	-0.76	0.00	0.00	0.00	0.00	0.00
SSP	Sway	m	-0.01	-0.61	-0.01	0.20	0.20	0.00	-0.11	0.00	0.00	-0.03	0.00	0.00
SSP	Heave	m	0.25	0.01	-0.02	-0.16	**-1.00**	0.00	-0.13	0.00	0.00	-0.01	0.00	0.00
SSP	Roll	deg	0.02	-0.10	0.00	**1.00**	-0.95	0.00	0.03	0.00	0.00	0.02	0.00	0.00
SSP	Pitch	deg	**1.00**	-0.15	0.00	0.07	0.85	0.00	0.11	0.00	0.00	0.01	0.00	0.00
SSP	Yaw	deg	0.16	**1.00**	-0.01	0.41	0.40	0.00	-0.12	0.00	0.00	-0.03	0.00	0.00
Spar	Surge	m	0.03	-0.14	**1.00**	0.00	0.05	0.00	**-1.00**	0.00	0.00	-0.08	0.00	0.00
Spar	Sway	m	0.00	0.00	0.00	0.00	0.00	0.00	0.00	0.00	0.66	0.00	0.66	**1.00**
Spar	Heave	m	0.00	0.00	0.00	0.00	0.00	0.00	0.00	**-1.00**	0.00	0.00	0.00	0.00
Spar	Roll	Deg	0.00	0.00	0.00	0.00	0.00	0.00	0.00	0.00	**-1.00**	0.00	**-1.00**	0.02
Spar	Pitch	deg	0.03	-0.14	0.99	0.00	0.06	0.00	**-1.00**	0.00	0.00	**-1.00**	0.00	0.00
Spar	Yaw	deg	0.00	0.01	-0.07	0.00	-0.01	**1.00**	-0.03	0.00	0.00	0.00	0.00	0.00

Motion characteristics

As mentioned, the SSP and spar hydrodynamic coefficients were imported into SIMA. These coefficients are calculated in the frequency domain using WAMIT and HydroD and are transferred into time domain using retardation functions.

It is of great interest to look at the motion characteristics of the coupled system. As the coupling elements change the characteristics of each object, it may reach a less favourable frequency range. The natural periods of the coupled system reveal the wave periods which should be avoided and tested. According to scatter diagram presented in appendix A (**Table A.0.1**) the rigid-body system natural frequencies corresponds to the most probable wave period of 8-12s in the North Sea. A irregular sea state consists of multiple wave peak periods and the natural periods does not have to be directly linked to the result for each respective wave period, commented in chapter 6.

Below are the important response parameters listed for the two floating bodies; SSP and spar. These are responses which will be analyzed and commented in the *Result and discussion* chapter.

Table 5.4: Selected response parameters to analyze. Important = I, Not important = NI

Response	Object	H_s	T_p	β
Surge motion	SSP	I	NI	I
	Spar	I	NI	I
Pitch motion	SSP	I	I	I
	Spar	I	I	I
Heave motion	SSP	I	I	NI
	Spar	I	I	NI
Relative motion	Docking cone	I	I	I
Force	Top grippers	I	I	I
	DX1/2 & DY1/2	I	I	I
	Mooring lines	I	NI	I

5.2 Installation procedure

The proposed installation procedure can be divided into three phases: Initial hanging position, lowered position and OWT released. These three phases are considered in the motion response analyses. Simulation parameters and specifications for each of the phases is presented in the sub-sections below.

5.2.1 Phase 1: Initial hanging position

Figure 5.3: OWT hanging in initial position.

In phase 1 is the OWT hanging 5m (15m above m. water level) centred over the spar, dampers between SSP and spar is connected and activated. It is hanging in the four lifting wires, controlled by four heave compensated winches. Phase 1 is simulated in the environmental conditions presented in **Table 5.2**, also the damper analyses and heave controller parametrization are done in this phase.

5.2.2 Phase 2: Lowered position

In phase 2 the OWT is lowered 3.5m, but not connected to the spar. This means that there is a small gap between the OWT and spar, see **Figure 5.4**. As mentioned, the contact forces in the docking cone are important to address. Environmental conditions simulated when OWT is in lowered position is listed in **Table 5.5**. Only Hs < 2m is considered for these analyses.

Table 5.5: Environmental conditions simulated to analyze the docking cone contact forces when lowered.

EC	Hs[m]	Tp[s]	β[deg]	C_v[m/s]
1	0.5	6, 8, 10, 12, 14, 16, 17	0	0.35
2	1.0	6, 8, 10, 12, 14, 16, 17	0	0.35
3	1.5	6, 8, 10, 12, 14, 16, 17	0	0.35
4	2.0	6, 8, 10, 12, 14, 16, 17	0	0.35
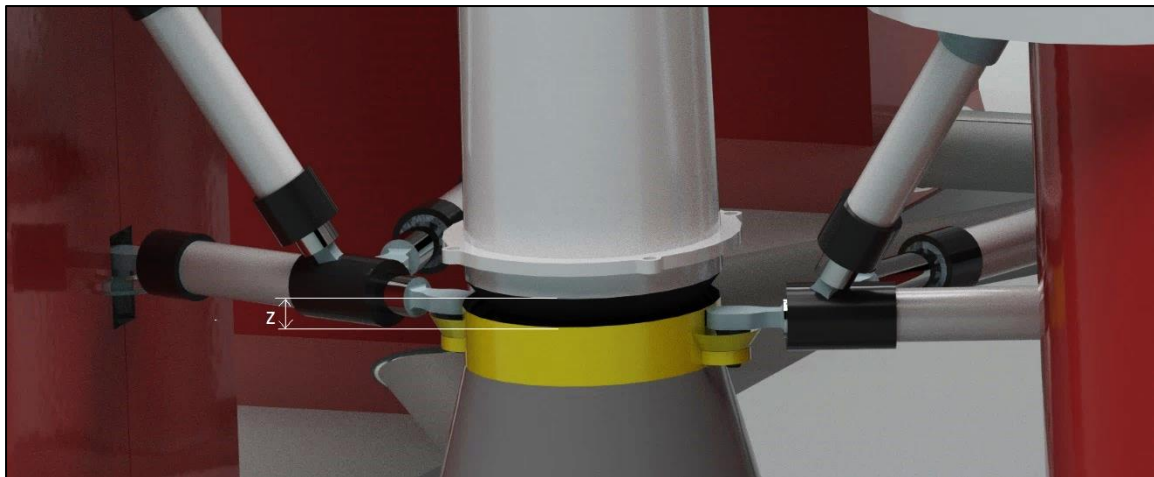
Figure 5.4: OWT in lowered position. Docking cone forces need to be addressed. Z = 0.5m.

5.2.3 Phase 3: OWT released

Figure 5.5: OWT is released from the installation vessel and attached to the spar.

OWT is in phase 3 mated and attached to the spar, presented visually in **Figure 5.5**. All the load is transferred to the spar buoy. According to SSP hydrostatics this means that the vessel will encounter large trim angle. More details and results from the static calculation in section 6.6. The intention is to automatically mate and lock the OWT firmly without direct human interaction.

6 Results and discussion

"Standard deviation is a number used to tell how measurements for a group are spread out from the average (mean), expected value. A low standard deviation means that most of the numbers are close to the average. A high standard deviation means that the numbers are more spread out." [24].

If nothing else is specified, standard deviation is the basis for all results presented in this chapter. Longer simulation time is needed to perform peak response analyses, but a "most probable maximum" can be found from the STD of a stochastic process as expressed below in equation (6.29). Where X_m is the max value, σ the STD and N the number of amplitudes over the time in question. Number of amplitudes (N) are assumed as simulation time divided by Tp, normally calculated based on the wave spectrum. Worth mentioning is that there exist multiple methods to estimate max values, but this simple estimation is considered sufficient. It is important to be aware that the max peak value could be four times the STD(σ) as relations below express:

$$H_S = 2\zeta_a, \qquad \sigma = \frac{\zeta}{2}, \qquad \zeta_{max} = 4\sigma$$

$$X_m = \sigma \cdot \sqrt{2\ln N} \tag{6.29}$$

For results where total force is plotted; it is defined as the resultant force of all three directions (X, Y, Z). For dampers DX and DY the standard deviation is noted, and for the top bumpers RMS (σ+mean) value is noted. Mean values of the forces in the top bumpers are highly relevant as the mean constitutes a large part of the total force. Reference error implies relative distance between reference point on top spar and bottom OWT. $\beta = 0$ if nothing else is specified in the plots. Tables with detailed values in appendix are referred to in each plot. Empirical "Most probable maximum" is calculated for the most relevant results – presented in *6.5 Most probable maximum*. No limiting values are considered, except radial outcrossing frequency, as the limits are usually based on client demands. Evaluations on what is considered as the limiting factor is included though.

6.1 Heave compensator

6.1.1 Controller parametrization

Tuned parameters for PD + FF and PID is presented in **Table 6.1** and **Table 6.2**, respectively. One environmental condition was considered when tuning the parameters; Hs = 3m, Tp = 12s. The control parameters were tuned one at a time, in chronological order as presented. Initial start value was set as provided for the temporary fixed parameters, and the variable parameter was tuned until the

smallest vertical reference error was achieved. All parameters tested in the controller is presented in appendix B (**Table B.0.2** to **Table B.0.11**) with relating vertical reference error. Parameters presented in **Table 6.1** is further used in the study – PD + FF gave the best result of the two controllers. It is a possibility that the PID could be a better choice with more in depth tuning, but after evaluation, it was decided that the PD + FF controller provided acceptable results for this study. Time history of the OWT and spar heave motion is presented in **Figure 6.1** – visual confirmation of the heave compensator. Results with and without the heave compensator in sub-section *6.1.2*.

Table 6.1: Result parameter tuning PD + FF.

Tf	0,95
Kf	2,3
Kp	8,5
Td	1,12
Tfd	1,1

Table 6.2: Result parameter tuning PID.

Kp	0,414
Kd	1
Ki	0,38
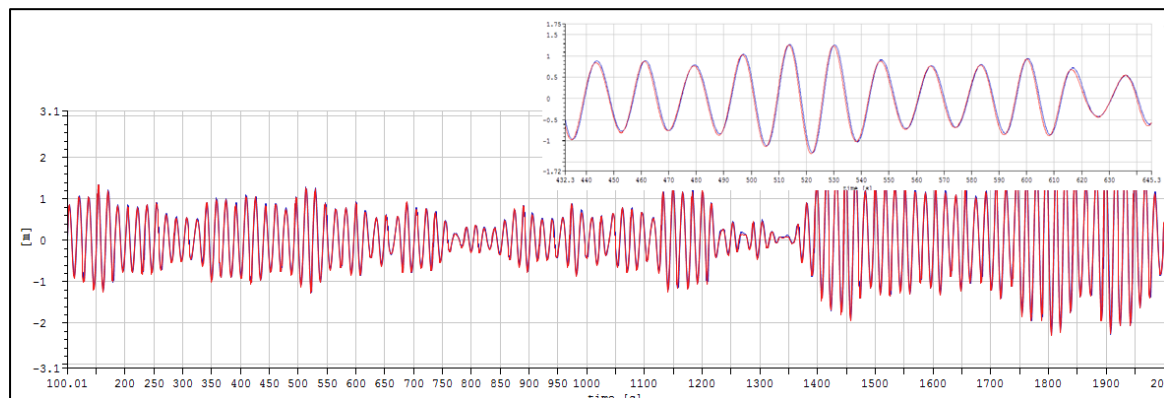
Figure 6.1: Time history of heave motion response of OWT(red line) and spar(blue line) with PD + FF controller. Hs = 3m, Tp = 12s.

6.1.2 Heave motion analyses
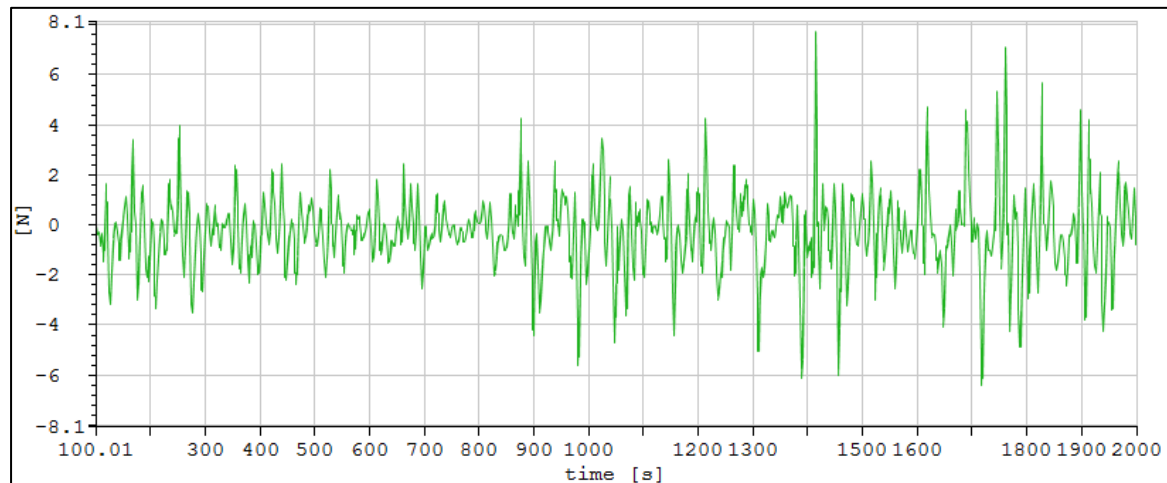
Figure 6.2: Time history of the vertical relative motion response between OWT and spar at mating point without couplings. Hs = 3.0m, Tp = 12.0s, β = 0 deg. STD: **1,482m.**

Without heave compensator the time history, see **Figure 6.2**, reveals large peaks of up to 8-9 meters, which is unacceptable when lowering the OWT. **Figure 6.3** presents vertical reference error at mating point in regard of wave peak period (Tp). The vertical reference error increases steadily with longer wave periods as expected.
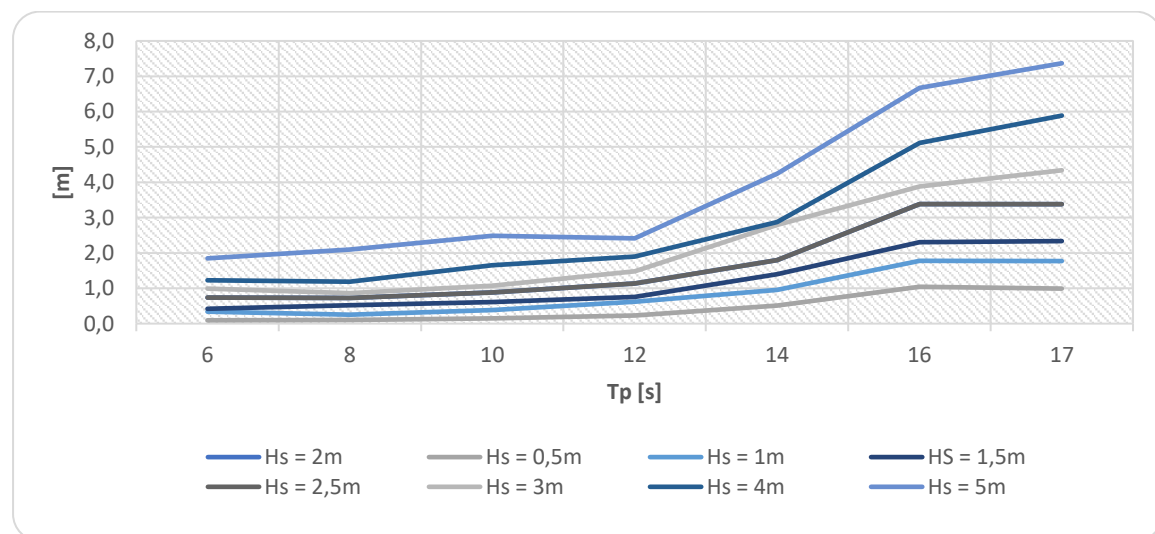
Figure 6.3: Standard deviation: Vertical reference error without couplings. (**Table B.0.21** in appendix B)
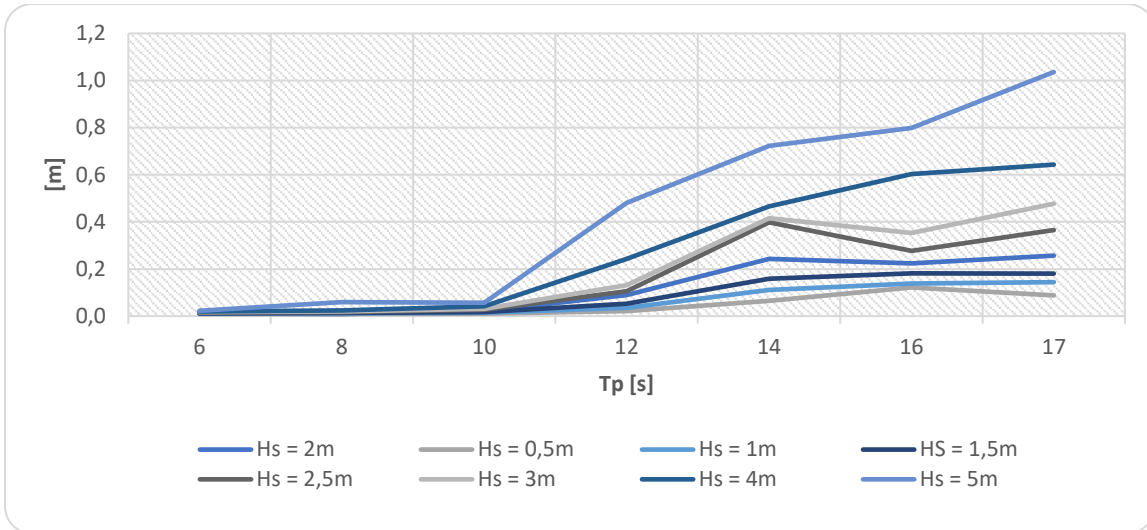
Figure 6.4: Standard deviation: Vertical reference error with couplings. (**Table B.0.20** in appendix B)

When heave compensator and horizontal dampers (DX/DY) are activated the vertical reference error is decreased significantly. At Tp =12s and Hs = 1,5m an improvement of ~1500% from 78cm to 5,3cm STD can be observed. Presented plots shows consistency, result is considered as valid. The immediate increase in reference error at Tp = 12s is due to the spar heave motion, the heave compensator is struggling to maintain constant distance. As expected the highest measured value is present at Tp = 17s; spar natural frequency in heave.

6.2 Phase 1: Initial hanging position

6.2.1 SSP and Spar total motion
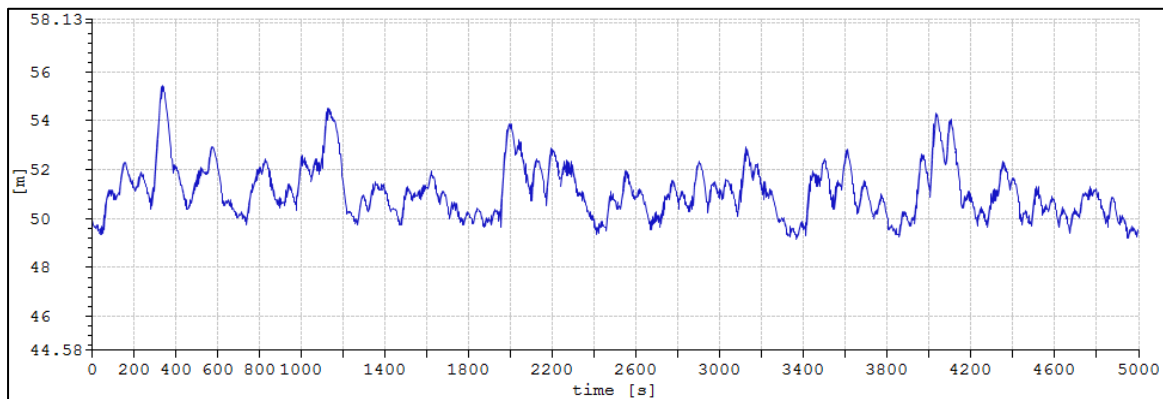
Figure 6.5: Time history of the SSP surge motion without couplings. Simulation time = 5000s, Hs = 2m, Tp = 8s. Acc. to global coordinates.

The intention with the time history presented above in **Figure 6.5** is to reveal or debunk the transient trend in the simulation. A small second order motion can be observed, which is connected to the different wave elevation phases. It seems that the solver is stable at an early stage of the simulation. This confirms that standard deviation results in simulation period 100-2000s is representative for the floating body responses.

Below in **Figure 6.6** and **Figure 6.7** are the SSP total motion without couplings presented. **Figure 6.8** and **Figure 6.9** presents the spar motion. Specifications are equivalent as presented for phase 1; β = 0 applies to all. The point of interest is to compare the result with and without couplings interacting total motion response. How does the couplings, especially the dampers, affect the total vessel and spar motion. Detailed result values can be inspected in appendix B, relating table is specified in each caption. Heave analyses result can be inspected in appendix B; **Figure B.0.7** and **Figure B.0.8** present the total motion coupled, and **Figure B.0.5** and **Figure B.0.6** presents the uncoupled heave responses. By comparing uncoupled and coupled the impact of the dampers (DX/DY) can be addressed. A spar heave motion decrease of around ~25% can be observed, and a slight increase in SSP heave motion.
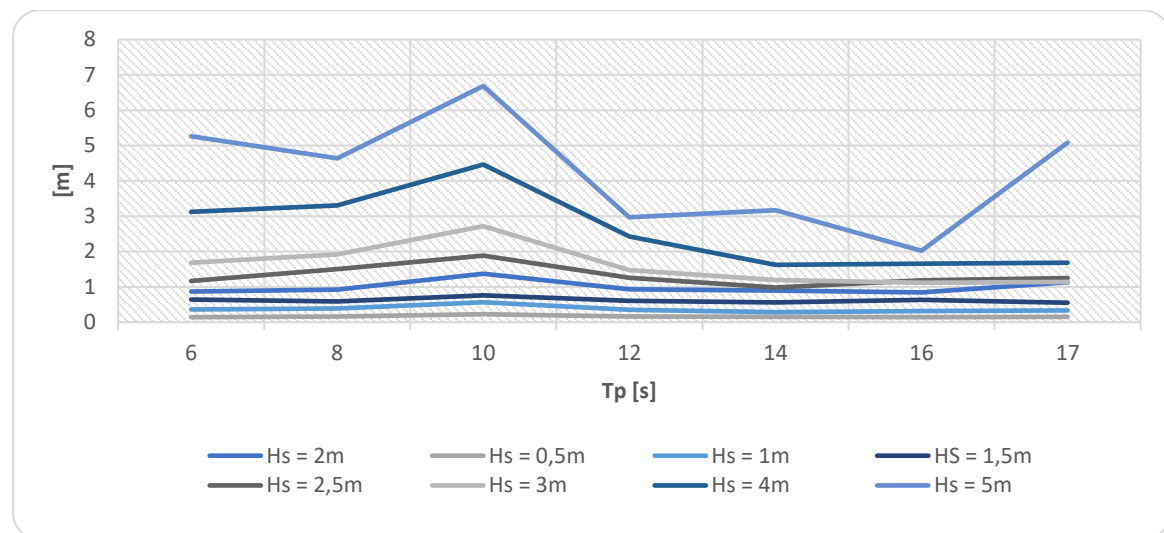
Figure 6.6: Standard deviation: SSP total motion in global X-direction without couplings (surge). (**Table B.0.12** in appendix B)
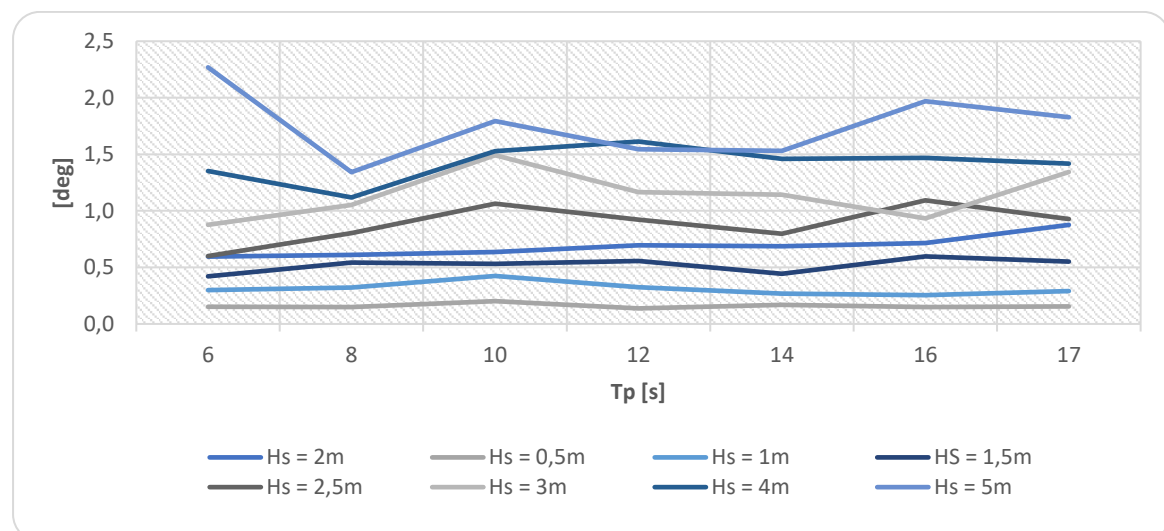
Figure 6.7: Standard deviation: SSP total motion rotation Y-axis without couplings (pitch). (**Table B.0.13** in appendix B)
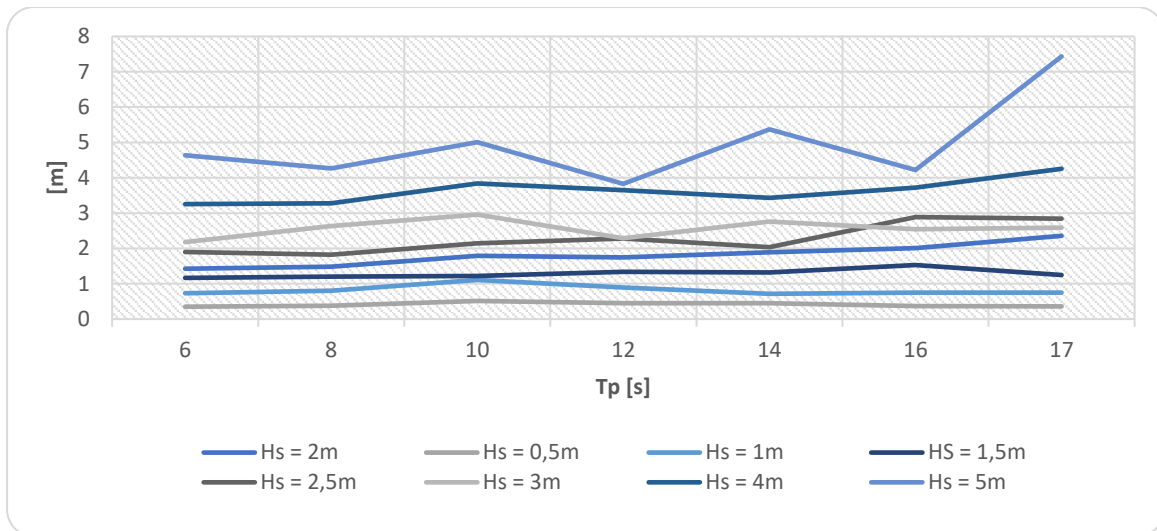
Figure 6.8: Standard deviation: Spar total motion in global X direction without couplings (surge). (**Table B.0.14** in appendix B)
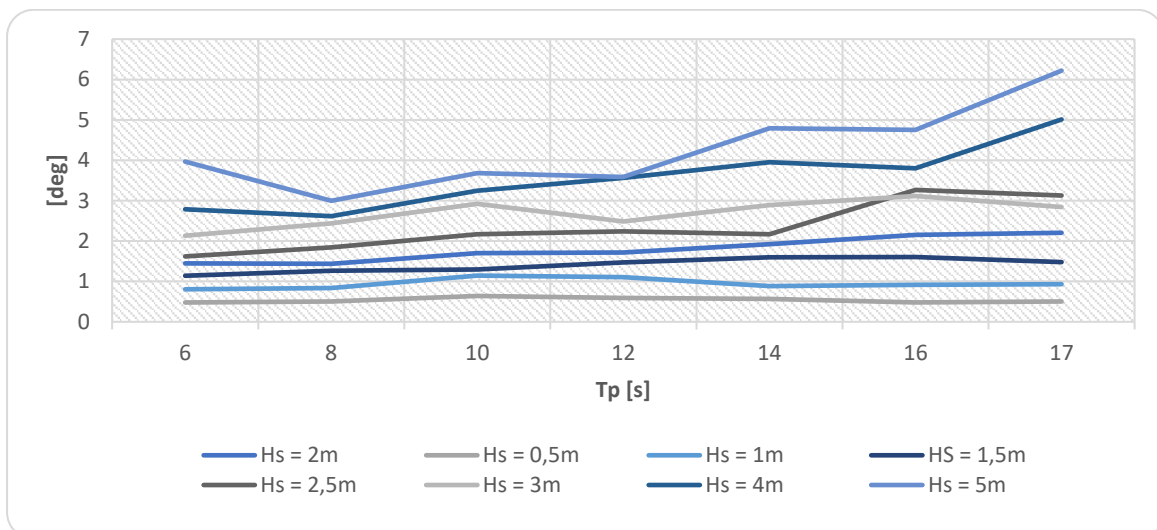
Figure 6.9: Standard deviation: Spar total motion rotation Y-axis without couplings(pitch). (**Table B.0.15** in appendix B)

Results presented in the figures below are the total motion response with couplings activated. Total motion for SSP and spar in surge is presented in **Figure 6.10** and **Figure 6.12**, respectively. **Figure 6.11** and **Figure 6.13** presents the pitch motion for each respective object.
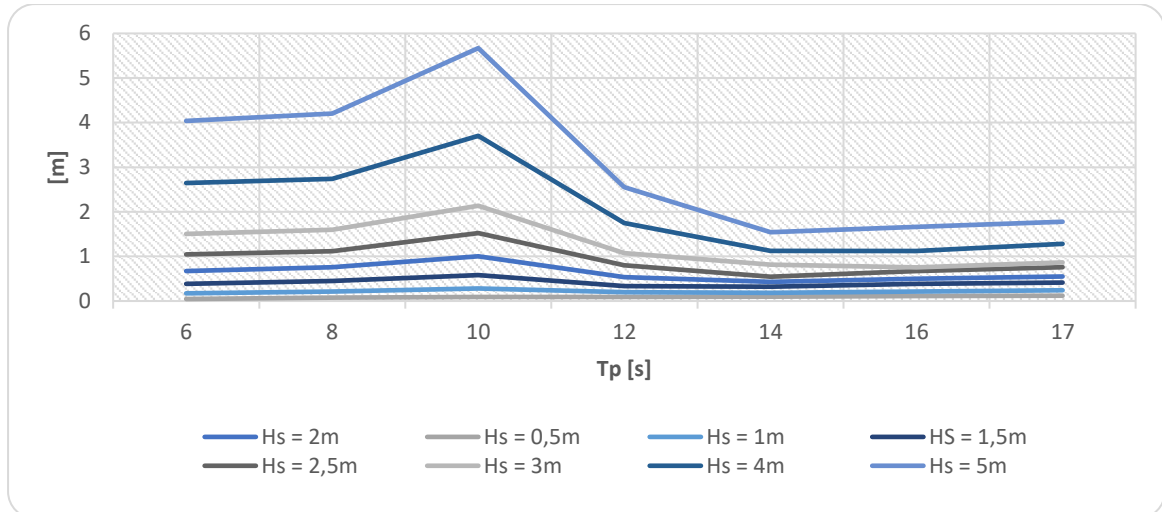
Figure 6.10: Standard deviation: SSP total motion in global X-direction with couplings (surge). (**Table B.0.16** in appendix B)
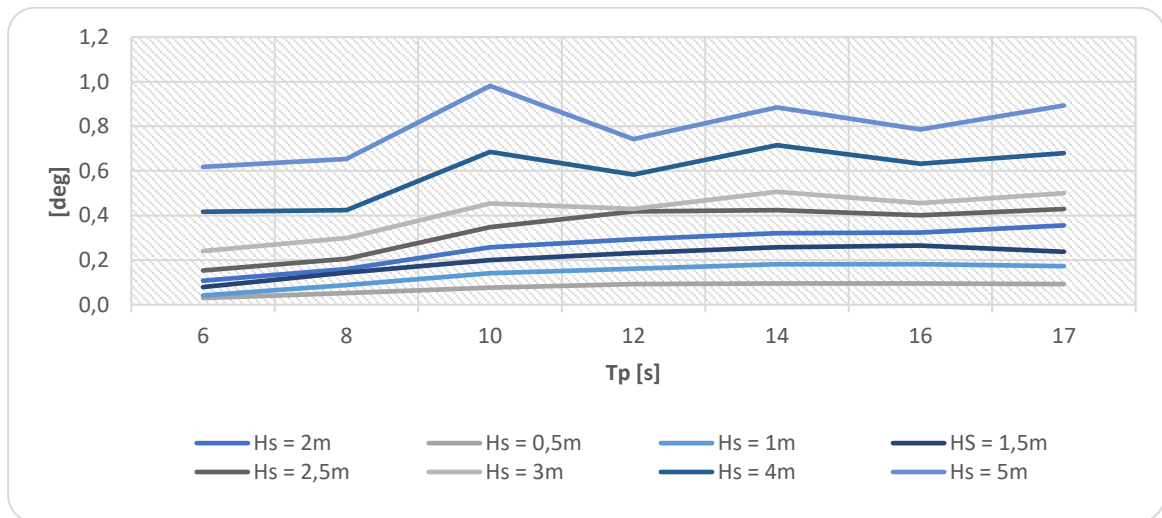
Figure 6.11: Standard deviation: SSP total motion rotation Y-axis with couplings (pitch). (**Table B.0.17** in appendix B)
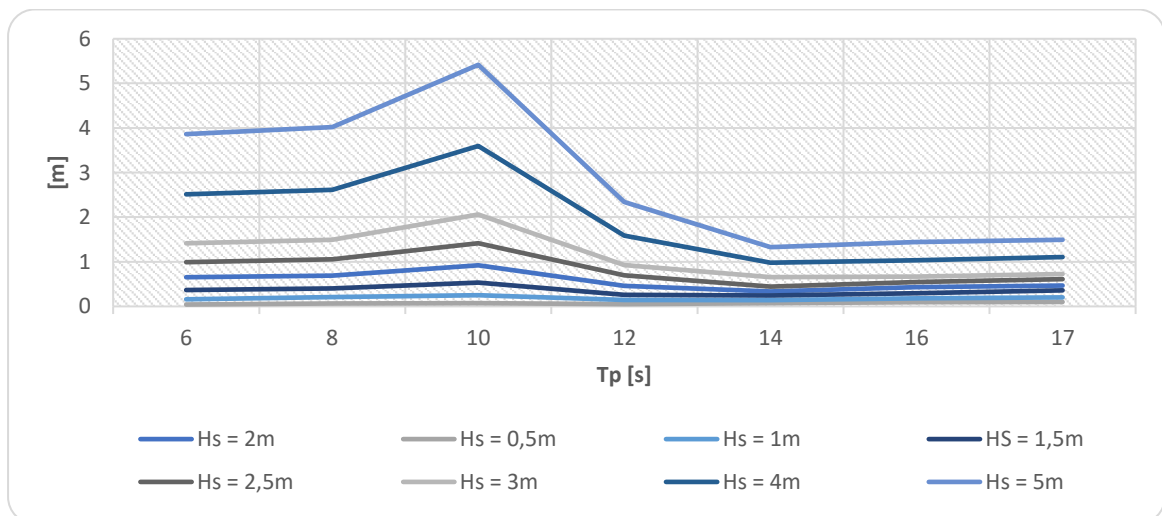
Figure 6.12: Standard deviation: Spar total motion in global X-direction with couplings (surge). (**Table B.0.18** in appendix B)
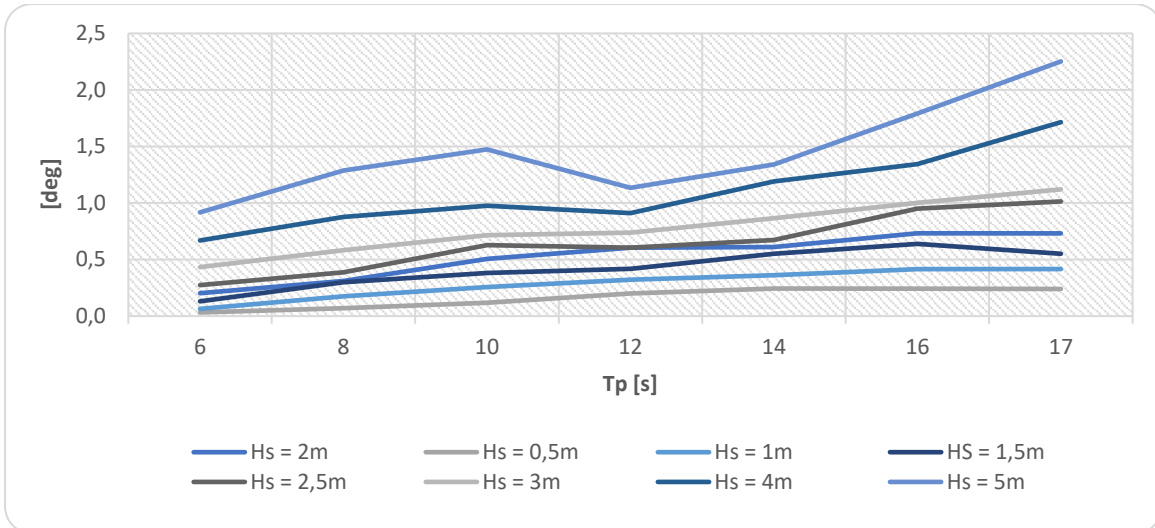
Figure 6.13: Standard deviation: Spar total motion rotation Y-axis with couplings (pitch). (**Table B.0.19** in appendix B)

The most responsive period for both SSP and spar is Tp = 10s with and without couplings. The couplings reduce the effect of the wave forces on both the SSP and spar, but the most sensitive period of 10s is unchanged. DX and DY reduce the total motion response of both object as well as significantly reducing the relative motion in hor. plane at reference point. Only surge motion responses are considered as the considered environmental direction was β = 0. The SSP surge motion response was expected to peak at a higher Tp, but it seems that the OWT mass hanging in initial position decrease the natural period of the SSP in surge. The transfer functions are presented in appendix A (**Figure A.0.1** to **Figure A.0.4**) and represents the SSP motion and spar wave force which express individually the most sensitive wave period. Also in pitch the dampers reduced the response for both SSP and spar, the total motion is reduced by 50% on average. The all over summary of improvement with couplings is that the surge motion is largely more synchronized, and the pitch motion response is significantly reduced especially for the spar.

6.2.2 Relative radial distance at reference point
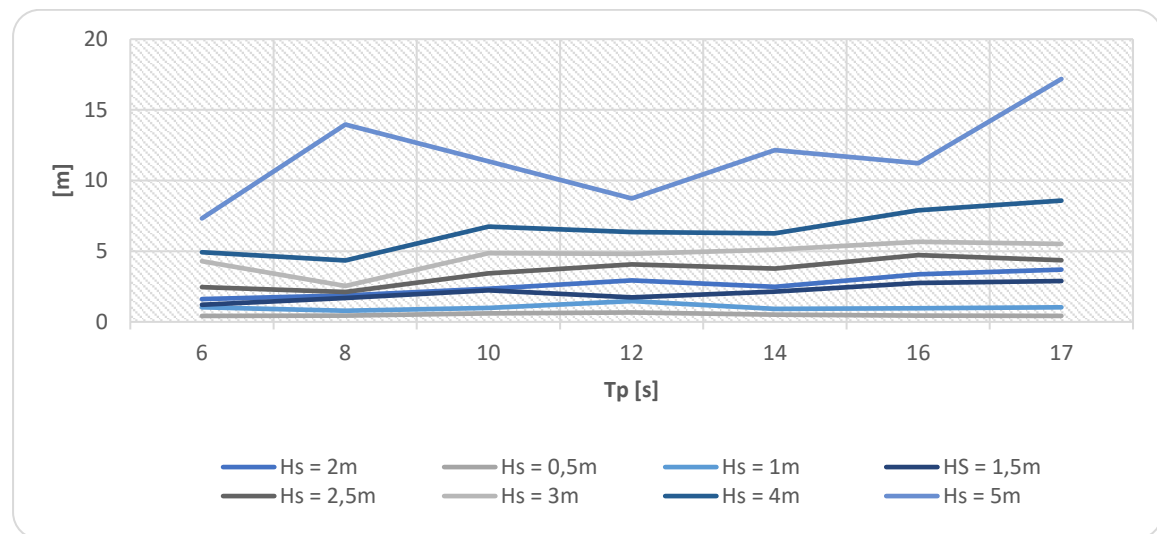
Figure 6.14: Standard deviation: Radial reference error, radius n. Without couplings. (**Table B.0.22** in appendix B)
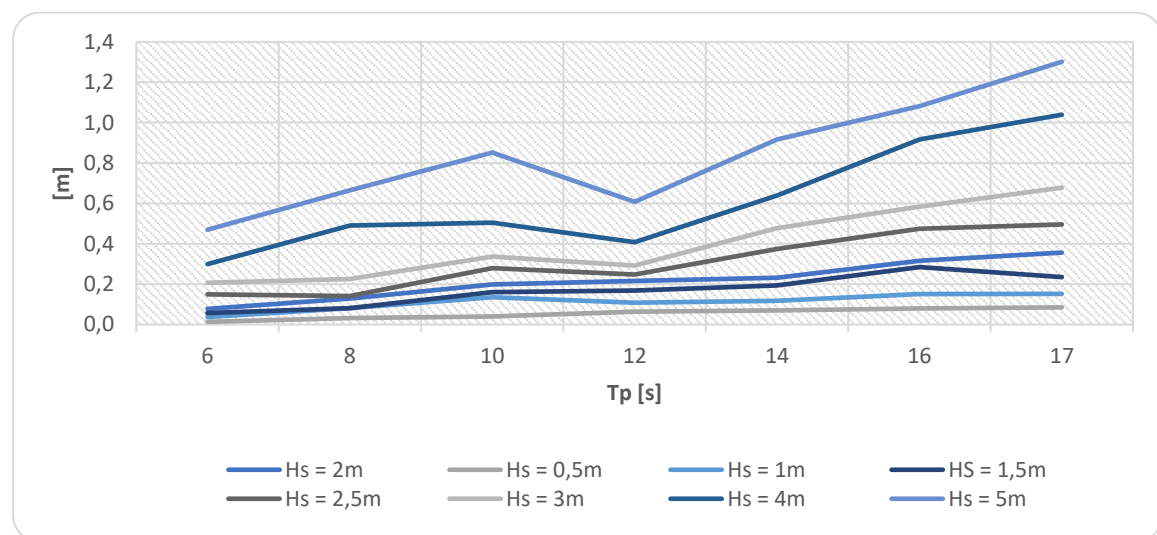
Figure 6.15: Standard deviation: Radial reference error, radius n. With couplings. (**Table B.0.23** in appendix B)

As claimed; surge motion response for SSP and spar is significantly more synchronized when couplings are activated. This means that the relative radial distance between OWT and spar is reduced. Improvement can be analyzed in **Figure 6.14** and **Figure 6.15**, where first figure presents the radial reference error (n) without couplings and second figure equally with couplings. Results from condition Hs = 1,5m and Tp = 12s presents an improvement from 0,76m to 0,17m or 450% decrease in STD. Most of the radial reference error is induced by spar pitch and SSP positioning system struggling to maintain position, especially when the wave forces increase at periods above 12s. The SSP positioning system is counteracting for the low frequent wave forces and DX/DY reduce the low frequent motions – the reason why the ref. error increases steadily at longer wave periods. As observed in **Figure 6.9** spar pitch is significant already at Hs = 1m. Only one

degree spar pitch equals ~0,6m displacement at mating point, if point of rotation is assumed in spar vertical centre.

Below in **Table 6.3** are the actual outcrossing rate for each environmental condition presented, red values indicate above limit. Results are based on one simulation per condition with wave seed 1. The R_{sb} are possibly assumed too large, but is considered feasible with assistance from the docking cone when finalizing the mating. These limitations are usually based on engineering experience from the industry. Note that below Hs = 1m, zero outcrossings can be observed.

Table 6.3: Outcrossing frequency. [Hz]*e-03.

Hs\Tp	8	10	12	14
0,5	0	0	0	0
1	0	0	0	0
1,5	0	0,53	0,53	0,53
2	0,53	4,21	6,84	6,84

6.2.3 Top bumpers
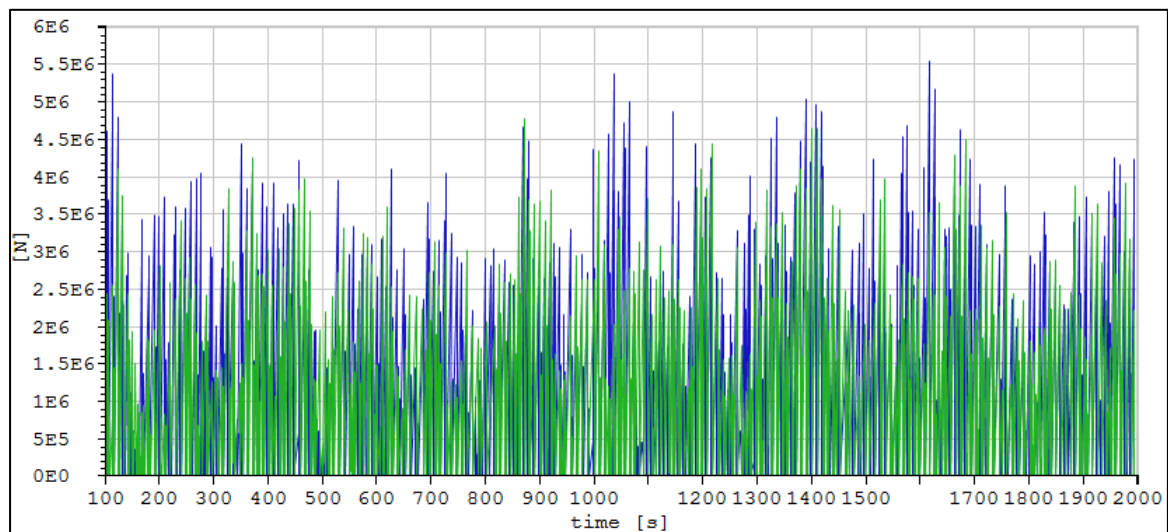
Figure 6.16: Time history of total force in top bumpers. Tp = 10s, Hs = 3m. Black and green line represents global Y-direction and blue and red represents X-direction.

Forces in top bumpers are primarily affected by the wave peak period and the rigid-body system natural frequencies. The force time history is dominated by peak forces, see **Figure 6.16**. This is due to the OWT swaying around dependent on the SSP motion response. This is arguably a common and realistic occurrence of forces in dynamic configurations like this. For the majority of the analyses the OWT is leaning slightly against one of the bumper elements – because of the 5 cm gap between the bumper elements. The bumper elements are modelled to obtain numerical stability, as the only function is to keep the OWT vertical. The RMS result presented is considered to provide an estimate of the forces in the top sliding arms.
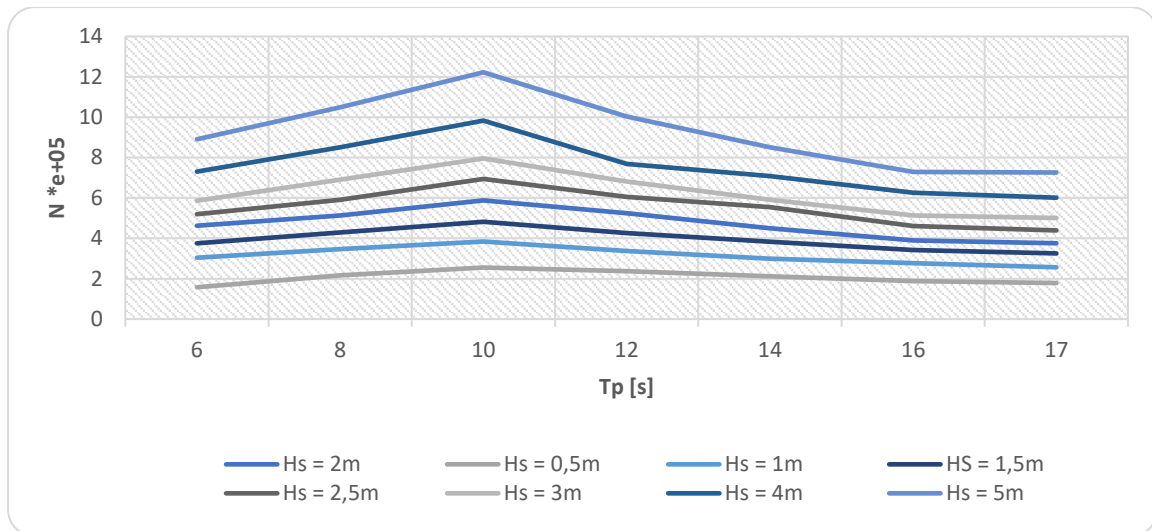
Figure 6.17: RMS: Total force top bumper element in global X-direction with couplings. (**Table B.0.29**)

Below in **Figure 6.18** are the total forces in Y-direction plotted, above **Figure 6.17** presents the total forces in X-direction. The largest forces in the top bumpers are present at Tp=10s - clearly relates to the SSP surge and pitch response. The environmental heading is also important when addressing the forces, as the OWT is swinging in regard of the SSP total motion. Forces in global X-direction is dominating in $\beta = 0$ because of the SSP pitch motion. Forces in global Y-direction can almost be neglected as they are not of any affecting magnitude at $\beta = 0$, but at $\beta = 30$ the forces are more dominant - see section *6.4*.
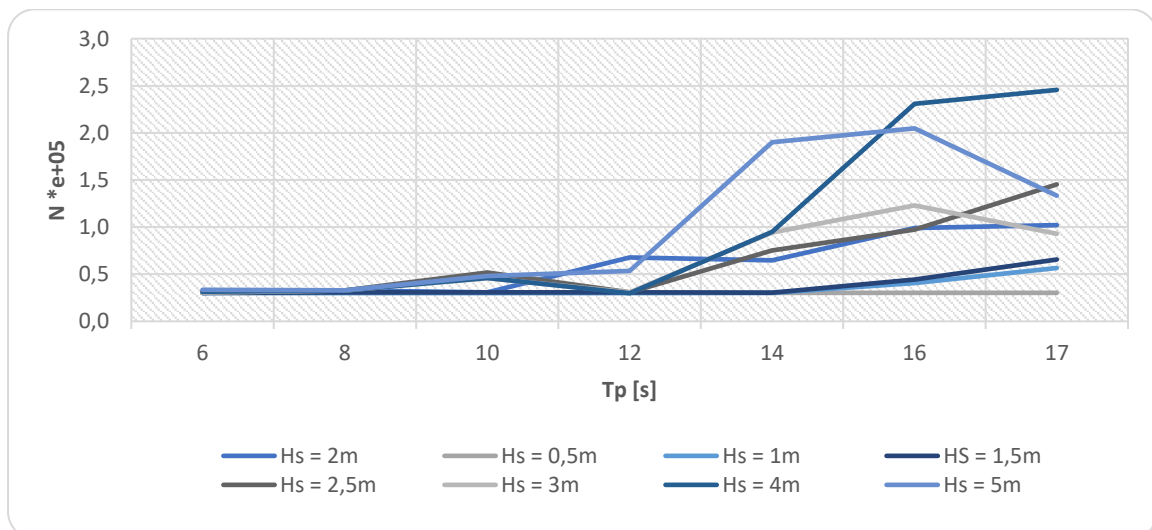
Figure 6.18: RMS: Total force top bumper element in global Y-direction with couplings. (**Table B.0.30**)

The proposed gripper arms will probably be more resistant towards forces in global Y-direction as the forces in X-direction would cause the lifting wagons to rotate. The correlation to reality of the calculated forces in top bumpers are assumed as a rough estimate.

6.2.4 Passive horizontal spar dampers

A simple horizontal damper (DX/DY) sensitivity analyses was conducted to find the compromise between total damper force and radial reference error. For damper results, STD estimates are valid as the mean is equal to zero. The procedure went as follows; Damping coefficient for all four damping elements were increased by $*10^1$ each step, radial ref. error and max total damper force was noted. Max total force is defined by resultant force from the largest force measured in X and Y damper. Total force magnitude is defined as the resultant of the total DX force and total DY force – total force acting on spar. Specific result from each condition is presented in Appendix B, where each of the plots represents one environmental condition (**Figure B.0.11** to **Figure B.0.19**). **Figure 6.19** presents the average values of Tp for each respective Hs - only valid for trend analyses or sensitivity analyses. As observed in the plot damping coefficient 1,0E+06 and 1,0E+07 is the most interesting. Total force in the damper elements increases rapidly when coefficient is increased to 1,0E+08, the system is entering the overdamped response phase. Underdamping when coefficient is below 1,0E+06. Damping coefficient 1,0E+07 were considered in this study when horizontal dampers are activated (coupled state). Max standard deviation force in elements is 7,3 N *e+05 (~73 tons) at Hs = 3m. According to equation (6.29) the estimated peak force equals ~232 tons. If a safety factor of 1,5 is considered the design load would be 348 tons.

For comparability to LIH's study a 2000s simulation run with regular waves with amplitude 1m and Tp = 6,66s was completed. Time history is presented in appendix B (**Figure B.0.20** and **Figure B.0.21**). From results a calculated magnitude force of 13,4e+05N acting on spar, around ~134tons. Max total force in damper pair is calculated to 6,7e+05N (67 tons).
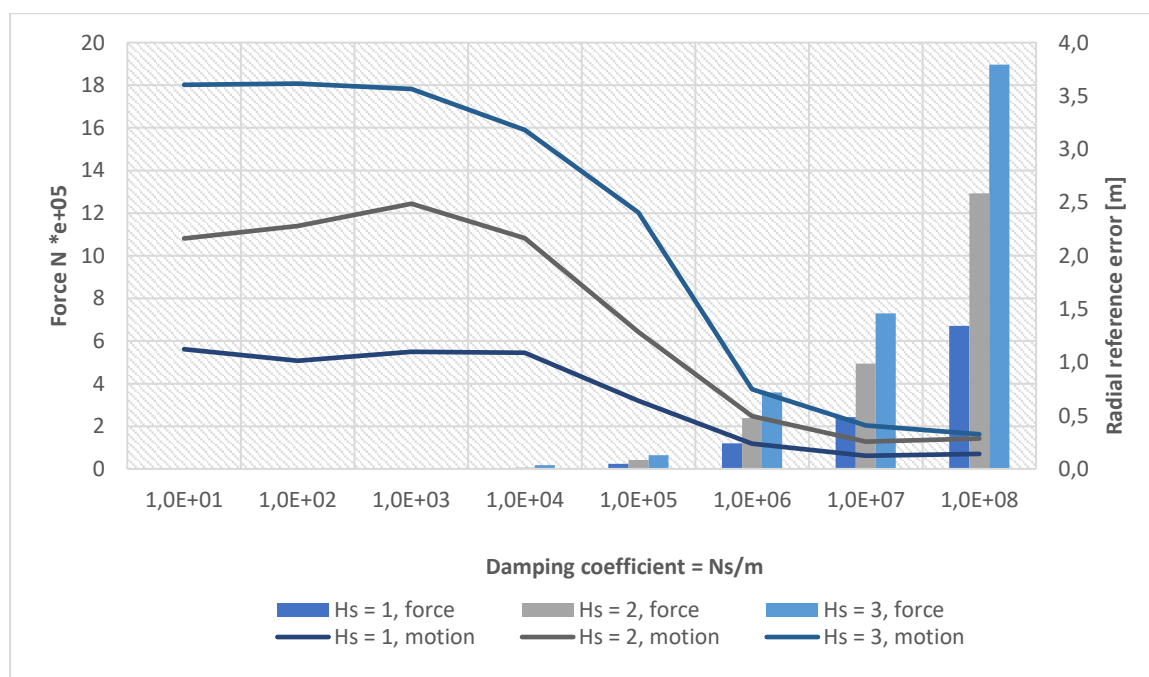
Figure 6.19: Standard deviation: Statistics of the max total force in damper elements and radial reference error in regard of damping coefficient. (**Table B.0.34** in appendix B)
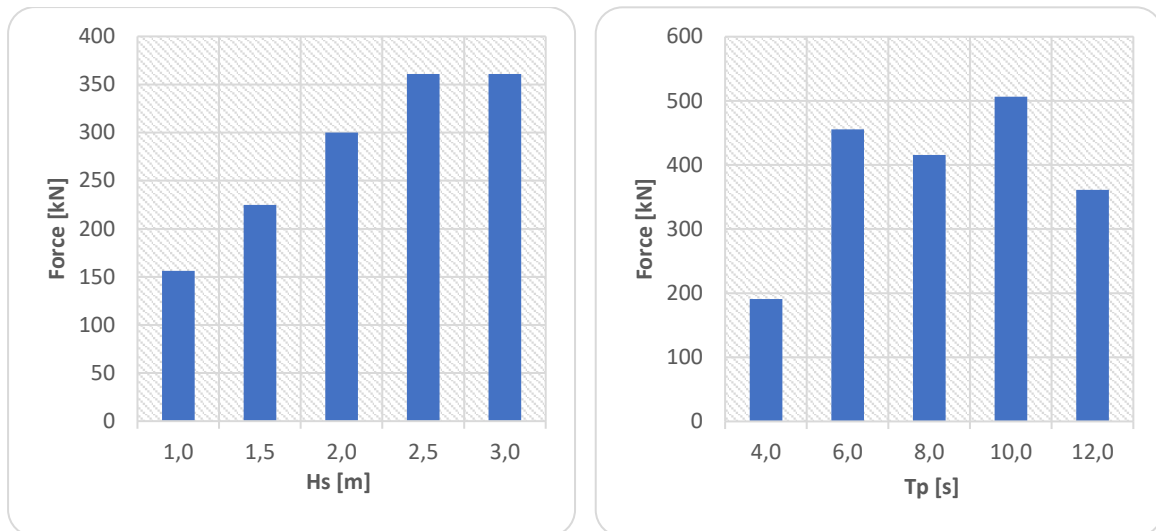
Figure 6.20: Standard deviation: Total force in damper. Left: Tp = 12s, β = 0. Right: Hs = 2,5m, β = 0.

Figure 6.20 presents the total force in the damper pair, which means the force resultant for X and Y damper component. Related estimation of probable max force is presented in **Figure 6.33**. Z. Jiang's got in his study ~1000kN gripper force and ~0,4m relative surge at ref. point in Hs = 2m, Tp = 12s, β =0 [3]. Comparable result extracted from this study; 300kN total damper force and 0,22m relative surge.

6.2.5 Lifting wires
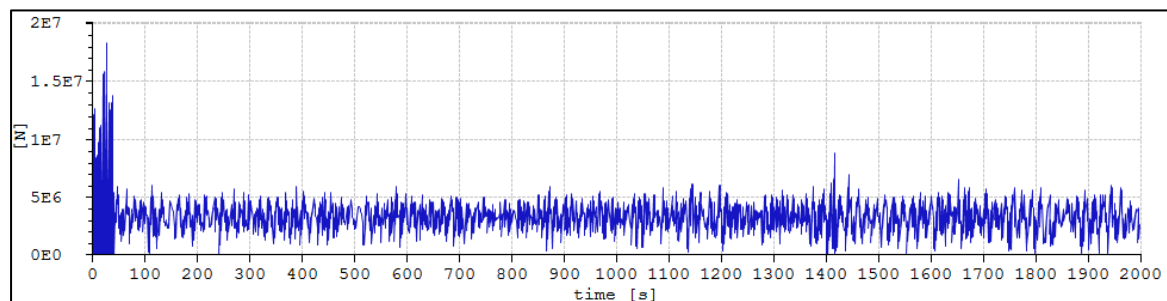
Figure 6.21: Time history of the total force in one of the lifting wires. Hs = 4m, Tp = 12s. STD = 1,07e+06N/mean = 3,24e+06N.

Above in **Figure 6.21** are the total force in one of the lifting wires presented, representative for all four wires. Large peak forces dominate in the first 50 seconds of the simulation, can be explained by the AHC settling. The numerical models need some time to stabilize. Generally, a pulsating force in the wire is to be expected because of dynamics. An estimate of the wire dimensions is earlier presented just for realization.

6.2.6 Mooring lines
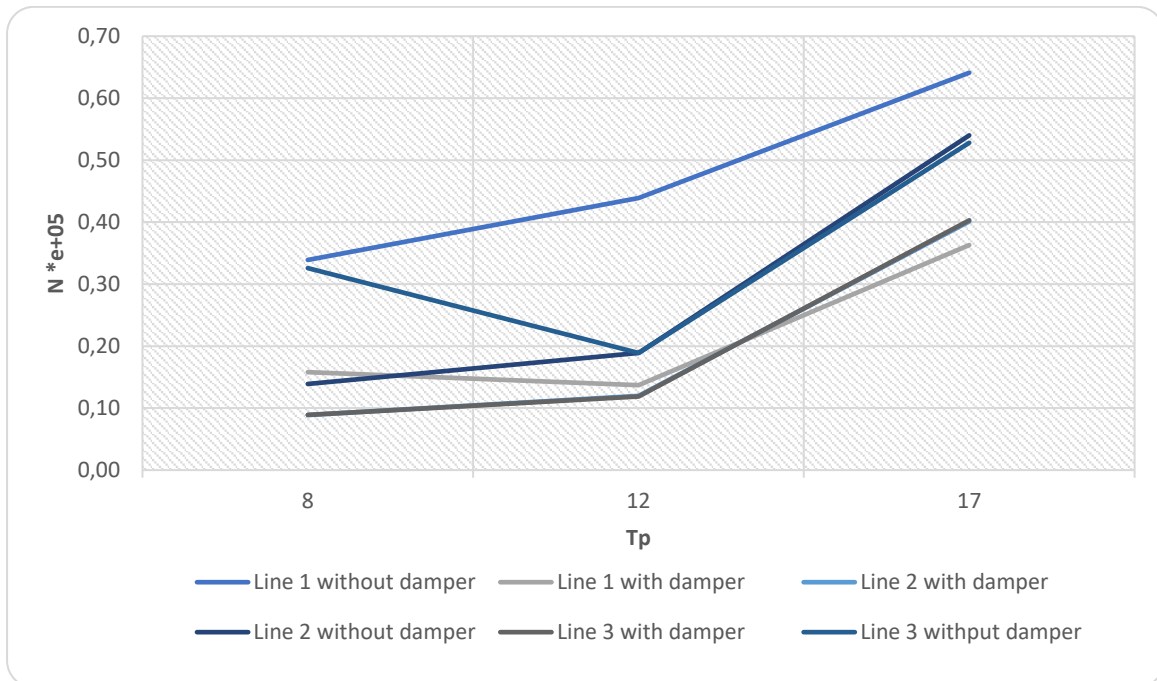
Figure 6.22: Standard deviation: Total forces in mooring lines. Comparison between with and without couplings.

As **Figure 6.22** presents total mooring line force it reveals that the forces are reduced when couplings are activated. This can be explained by restoring forces by the SSP positioning system, since the control system corrects in regard of a globally fixed point. Throughout the study it was experienced that globally fixed point for the SSP control system provided less relative motion between the floating objects. One positive bi-effect is reduction in forces on the mooring line system.

6.2.7 OWT pitching
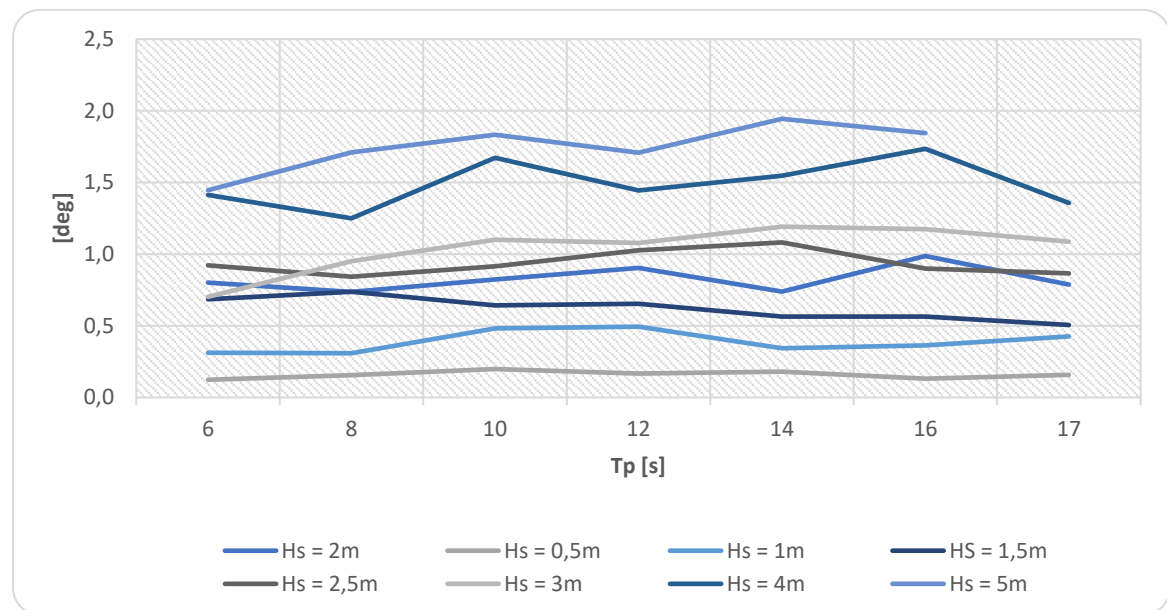
Figure 6.23: Standard deviation: OWT rotation about Y-axis. Without couplings. (**Table B.0.24** in appendix B).
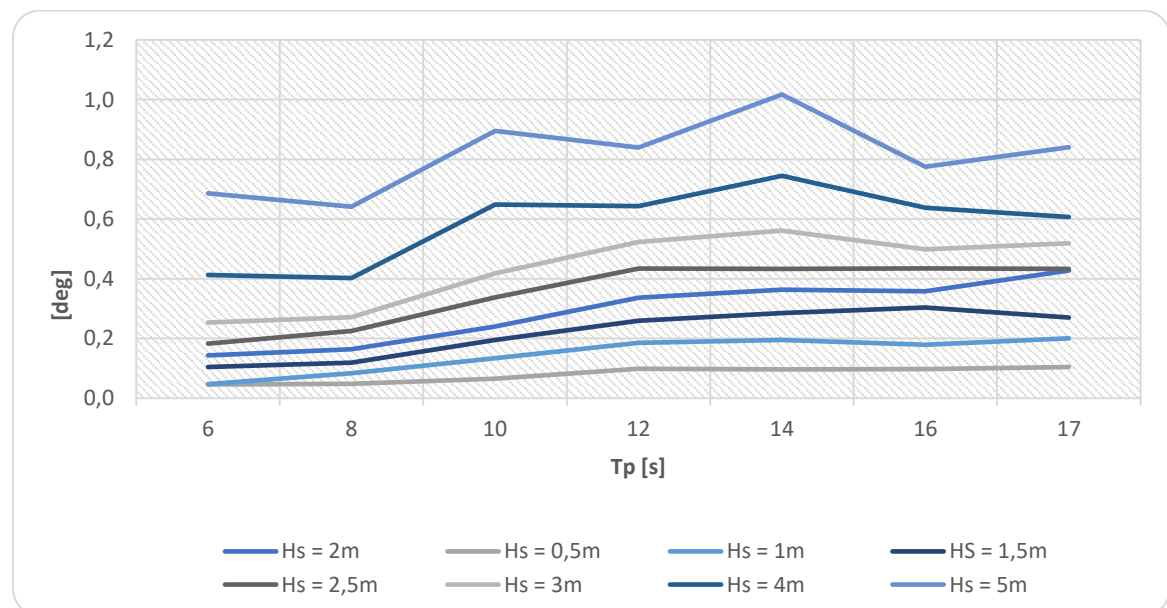
Figure 6.24: Standard deviation: OWT rotation about Y-axis. With couplings. (**Table B.0.25** in appendix B).

One of the crucial parts of the mating phase is the OWT angle or tilting angle. Only rotation about Y-axis (pitch) is considered in this study. As observed in **Figure 6.23** and **Figure 6.24** the average tilting angle is reduced when couplings are activated. This can be explained by increased stiffness between SSP and spar induced by DX and DY - the dampers counteracts the SSP and spar relative vertical motion. This means especially reduced pitching for SSP, can be observed in **Figure 6.11**. The dampers act as a counteracting momentum arm or force to reduce OWT pitching.

6.3 Phase 2: Lowered position

6.3.1 Docking cone forces
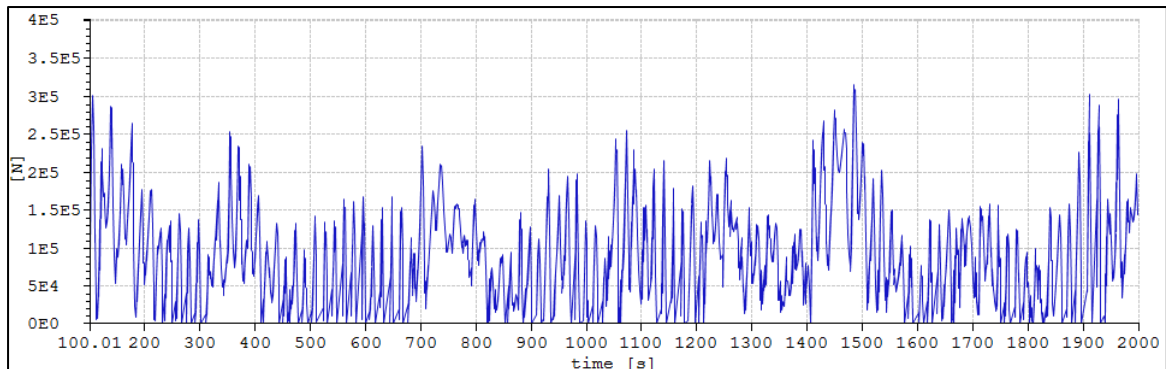
Figure 6.25: Time history of the total force in docking pin. Hs = 2m, Tp = 17s, β = 0 deg. (STD ~92kN).

Environmental conditions presented in **Table 5.5** was simulated and standard deviation of total forces in docking pin was noted. As mentioned, in lowered position is the OWT and spar initially not in contact but contact forces will occur when the OWT starts moving relatively to spar. Peak forces can be observed in the time history presented in **Figure 6.25**. **Figure 6.26** present the plot of total force in docking pin in regard of Tp. High peak forces in the docking cone could be the deal breaker, should be specially considered.
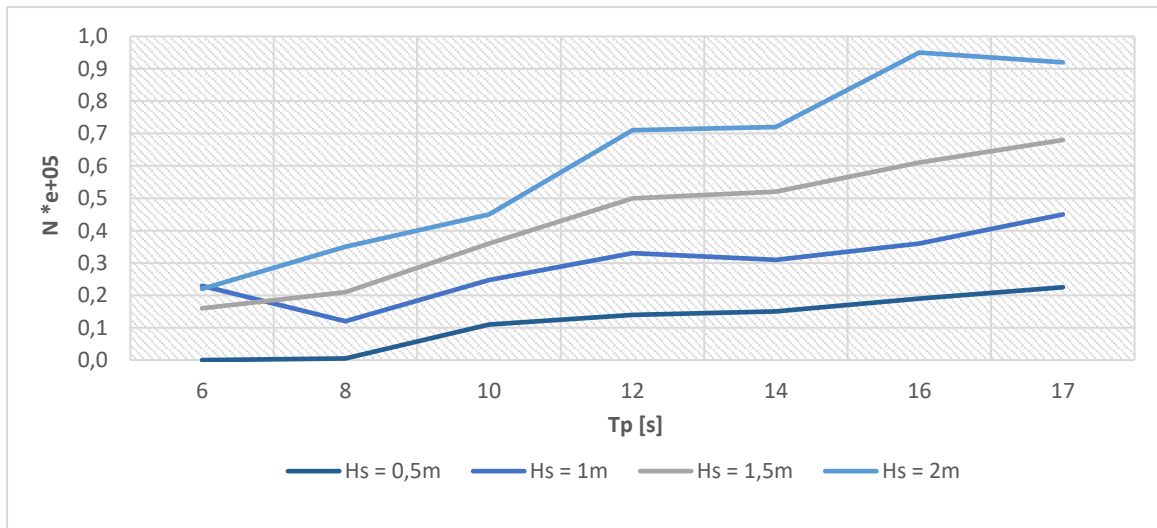
Figure 6.26: Standard deviation: Statistics of the total force in the docking pin element. (**Table B.0.26**)
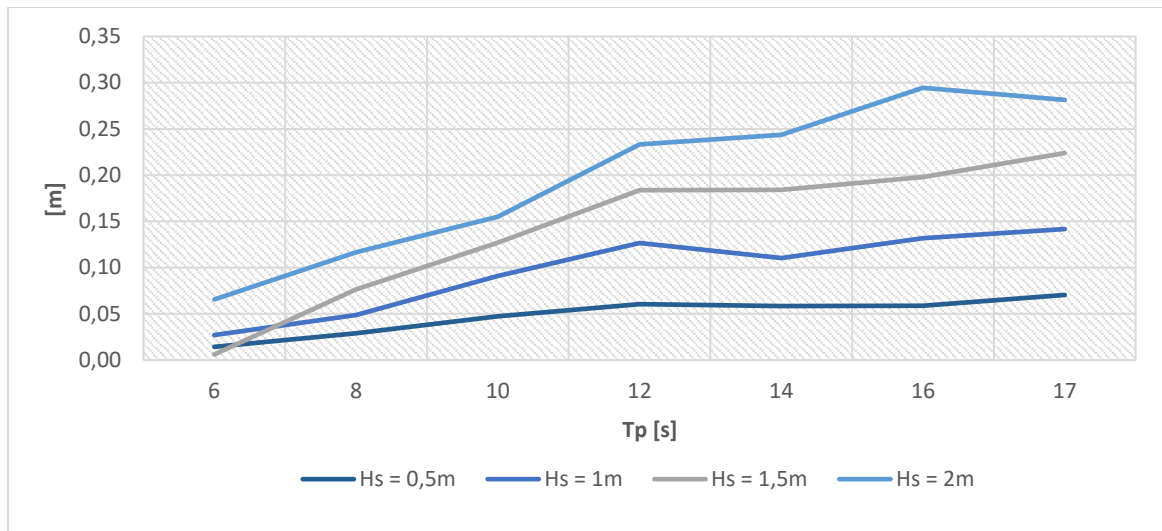
Figure 6.27: Standard deviation: Statistics of the radial distance, n, at reference point when OWT is in lowered position. (X-dir: **Table B.0.27**, Y-dir: **Table B.0.28** in appendix B)

A slight increase in radial reference error can be observed: increase from 0,22m in initial position to 0,23m when lowered in Hs = 2m, Tp = 12s. It seems that the contact forces influent the OWT radial motion negatively in all analyzed conditions.

6.4 Sensitivity analyses

All result presented is with couplings activated.
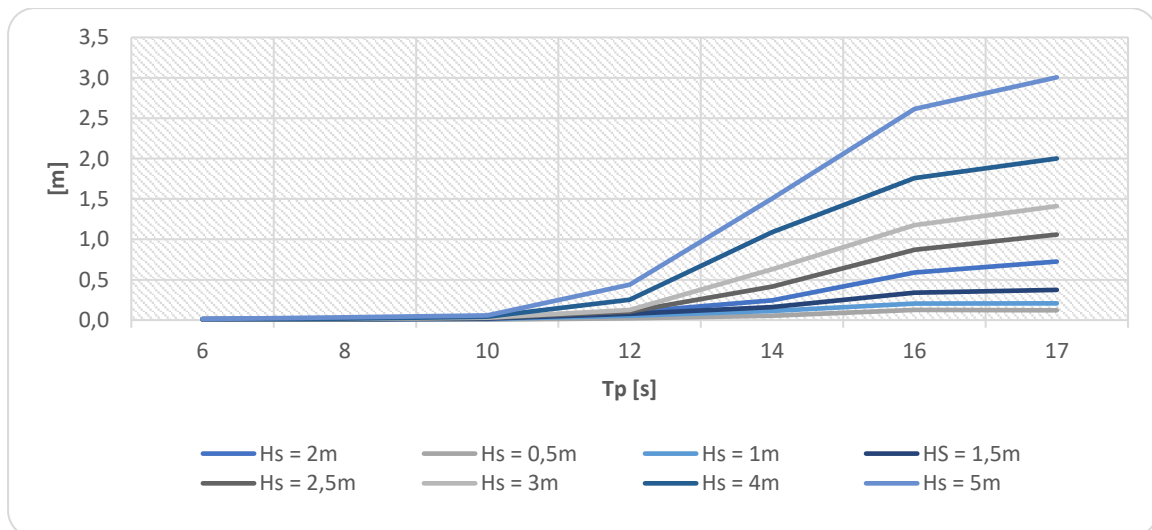
Figure 6.28: Standard deviation: Vertical reference error. β = 30 deg. (**Table B.0.31**)
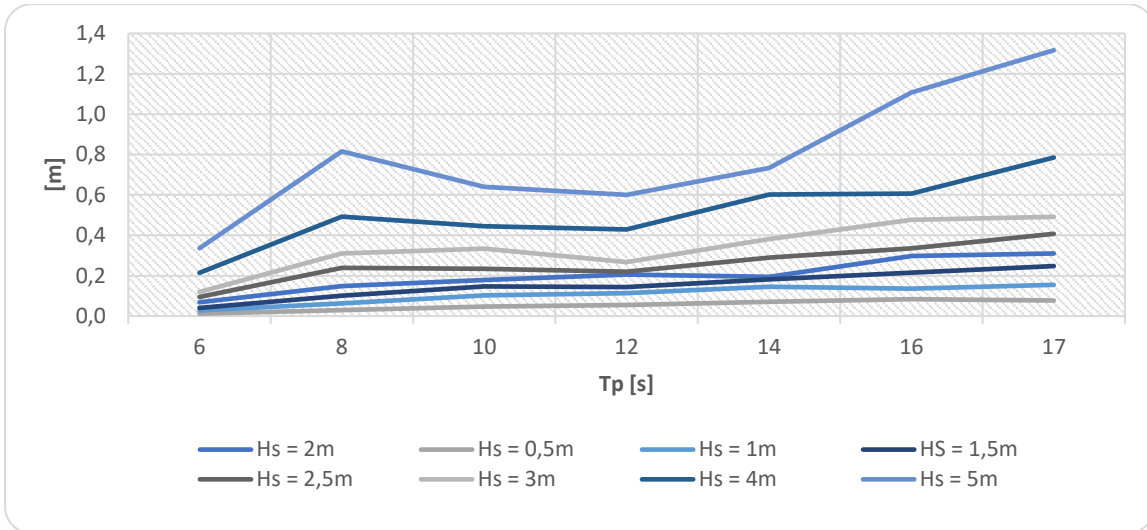
Figure 6.29: Standard deviation: Radial reference error, n. β = 30 deg. (**Table B.0.32**)
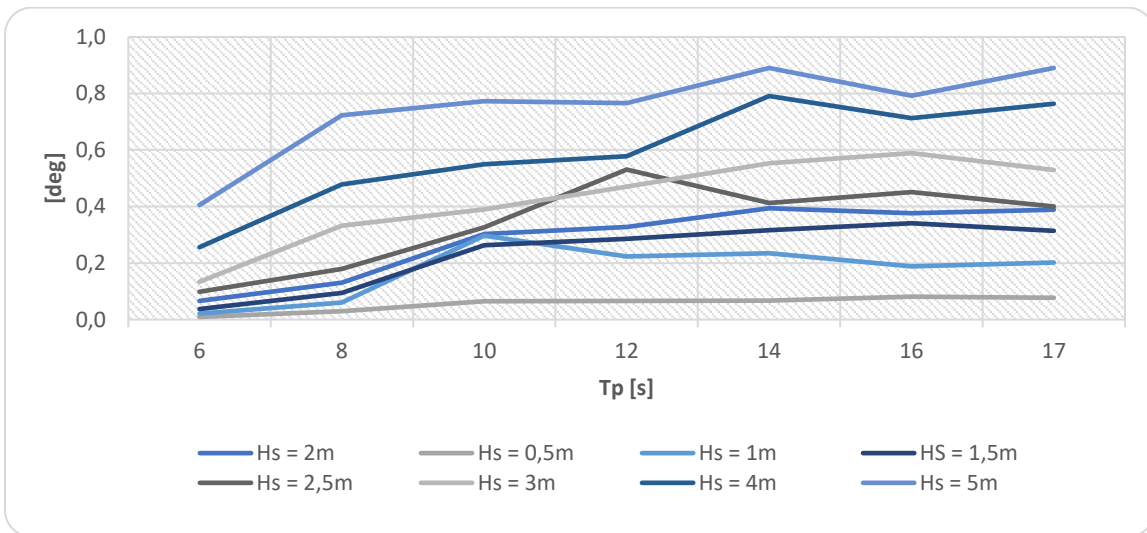
Figure 6.30: Standard deviation: OWT rotation Y-axis (pitch). β = 30 deg. (**Table B.0.33**)

A sensitivity analyses with environmental direction β = 30 deg was performed with env. conditions as presented in **Table 5.2**. Result is presented in **Figure 6.28**, **Figure 6.29** and **Figure 6.30**. With different env. heading the system responses are deviating a bit compared to head seas (β = 0 deg). As the radial error results clearly confirms; Tp = 8s becomes a resonant period for the coupled system. The sensitive periods are directly related to the natural frequencies; Tp ≈ 8s is as the eigenvectors reveals a period which induces heavy response in all modes expect surge for the SSP and yaw for the spar. Vertical reference error is increasing exponentially with longer wave periods, as expected. The OWT pitch STD is similar to the results from head seas.

Top bumper forces in X and Y direction can be inspected in **Figure B.0.9** and **Figure B.0.10,** respectively. The result shows that Tp around 8-10s is the period with largest forces in the top bumpers, this relates to the natural periods. A high radial ref. error can also be observed in these periods, which confirms the

indications in the previous sections. Compared to bumper forces at head seas the magnitude is almost equal.

6.5 Most probable maximum

Below in **Figure 6.31** and **Figure 6.32** is the most probable maximum presented, calculated with equation (6.29).
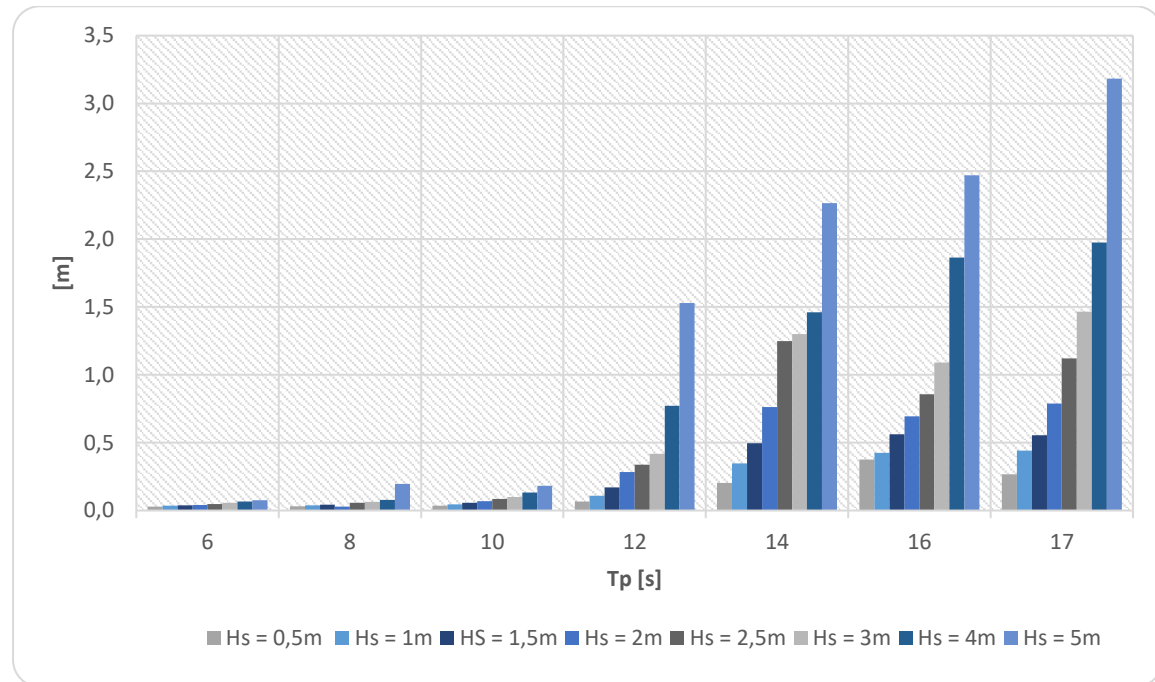
Figure 6.31: Estimation of most probable maximum: Vertical reference error. With couplings.
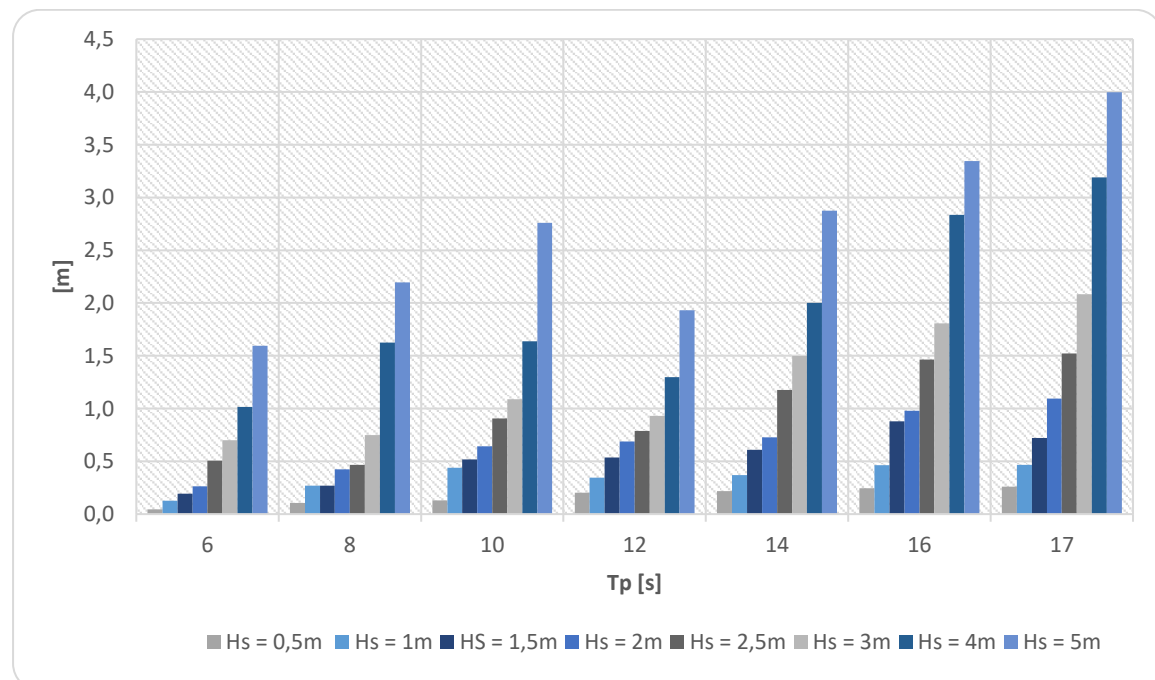
Figure 6.32: Estimation of most probable maximum: Radial reference error. With couplings.

It is likely that the calculated maximums can be exceeded, as there will be statistical variations of the extreme values.

In **Figure 6.33** are the most probable max of DX and DY estimated. 1600kN equals around 160 ton at Tp = 10s. Design limits are depending on the engineering and is usually deeply affected by finances. The result can be directly compared to Z. Jiang's study [3].
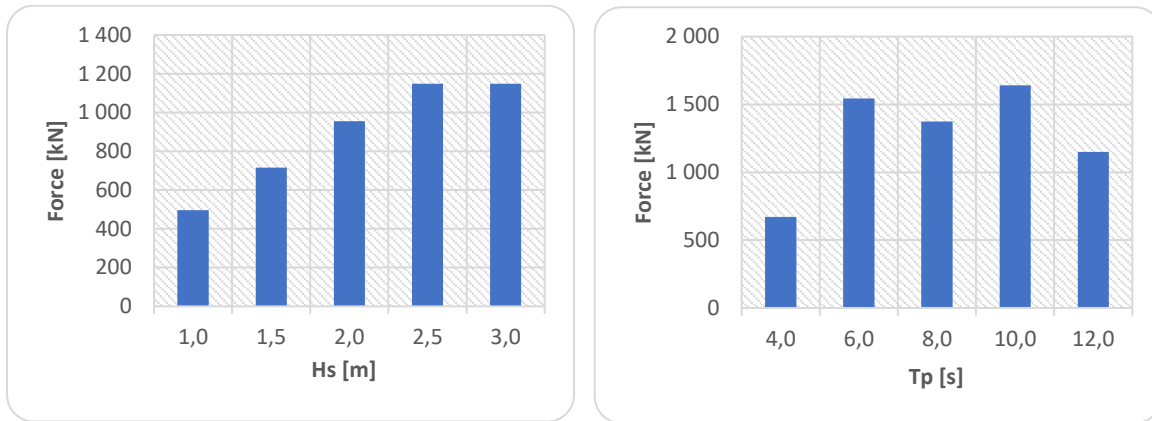
Figure 6.33: Estimation of probable maximum based: Max total damper forces (DX/DY). Left: Tp = 12s, β = 0. Right: Hs = 2,5m, β = 0.
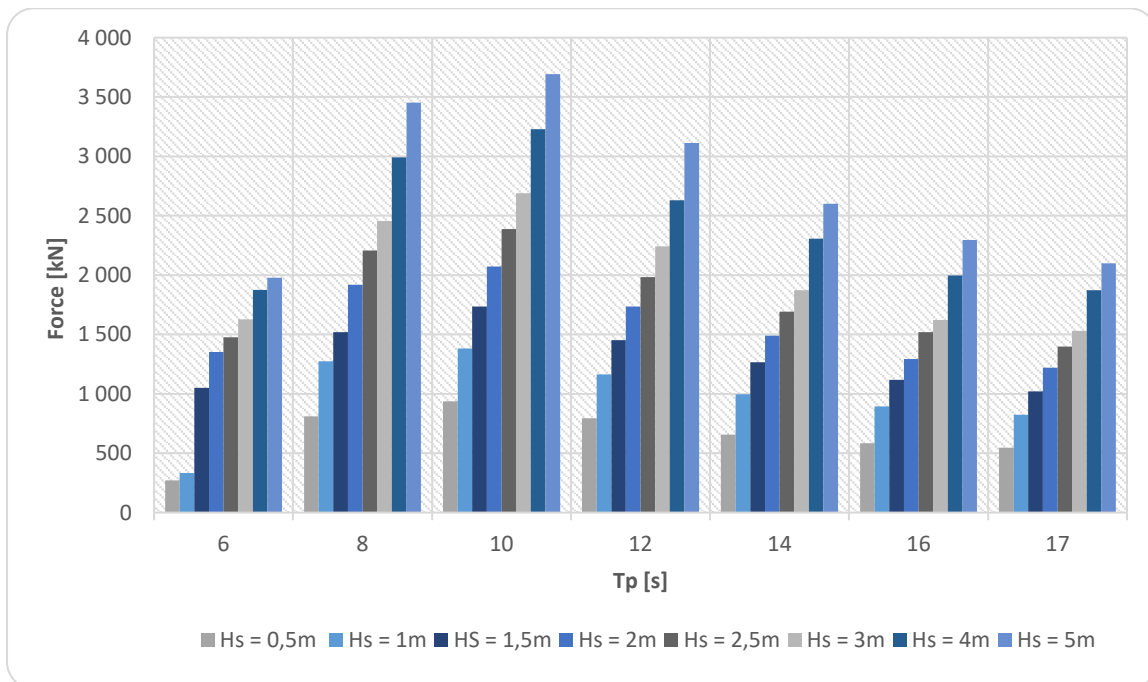
Figure 6.34: Estimation of most probable maximum: Top bumper element. With couplings.

Most probable maximum presented in **Figure 6.34** are estimated based upon the resultant max force in top bumper elements. Calculated by using equation (6.29) plus mean value. A maximum force of +3500 kN can be observed at Tp = 10s, Hs = 5m. Taken the mass of the OWT and the momentum into account these forces can rapidly change in magnitude in e.g. bad weather or sudden change in ballast. Margins should be evaluated with care.

6.6 Phase 3: OWT released

The spar draft has in phase 3 increased by ~10m and the static result shows that SSP has an aft trim of 15 deg with initial ballast. To counteract for the large mass shift a high capacity ballast system would normally be fitted to the SSP. There are physical and financial limitations regarding what is possible and profitable with a common ballast system - other solutions should be considered. A more suitable suggestion is to have a sliding mass underneath the deck and increased waterplane area, extra volume added on each pontoon end, as mentioned in section 4.1. The mass shall be moved according to the different load conditions of the SSP under installation. The goal is to manage fast mass shifting such that the SSP stays in equilibrium and the time in the critical phase 2 of the installation is kept to a minimum. Throughout the study one other proposed solution to ensure smooth OWT mating, and reduce contact forces, was to lift the spar and slowly pay out wire when the connection is completed. But according to the SSP hydrostatical characteristics challenges with trim would occur - adding more mass to the SSP is not preferable. The proposal was not considered any further. Static stability should always be considered for all kinds of possible load conditions, especially when large weight concentrations are shifted.

7 Conclusion

7.1 Conclusion from results and discussion

From the result and discussion, it can be seen that the method used to analyse motion responses for the coupled rigid-body is satisfactory. STD and RMS values are considered to give an estimate of the total response of the system and forces in all phases of the installation procedure.

Short term statistics was the basis for this study and long-term statistics was evaluated and commented. The installation concept was subjected to varying wave heights and wave peak periods, and the result presented some promising improvements in reference error at mating point. Collectively the most responsive periods for the rigid-body system are the ones that frequently occur in the long-term statistics - around Tp = 8-10s and 17s. Different composition of the coupling specifications is arguably preferred to change the eigenvalues of the system based on the long-term statistics, but compared to uncoupled and similar studies the weather window is increased.

The horizontal dampers DX and DY serves its purpose of reducing the high frequent relative motion between spar and SSP. The damper sensitivity analyses revealed the exponential increase in coupling forces when the phase of overdamping is reached. When preferred damping coefficient is applied a significant reduction in coupling forces and radial reference error compared to similar studies is observed, this verifies the parametrization of the damper characteristic. A non-intentional reduction in vertical reference error by the dampers can also be observed. With the combination of dampers and heave compensator the OWT heave motion is nearly synchornized to the spar heave motion in wave periods below 10s. The simple parametrization of the PD + FF controller was considered as adequate for this study, as a detailed or more in depth parametrization would have been too time consuming in SIMA.

The sensitivity analyses of the concept were successfully completed after tuning of the simulation time step. Similar responses are observed in the sensitivity analyses result as for head seas, both for radial and vertical ref. error. The result presented with head seas can be considered valid by the validation of the sensitivity analyses. Combined they amplify the plausibility of the proposed conceptual installation model.

As previously stated, the SSP hydrostatical characteristics could cause some challenges when large amount of weight is shifted. High load sensitivity due to the small waterplane area is one of the main concerns. A high capacity ballast system or mass shifting arrangement is necessary otherwise the SSP is technically not favored as installation vessel.

In conclusion, this paper has presented a valid installation procedure. Further development of the concept is still needed and should be substantiated by other similar studies, but at preliminary level this study proves the feasibility.

7.2 Suggestion for further work

Implementation of motion compensation in horizontal plane using the four lifting wires should be implemented. The intention is that if controlled, they will further improve the radial reference error. A controller which controls all four winches both in horizontal and vertical plane is complex. As mentioned, the heave compensator control used in this study is quite simple and further development is necessary to include all influential variables.

Wind analyses of the concept model assembly is an important part of the development and should be prioritized in the next step. Wind forces acting on the turbine assembly could be substantial and cause inadequate stability margins, confirmed by Z. Jiangs study [3].

Hydrodynamic coupling between SSP and spar should be calculated in suitable software, e.g. WAMIT, and implemented in the SIMA model.

Structural analyses of the involved elements in the proposed installation concept. Especially the horizontal spar dampers and the top sliding gripper arms should be prioritized.

7.3 Practical improvement and experiences

Post-processing was in this study time-consuming and should be more efficiently executed with e.g. exporting *.csv* file to Mathlab and more easily extract the important result. SIMA has an integrated post-processing tool which is helpful, but with its limitations.

When simulating different environments or parameters each run has to be manually started and each result parameter must be noted. SIMA has the possibility to run a set of variables, named *condition set.* But due to computer capacity limitations this was not possible to utilize, this resulted in time consuming parametrizations.

Summarized, the SIMA modelling software served its purpose. Some time was used to understand the feedback and physical definitions but the graphical feedback makes the modelling easy to understand.

References

[1]   DNV GL, "DNV GL - SIMA," 2018. [Online]. Available: https://www.dnvgl.com/services/simulation-of-marine-operations-sima-2324. [Accessed 02 11 2018].

[2]   Equinor, "Video: Installation of worlds first offshore wind farm," Equinor, 2017. [Online]. Available: https://www.youtube.com/watch?v=PUlfvXaISvc. [Accessed 01 11 2017].

[3]   Z. Jiang, L. Li, Z. Gao, K. H. Halse and P. C. Sandvik, "Dynamic response analyses of a catamaran installation vessel during the positioning of a wind turbine assembly onto a spar foundation," Elsevier Ltd., Ålesund, 2018.

[4]   J. Kosowatz, "ASME.org," 2015. [Online]. Available: https://www.asme.org/engineering-topics/articles/energy/developing-verifying-deepwater-offshore-wind. [Accessed 07 11 2018].

[5]   The university of Maine, "The VolturnUS 1:8 Floating Wind Turbine," 2017. [Online]. Available: https://www.osti.gov/servlets/purl/1375022. [Accessed 14 11 2018].

[6]   Equinor, "Hywind wind farm project," 2017. [Online]. Available: https://www.equinor.com/en/what-we-do/hywind-where-the-wind-takes-us.html. [Accessed 14 11 2018].

[7]   K. M. Hovland, "E24: Equinors flytende vindpark leverer over all forventning: – En kjempesuksess," 24 11 2018. [Online]. Available: https://e24.no/energi/vindkraft/equinors-flytende-vindpark-leverer-over-all-forventning-en-kjempesuksess/24500938. [Accessed 24 11 2018].

[8]   P. Bernard, "Master Thesis: An Innovative method for the installation of Offshore Wind Turbines," NTNU Ålesund, Ålesund, 2017.

[9]   Atkins, "Hywind floating installation challenge," [Online]. Available: https://www.atkinsglobal.com/en-gb/projects/hywind-installation-challenge. [Accessed 24 11 2018].

[10]   L. I. Hatledal , Z. Houxiang , K. H. Halse and H. P. Hildre , "Numerical study for a catamaran gripper-monopile mechanism of a novel offshore wind turbine assembly installation procedure," Department of Ocean Operations and Civil engineering , Ålesund, 2017.

[11]   P. Dvorak, "Windpower engineering," 13 03 2017. [Online]. Available: https://www.windpowerengineering.com/projects/offshore-wind/foundations-that-float/. [Accessed 24 11 2018].

[12]   SINTEF Ocean, "SIMA User Manual," SINTEF Ocean, Marintek, Ålesund, 2017.

[13]   K. Dooley, "Simulation Research Methods," Arizona State University, Departments of Management and Industrial Engineering , Arizona , 2002.

[14]   K. H. Halse, Interviewee, *Supervisor.* [Interview]. 01-06 2019.

[15]   F. Solaas, "Introduction course," SINTEF Ocean, Ålesund, 2019.

[16]   J. L. B. Børkja, "Master Thesis: Dynamic analysis of floating dock strcutures," NTNU, Trondheim, 2015.

[17]   H. Gill, "Quora," 10 06 2016. [Online]. Available: https://www.quora.com/What-are-over-damped-critically-and-under-damped-systems. [Accessed 19 05 2019].

[18]   K. Torsethaugen and S. Haver, "Simplified double peak spectral model for ocean waves," 2004.

[19]   J. Woodacre, R. Bauer and R. Irani, "A review of vertical motion heave compensation systems," Elsevier , Canada, 2015.

[20]   J. Balchen , N. Jensen, E. Mathisen and S. Sælid, "A dynamic positioning system based on kalman filtering and optimal control," 1980.

[21]   United Shipbuilding Corporation, "Vessels and equipment for offshore field development," 2019. [Online]. Available: http://www.aoosk.ru/en/products/semi-submersible-drilling-rig-moss-cs-50-mk-ii-severnoye-siyanie/. [Accessed 24 01 2019].

[22]   Det Norske Veritas, "Environmental conditions and environmental loads," DNV, 2010.

[23]   C. H. L. Gunawan Suwarno, "Wave Seed Selection on Irregular Wave Analyses and the Max Extreme Time Windows from 3 Hours Simulations," Offshore Technology conference , 2016.

[24]   H. M. Walker, Studies in the history of statistical method, Baltimore : THE WILLIAMS AND WILKINS COMPANY , 1929.

[25]   J. Smuts, "Control notes," [Online]. Available: http://blog.opticontrols.com/archives/297. [Accessed 07 05 2019].

[26]   O. M. E. S. Khayal, "Tutorial - Damped vibrations," ResearchGate , Sudan, 2017.

[27]   Z. Jiang, "A numerical study of a catamaran installation vessel for installaling offshore wind turbines," 18 01 2018. [Online]. Available: https://www.sintef.no/globalassets/project/eera-deepwind-2018/presentations/e2_jiang.pdf. [Accessed 09 11 2018].

[28]   S. McLeod, "Symplypsychology.org," 2017. [Online]. Available: https://www.simplypsychology.org/qualitative-quantitative.html. [Accessed 17 11 2018].

[29]   Andrea, "SWELLBEAT," 27 07 2016. [Online]. Available: https://swellbeat.com/mean-and-peak-wave-periods/. [Accessed 22 05 2019].

Appendix

A. Input files

Scatter diagram

Table A.0.1: All year scatter diagram for Statfjord for Statoil in 2003. Used to determine most probable occurring sea state.

H$_s$	SPECTRAL PEAK PERIOD																				SUM
	0-3	3-4	4-5	5-6	6-7	7-8	8-9	9-10	10-11	11-12	12-13	13-14	14-15	15-16	16-17	17-18	18-19	19-20	<20	
0-1	21	179	529	859	977	889	701	503	337	217	135	82	49	29	17	10	6	4	5	5550
1-2	5	141	959	2762	4683	5644	5411	4430	3245	2193	1399	855	507	294	167	94	53	29	36	32909
2-3	0	9	168	956	2604	4359	5230	4964	3980	2819	1822	1099	629	346	185	97	50	25	25	29368
3-4	0	0	9	127	634	1629	2633	3053	2777	2109	1398	835	461	239	118	56	26	12	9	16126
4-5	0	0	0	8	88	397	955	1460	1593	1349	941	566	303	148	67	29	12	5	3	7924
5-6	0	0	0	0	7	66	268	594	838	836	639	397	210	97	41	16	6	2	1	4019
6-7	0	0	0	0	0	6	49	177	352	445	393	263	141	63	25	9	3	1	0	1928
7-8	0	0	0	0	0	0	5	36	111	192	209	159	90	40	15	5	1	0	0	863
8-9	0	0	0	0	0	0	0	5	25	64	93	85	54	25	9	3	1	0	0	363
9-10	0	0	0	0	0	0	0	0	4	16	33	39	29	15	6	2	0	0	0	145
10-11	0	0	0	0	0	0	0	0	0	3	9	15	14	8	3	1	0	0	0	55
11-12	0	0	0	0	0	0	0	0	0	0	2	5	6	4	2	1	0	0	0	20
12-13	0	0	0	0	0	0	0	0	0	0	0	1	2	2	1	0	0	0	0	7
13-14	0	0	0	0	0	0	0	0	0	0	0	0	1	1	0	0	0	0	0	2
14-15	0	0	0	0	0	0	0	0	0	0	0	0	0	0	0	0	0	0	0	1
SUM	25	329	1667	4712	8993	12991	15255	15222	13262	10243	7075	4403	2495	1312	657	322	158	78	81	99280

RAO for SSP and spar
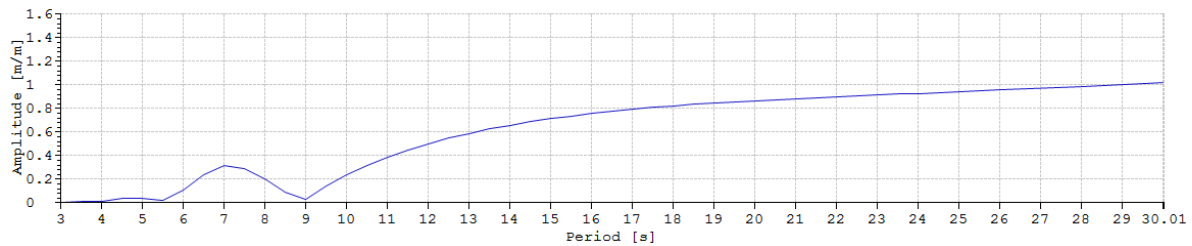
Figure A.0.1: First order motion transfer function for SSP surge. β = 0.
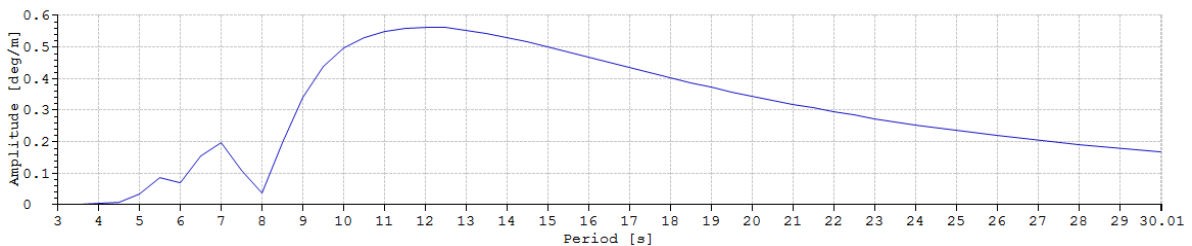
Figure A.0.2: First order motion transfer function for SSP pitch. β = 0.
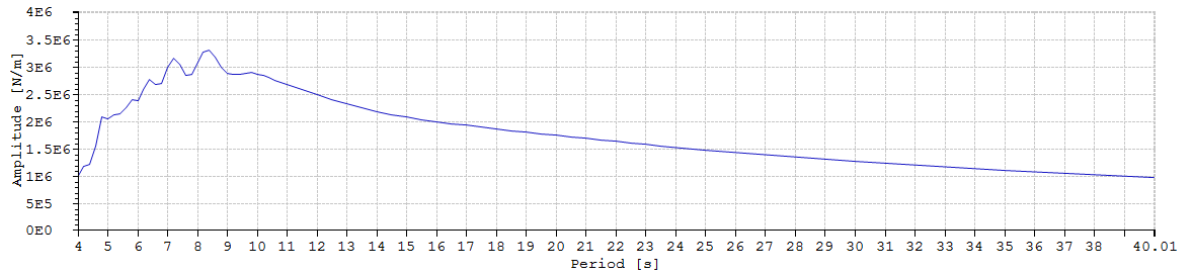
Figure A.0.3: First order wave force transfer function for spar surge. β = 0.
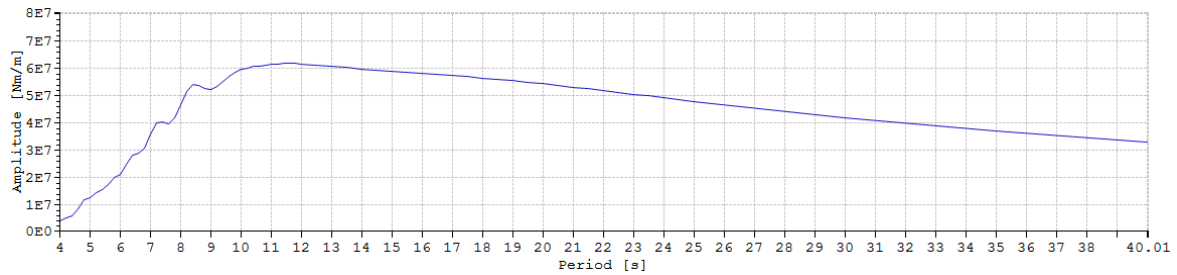
Figure A.0.4: First order wave force transfer function for spar pitch. β = 0.

B. Result files

Heave compensator parameter tuning

PD + FF controller

Table B.0.2: Parameter tuning Kf.

Kf	1	2	2,1	2,2	2,3	2,4	2,5	2,6	2,7	2,75	2,8	2,85	3	3,2	3,5
STD	-	0,42	0,41	0,48	**0,39**	0,4	0,4	0,48	0,57	0,46	0,51	0,51	0,46	0,44	0,6
Kp	3
Td	1,12
Tfd	1,1
Tf	0,95

Table B.0.3: Parameter tuning Kp.

Kp	1	2	3	4	5	6	7	8	8,4	8,5	8,6	7,75	9	10	20
STD	0,93	0,63	0,39	0,28	0,23	0,19	0,18	0,15	0,1506	**0,14**	0,16	0,17	0,24	0,24	1,34
Td	1,12
Kf	2,3
Tfd	1,1
Tf	0,95

Table B.0.4: Parameter tuning Tf.

Tf	0,1	0,4	0,6	0,8	0,9	0,92	0,94	0,95	0,96	0,98	1	1,5
STD	1,44	-	0,98	0,24	0,29	0,2	0,19	**0,14**	0,168	0,27	0,16	2,24
Kf	2,3											
Kp	8,5											
Td	1,12											
Tfd	1,1											

Table B.0.5: Parameter tuning Tfd.

Tfd	1	1,05	1,1	1,15	1,2	2	3	5
STD	0,21	0,19	**0,14**	0,14	0,17	0,16	0,2	0,35
Kf	2,3							
Kp	8,5							
Td	0,91							
Tf	0,95							

Table B.0.6: Parameter tuning first part Td.

Td	0,1	0,15	0,19	0,2	0,21	0,25	0,3	0,4	0,5	0,6	0,7	0,8	0,89	0,9	0,91
STD	-	0,27	0,27	**0,12**	0,12	0,26	0,26	0,23	0,2	0,19	0,17	0,16	0,18	0,14	0,14
Kf	2,3														
Kp	8,5														
Tfd	1,1														
Tf	0,95														

Table B.0.7: Parameter tuning second part Td.

Tfd	0,92	1	1,01	1,05	1,1	1,11	1,115	1,12	2
STD	0,2	0,205	0,192	0,217	0,145	0,191	0,204	**0,143**	1,69
Kf	2,3								
Kp	8,5								
Tfd	1,1								
Tf	0,95								

PID controller

Table B.0.8: Parameter tuning Kp.

Kp	0,1	0,5	1	1,05	1,1	1,075	2	3	4	5
STD	1,479	1,353	0,795	0,779	**0,414**	1,267	1,367	2,200	-	2,563
Kd	1									
Ki	1									

Table B.0.9: Parameter tuning first part Kd.

Kd	0,1	0,2	0,3	0,4	0,5	0,6	0,7	0,8	0,99	0,9	1	1,01	1,1	1,2
STD	2,170	2,083	2,049	1,730	1,578	1,319	1,119	0,852	0,924	0,4919	**0,414**	0,44	1,008	0,820
Kp		1,1												
Ki			1											

Table B.0.10: Parameter tuning second part Kd.

Kd	1,3	1,4	2
STD	1,053	0,835	0,718
Kp	1,1		
Ki	1		

Table B.0.11: Parameter tuning Ki.

Ki	0,1	0,2	0,3	0,38	0,39	0,4	0,5	0,6	0,7	0,8	0,9	1	1,1	1,2	1,3
STD	0,546	0,659	0,523	0,350	0,370	0,420	0,626	0,503	0,4563	0,748	0,759	0,444	0,475	0,812	1,154
Kp	1,1														
Kd	1														

Total motion SSP and spar

Uncoupled total motion

Table B.0.12: Standard deviation: Total motion SSP surge uncoupled. [m]

Hs\Tp [m]	6	8	10	12	14	16	17
0,5	0,1425	0,1583	0,2268	0,1658	0,1575	0,1437	0,1516
1	0,3614	0,3845	0,5653	0,3550	0,2854	0,3185	0,3336
1,5	0,6423	0,5846	0,7604	0,6103	0,5611	0,6377	0,5513
2	0,8682	0,9200	1,3720	0,9338	0,9002	0,8438	1,1270
2,5	1,1670	1,5020	1,8850	1,2540	0,9825	1,1830	1,2530
3	1,6820	1,9240	2,7190	1,4720	1,1990	1,1170	1,1416
4	3,1250	3,3070	4,4640	2,4290	1,6240	1,6530	1,6870
5	5,2620	4,6410	6,6840	2,9730	3,1666	2,0220	5,0790

Table B.0.13: Standard deviation: Total motion SSP pitch uncoupled. [deg]

Hs\Tp [deg]	6	8	10	12	14	16	17
0,5	0,1508	0,1501	0,2013	0,1373	0,1691	0,1490	0,1553
1	0,3003	0,3206	0,4241	0,3241	0,2684	0,2542	0,2894
1,5	0,4209	0,5430	0,5314	0,5555	0,4437	0,5970	0,5510
2	0,5951	0,6112	0,6357	0,6955	0,6879	0,7156	0,8758
2,5	0,6000	0,8041	1,0640	0,9223	0,7975	1,0930	0,9272
3	0,8766	1,0530	1,4920	1,1640	1,1430	0,9335	1,3430
4	1,3510	1,1184	1,5280	1,6130	1,4600	1,4690	1,4160
5	2,2690	1,3420	1,7940	1,5450	1,5300	1,9690	1,8280

Table B.0.14: Standard deviation: Total motion spar surge uncoupled. [m]

Hs\Tp [m]	6	8	10	12	14	16	17
0,5	0,3512	0,3739	0,5137	0,4468	0,4544	0,3673	0,3625
1	0,7269	0,8047	1,1080	0,8949	0,7156	0,7495	0,7505
1,5	1,1660	1,1990	1,2160	1,3380	1,3210	1,5300	1,2440
2	1,4260	1,4860	1,7870	1,7430	1,8888	2,0110	2,3570
2,5	1,8980	1,8230	2,1460	2,2780	2,0370	2,8870	2,8390
3	2,1800	2,6360	2,9570	2,2900	2,7650	2,547	2,5870
4	3,2540	3,2790	3,8370	3,6450	3,4320	3,7220	4,254
5	4,6390	4,2600	5,0030	3,8270	5,3690	4,2220	7,4340

Table B.0.15: Standard deviation: Total motion spar pitch uncoupled. [deg]

Hs\Tp [deg]	6	8	10	12	14	16	17
0,5	0,4781	0,5048	0,6397	0,5920	0,5648	0,4803	0,5033
1	0,8047	0,8334	1,1440	1,1050	0,8800	0,9177	0,9342
1,5	1,1400	1,2660	1,2970	1,4730	1,5960	1,6040	1,4790
2	1,4460	1,4360	1,7000	1,7130	1,9250	2,149	2,204
2,5	1,6190	1,8460	2,1640	2,2410	2,1650	3,2650	3,1280
3	2,1320	2,4390	2,9230	2,4850	2,8860	3,1150	2,8430
4	2,7900	2,6150	3,2490	3,5600	3,9530	3,7980	5,0100
5	3,9650	2,9960	3,6800	3,5890	4,7910	4,7510	6,2190

[m]		6	8	10	12	14	16	17
	Hs = 2m	0,0278	0,0452	0,1214	0,2066	0,2443	0,2704	0,2746
	Hs = 0,5m	0,0065	0,0102	0,0301	0,0514	0,0613	0,06751	0,0679
	Hs = 1m	0,0131	0,0204	0,0603	0,1029	0,1226	0,1357	0,1355
	HS = 1,5m	0,0200	0,0311	0,0909	0,1545	0,1847	0,2063	0,2230
	Hs = 2,5m	0,0338	0,0525	0,1510	0,2573	0,3077	0,3345	0,3357
	Hs = 3m	0,0421	0,0634	0,1821	0,3088	0,3673	0,4052	0,4097
	Hs = 4m	0,0552	0,0836	0,2423	0,4114	0,4907	0,5346	0,5456
	Hs = 5m	0,0791	0,1046	0,3012	0,5162	0,6126	0,6787	0,6816

Tp [s]

Hs = 2m   Hs = 0,5m   Hs = 1m   HS = 1,5m
Hs = 2,5m   Hs = 3m   Hs = 4m   Hs = 5m

Figure B.0.5: Standard deviation: Total motion SSP heave. Uncoupled.
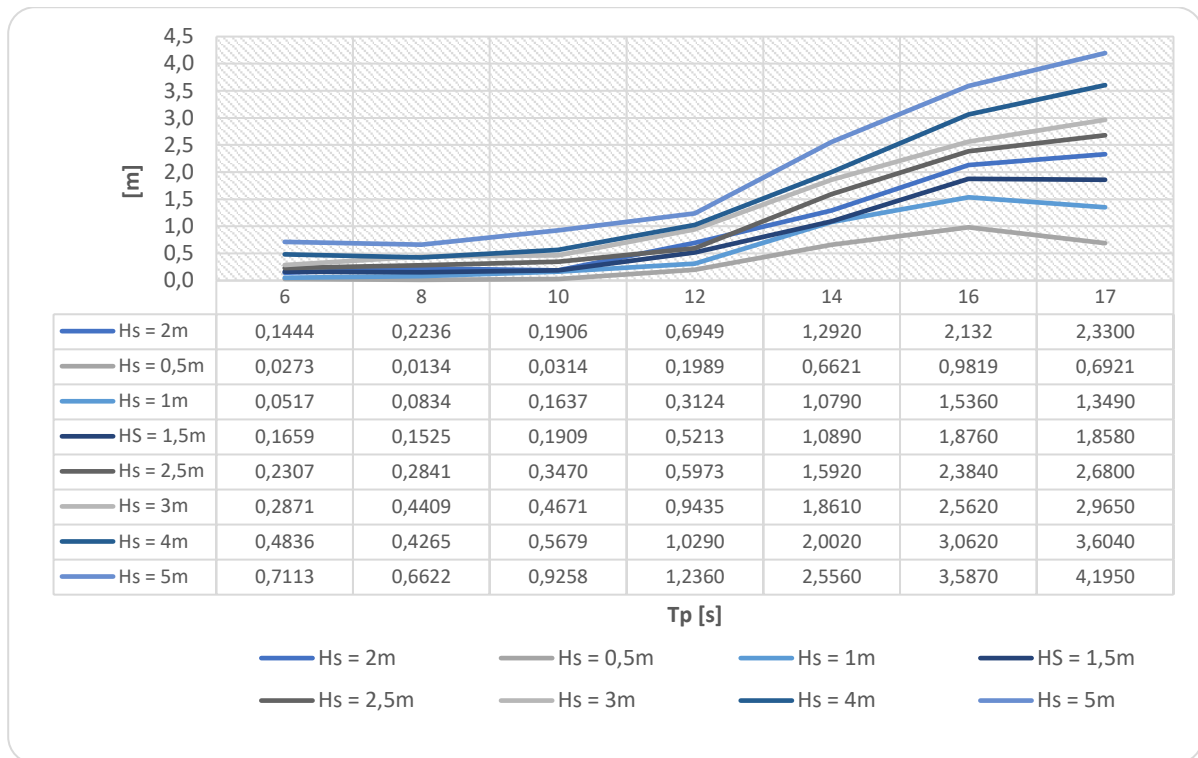
Figure B.0.6: Standard deviation: Total motion spar heave. Uncoupled.

Coupled total motion

Table B.0.16: Standard deviation: Total motion SSP surge coupled. [m]

Hs\Tp [m]	6	8	10	12	14	16	17
0,5	0,0456	0,0795	0,0930	0,0877	0,0972	0,1089	0,1196
1	0,1725	0,2135	0,2816	0,1964	0,1827	0,2132	0,2382
1,5	0,3853	0,4487	0,5814	0,3354	0,3211	0,3866	0,4172
2	0,6698	0,7571	1,0030	0,5327	0,4297	0,5029	0,5518
2,5	1,0480	1,1200	1,5230	0,7987	0,5454	0,6723	0,7571
3	1,5030	1,6010	2,1360	1,0720	0,8137	0,7544	0,8662
4	2,6430	2,7410	3,7040	1,7500	1,1270	1,1220	1,2810
5	4,0360	4,2020	5,6700	2,5510	1,5430	1,6640	1,7750

Table B.0.17: Standard deviation: Total motion SSP pitch coupled. [deg]

Hs\Tp [m]	6	8	10	12	14	16	17
0,5	0,0299	0,0520	0,0772	0,0928	0,0953	0,0951	0,0917
1	0,0416	0,0883	0,1407	0,1612	0,1810	0,1818	0,1734
1,5	0,0792	0,1440	0,1995	0,2318	0,2573	0,2652	0,2378
2	0,1076	0,1593	0,2578	0,2936	0,3210	0,323	0,3556
2,5	0,1536	0,2054	0,3486	0,4187	0,4235	0,4011	0,4292
3	0,2406	0,2995	0,4537	0,4293	0,5062	0,4549	0,4994
4	0,4168	0,4236	0,6852	0,5839	0,7153	0,6316	0,6800
5	0,6181	0,6531	0,9812	0,7428	0,8855	0,7851	0,8940

Table B.0.18: Standard deviation: Total motion spar surge coupled. [m]

Hs\Tp [m]	6	8	10	12	14	16	17
0,5	0,0421	0,0674	0,0700	0,0546	0,0750	0,0966	0,0998
1	0,1623	0,2083	0,2512	0,1420	0,1412	0,1821	0,2033
1,5	0,3678	0,4025	0,5338	0,2627	0,2453	0,2960	0,3582
2	0,6523	0,6915	0,9212	0,4587	0,3346	0,4325	0,4681
2,5	0,9899	1,0590	1,4160	0,6937	0,4436	0,5475	0,6103
3	1,4150	1,4920	2,0610	0,9244	0,6561	0,6655	0,7282
4	2,5100	2,6100	3,5970	1,5890	0,9795	1,0320	1,109
5	3,8600	4,0200	5,4170	2,3440	1,3280	1,4460	1,4960

Table B.0.19: Standard deviation: Total motion spar pitch coupled. [deg]

Hs\Tp [deg]	6	8	10	12	14	16	17
0,5	0,0321	0,0711	0,1192	0,1995	0,2436	0,2422	0,2398
1	0,0639	0,1753	0,2575	0,3206	0,3621	0,4149	0,4160
1,5	0,1306	0,2993	0,3811	0,4194	0,5525	0,6387	0,5511
2	0,2026	0,3111	0,5054	0,6052	0,6106	0,7313	0,7316
2,5	0,2741	0,3884	0,6283	0,6062	0,6736	0,9499	1,0140
3	0,4332	0,5810	0,7150	0,7381	0,8650	1,0020	1,1210
4	0,6690	0,8775	0,9772	0,9122	1,1920	1,3450	1,7150
5	0,9174	1,2860	1,4730	1,1350	1,3410	1,7920	2,2520

	6	8	10	12	14	16	17
Hs = 2m	0,0147	0,0368	0,1180	0,2325	0,2548	0,2676	0,2729
Hs = 0,5m	0,0037	0,0093	0,0296	0,0524	0,0641	0,06772	0,0698
Hs = 1m	0,0191	0,0185	0,0591	0,1568	0,1277	0,1339	0,1371
Hs = 1,5m	0,0111	0,0277	0,0885	0,2090	0,1911	0,2004	0,2055
Hs = 2,5m	0,0184	0,0461	0,1475	0,2611	0,3180	0,3340	0,3412
Hs = 3m	0,0222	0,0554	0,1769	0,3132	0,3821	0,4000	0,4106
Hs = 4m	0,0298	0,0742	0,2360	0,4175	0,5091	0,5332	0,5438
Hs = 5m	0,0372	0,0933	0,2951	0,5218	0,6323	0,6631	0,6763

Tp [s]

Hs = 2m   Hs = 0,5m   Hs = 1m   Hs = 1,5m   Hs = 2,5m   Hs = 3m   Hs = 4m   Hs = 5m
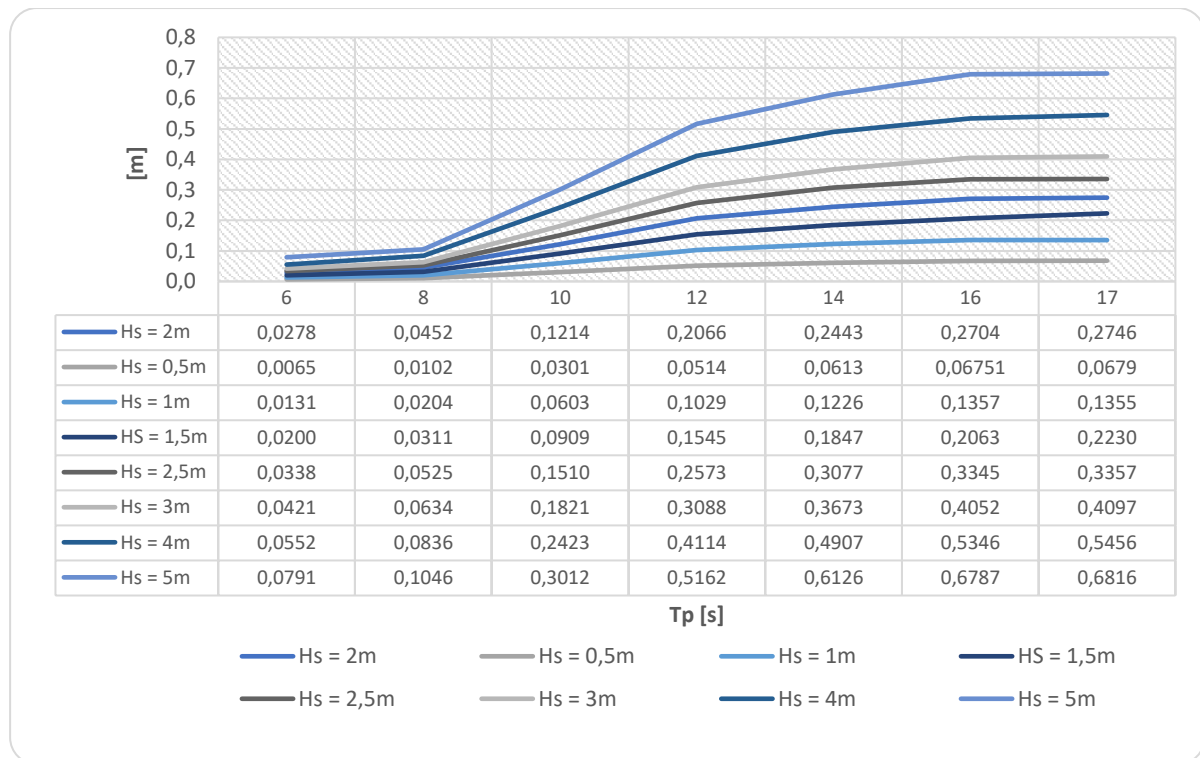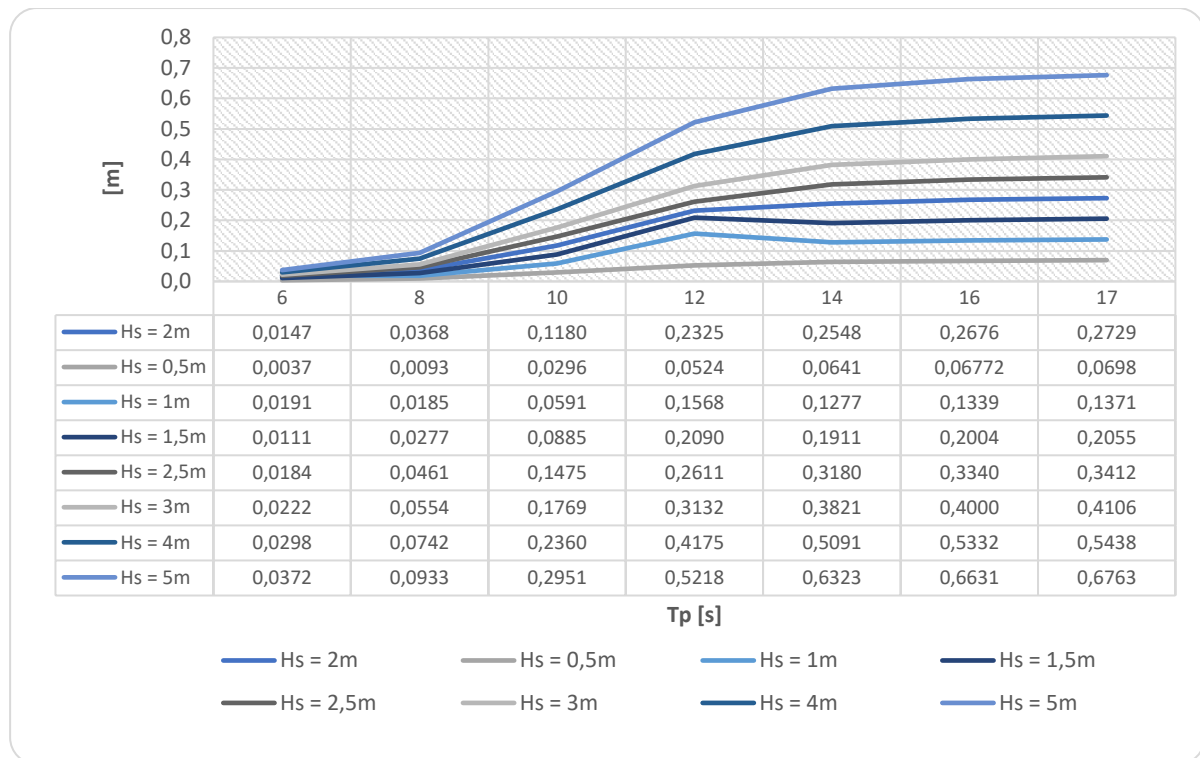
Figure B.0.7: Standard deviation: Total motion SSP heave (COG). Coupled.
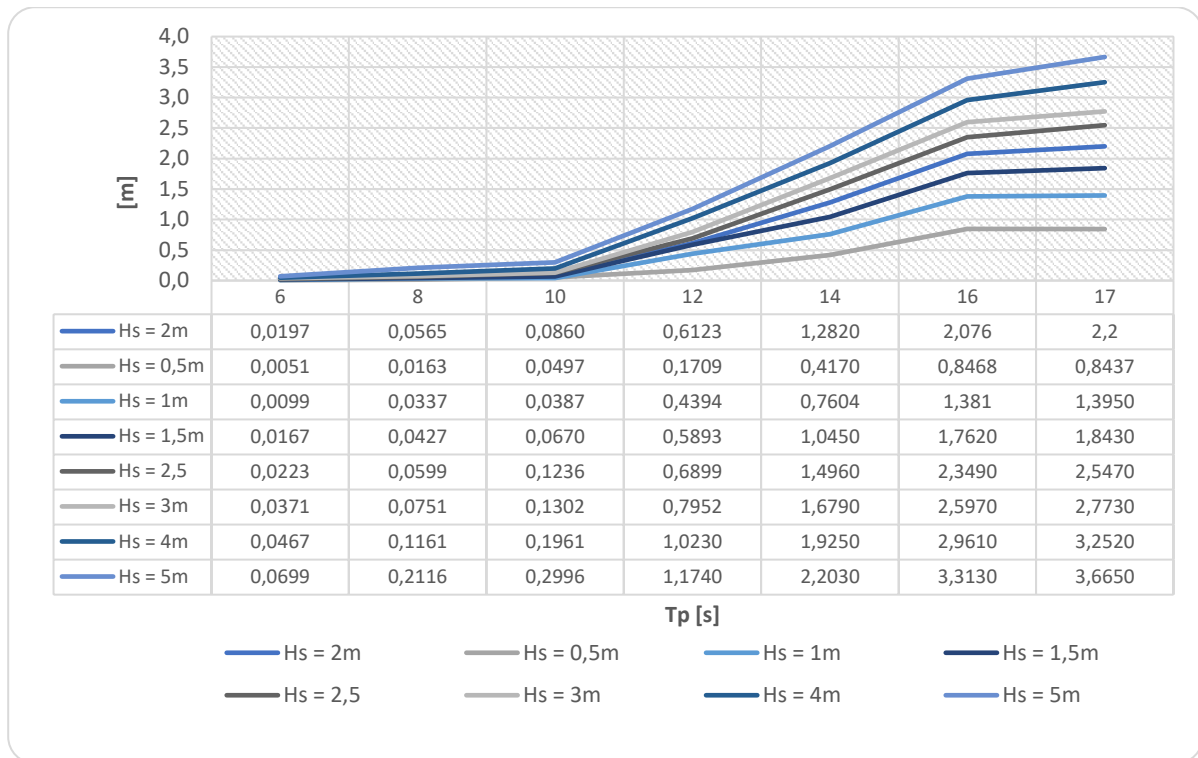
Figure B.0.8: Standard deviation: Total motion spar heave (COG). Coupled.

Relative motion raw data

Table B.0.20: Standard deviation: Vertical reference error coupled.

Hs\Tp [m]	6	8	10	12	14	16	17
0,5	0,0088	0,0093	0,0108	0,0210	0,0647	0,1216	0,0874
1	0,0107	0,0117	0,0139	0,0346	0,1112	0,1376	0,1441
1,5	0,0112	0,0129	0,0179	0,0532	0,1585	0,1815	0,1810
2	0,0117	0,0152	0,0214	0,0889	0,2434	0,2243	0,2567
2,5	0,0140	0,0172	0,0267	0,1058	0,3981	0,2774	0,3648
3	0,0171	0,0198	0,0305	0,1315	0,4152	0,3530	0,4770
4	0,0195	0,0236	0,0413	0,2427	0,4660	0,6034	0,6431
5	0,0227	0,0597	0,0566	0,4806	0,7231	0,7990	1,0360

Table B.0.21: Standard deviation: Vertical reference error uncoupled.

Hs\Tp [m]	6	8	10	12	14	16	17
0,5	0,0935	0,1059	0,1444	0,2316	0,5069	1,0430	0,9950
1	0,3342	0,2525	0,3814	0,6206	0,9569	1,7770	1,7670
1,5	0,4198	0,5230	0,6144	0,7559	1,3970	2,3010	2,3350
2	0,5604	0,6001	0,6244	1,0060	1,8260	2,8840	2,8590
2,5	0,7349	0,7263	0,8782	1,1320	1,7960	3,3790	3,3800
3	0,9882	0,8622	1,0720	1,4820	2,7910	3,8790	4,3390
4	1,2250	1,1860	1,6530	1,8960	2,8710	5,1100	5,8870
5	1,8470	2,0970	2,4860	2,4170	4,2440	6,6670	7,3680

Table B.0.22: Standard deviation: Radial reference error uncoupled.

Hs\Tp [m]	6	8	10	12	14	16	17
0,5	0,4210	0,4457	0,5984	0,6636	0,5049	0,4524	0,4196
1	1,0310	0,7861	0,9959	1,4690	0,9140	0,9721	1,0376
1,5	1,2090	1,6881	2,2380	1,7414	2,1476	2,7404	2,8894
2	1,6121	1,8781	2,3391	2,9418	2,4782	3,3663	3,6975
2,5	2,4634	2,1144	3,4298	4,0699	3,7691	4,7211	4,3680
3	4,2864	2,5407	4,8466	4,8094	5,0976	5,6627	5,5238
4	4,9353	4,3440	6,7427	6,3487	6,2642	7,8884	8,5773
5	7,3183	13,9720	11,3482	8,7209	12,1547	11,2153	17,1837

Table B.0.23: Standard deviation: Radial reference error coupled.

Hs\Tp [m]	6	8	10	12	14	16	17
0,5	0,0135	0,0320	0,0400	0,0634	0,0700	0,0793	0,0851
1	0,0373	0,0814	0,1354	0,1089	0,1176	0,1502	0,1519
1,5	0,0571	0,0818	0,1600	0,1683	0,1944	0,2845	0,2354
2	0,0776	0,1481	0,1985	0,2161	0,2321	0,3165	0,3564
2,5	0,1490	0,1412	0,2794	0,2478	0,3752	0,4742	0,4957
3	0,2067	0,2261	0,3358	0,2924	0,4777	0,5845	0,6779
4	0,2993	0,4909	0,5051	0,4076	0,6390	0,9169	1,0392
5	0,4697	0,6642	0,8520	0,6071	0,9173	1,0822	1,3015

OWT rotation around Y-axis (pitch)

Table B.0.24: Standard deviation: Rotation around Y-axis (pitch) uncoupled.

Hs\Tp [deg]	6	8	10	12	14	16	17
0,5	0,1237	0,1548	0,1986	0,1674	0,1794	0,1319	0,1569
1	0,3120	0,3088	0,4814	0,4941	0,3442	0,3635	0,4268
1,5	0,6858	0,7375	0,6422	0,6536	0,5639	0,5643	0,5058
2	0,8020	0,7367	0,8230	0,9036	0,7382	0,9868	0,7874
2,5	0,9213	0,8426	0,9157	1,0260	1,0820	0,9005	0,8670
3	0,7025	0,9498	1,1000	1,0780	1,1920	1,1750	1,0870
4	1,4130	1,2500	1,6720	1,4440	1,5480	1,7350	1,3580
5	1,4460	1,7110	1,8340	1,7090	1,9440	1,8440	

Table B.0.25: Standard deviation: Rotation around Y-axis (pitch) coupled.

Hs\Tp [deg]	6	8	10	12	14	16	17
0,5	0,0459	0,0487	0,0654	0,0990	0,0963	0,0977	0,1044
1	0,0472	0,0841	0,1343	0,1856	0,1952	0,1793	0,2006
1,5	0,1045	0,1192	0,1955	0,2599	0,2856	0,3037	0,2700
2	0,1433	0,1636	0,2402	0,3363	0,3634	0,3584	0,4276
2,5	0,1828	0,2249	0,3380	0,4340	0,4335	0,4346	0,4330
3	0,2535	0,2715	0,4184	0,5227	0,5612	0,4990	0,5191

4	0,4128	0,4023	0,6486	0,6430	0,7449	0,6380	0,6070
5	0,6865	0,6413	0,8954	0,8396	1,0170	0,7756	0,8410

Phase 3: Lowered position

Table B.0.26: Standard deviation: Max total force in docking pin element. Coupled.

Hs\Tp [N*e5]	6	8	10	12	14	16	17
0,5	0,00	0,01	0,11	0,14	0,15	0,19	0,23
1	0,23	0,12	0,25	0,33	0,31	0,36	0,45
1,5	0,16	0,21	0,36	0,50	0,52	0,61	0,68
2	0,22	0,35	0,45	0,71	0,72	0,95	0,92

Table B.0.27: Standard deviaion: Reference error X-direction (surge). Coupled.

Hs\Tp [m]	6	8	10	12	14	16	17
0,5	0,014	0,029	0,047	0,061	0,058	0,059	0,07
1	0,027	0,049	0,091	0,127	0,110	0,122	0,141
1,5	0,005	0,076	0,125	0,179	0,177	0,197	0,214
2	0,066	0,117	0,155	0,233	0,235	0,285	0,272

Table B.0.28: Standard deviaion: Reference error Y-direction (sway). Coupled.

Hs\Tp [m]	6	8	10	12	14	16	17
0,5	0,004	0,004	0,003	0,003	0,003	0,004	0,006
1	0,004	0,003	0,003	0,008	0,008	0,051	0,012
1,5	0,003	0,003	0,025	0,040	0,052	0,023	0,066
2	0,003	0,005	0,004	0,005	0,062	0,076	0,071

Top bumper forces

Coupled

Table B.0.29: RMS: Total force top bumper element in global X-direction with couplings.

Hs\Tp [N*e+05]	6	8	10	12	14	16	17
0,5	1,58	2,17	2,55	2,37	2,12	1,88	1,78
1	3,03	3,46	3,84	3,36	3,00	2,77	2,57
1,5	3,75	4,29	4,82	4,27	3,84	3,42	3,25
2	4,63	5,13	5,88	5,25	4,50	3,90	3,76
2,5	5,19	5,90	6,94	6,06	5,55	4,62	4,39
3	5,85	6,91	7,96	6,81	5,90	5,14	5,01
4	7,31	8,51	9,83	7,68	7,08	6,26	6,01
5	8,91	10,49	12,22	10,03	8,51	7,29	7,26

Table B.0.30: RMS: Total force top bumper element in global Y-direction with couplings.

Hs\Tp [N*e+05]	6	8	10	12	14	16	17
0,5	0,30	0,30	0,30	0,30	0,30	0,30	0,30
1	0,30	0,30	0,30	0,30	0,30	0,41	0,57
1,5	0,30	0,31	0,31	0,31	0,30	0,44	0,66
2	0,30	0,33	0,31	0,68	0,65	0,99	1,02
2,5	0,30	0,33	0,52	0,31	0,75	0,97	1,45
3	0,30	0,33	0,46	0,31	0,94	1,23	0,93
4	0,31	0,33	0,46	0,30	0,95	2,31	2,46
5	0,34	0,33	0,48	0,54	1,90	2,05	1,33

Sensitivity analyses

Table B.0.31: Standard deviation: Vertical reference error. $\beta = 30$ deg.

Hs\Tp [m]	6	8	10	12	14	16	17
0,5	0,0080	0,0085	0,0080	0,0243	0,0554	0,1264	0,1229
1	0,0090	0,0104	0,0129	0,0538	0,1128	0,2055	0,2073
1,5	0,0104	0,0116	0,0193	0,0765	0,1598	0,3394	0,3743
2	0,0109	0,0131	0,0195	0,0977	0,2454	0,5908	0,7248
2,5	0,0121	0,0110	0,0255	0,1063	0,4149	0,8698	1,0590
3	0,0141	0,0137	0,0306	0,1263	0,6275	1,1770	1,4110
4	0,0131	0,0204	0,0422	0,2534	1,0900	1,7580	2,0010
5	0,0134	0,0344	0,0593	0,4382	1,5042	2,6150	3,0060

Table B.0.32: Standard deviation: Radial reference error. $\beta = 30$ deg.

Hs\Tp [m]	6	8	10	12	14	16	17
0,5	0,0122	0,0302	0,0471	0,0552	0,0711	0,0838	0,0774
1	0,0279	0,0632	0,1030	0,1133	0,1448	0,1366	0,1549
1,5	0,0405	0,1016	0,1462	0,1441	0,1818	0,2153	0,2478
2	0,0685	0,1481	0,1788	0,2054	0,1942	0,2971	0,3102
2,5	0,0948	0,2389	0,2345	0,2192	0,2894	0,3362	0,4076
3	0,1196	0,3103	0,3343	0,2680	0,3817	0,4769	0,4917
4	0,2145	0,4930	0,4451	0,4291	0,6016	0,6072	0,7854
5	0,3359	0,8157	0,6399	0,6007	0,7342	1,1075	1,3166

Table B.0.33: Standard deviation: OWT rotation around Y-axis (pitch). $\beta = 30$ deg.

Hs\Tp [deg]	6	8	10	12	14	16	17
0,5	0,0094	0,0298	0,0647	0,0659	0,0669	0,0811	0,0777
1	0,0212	0,0609	0,2969	0,2240	0,2352	0,1886	0,2020
1,5	0,0375	0,0947	0,2632	0,2863	0,3160	0,3409	0,3143
2	0,0662	0,1305	0,3026	0,3275	0,3940	0,3764	0,389
2,5	0,0985	0,1795	0,3269	0,5308	0,4123	0,4510	0,4002

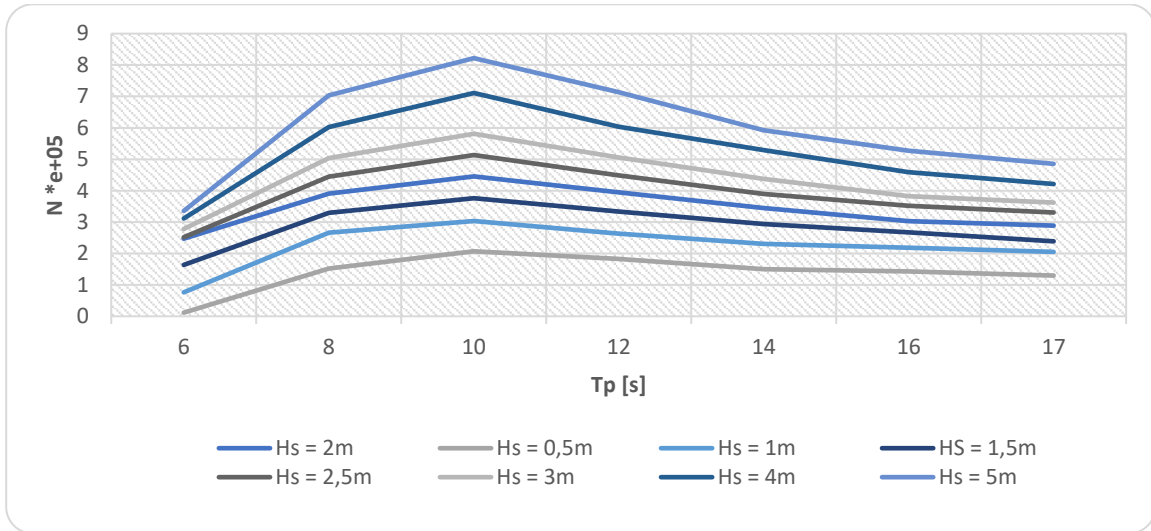|							
3	0,1339	0,3317	0,3902	0,4700	0,5532	0,5889	0,5287
4	0,2561	0,4785	0,5492	0,5780	0,7909	0,7121	0,7631
5	0,4054	0,7225	0,7724	0,7660	0,8902	0,7916	0,8902

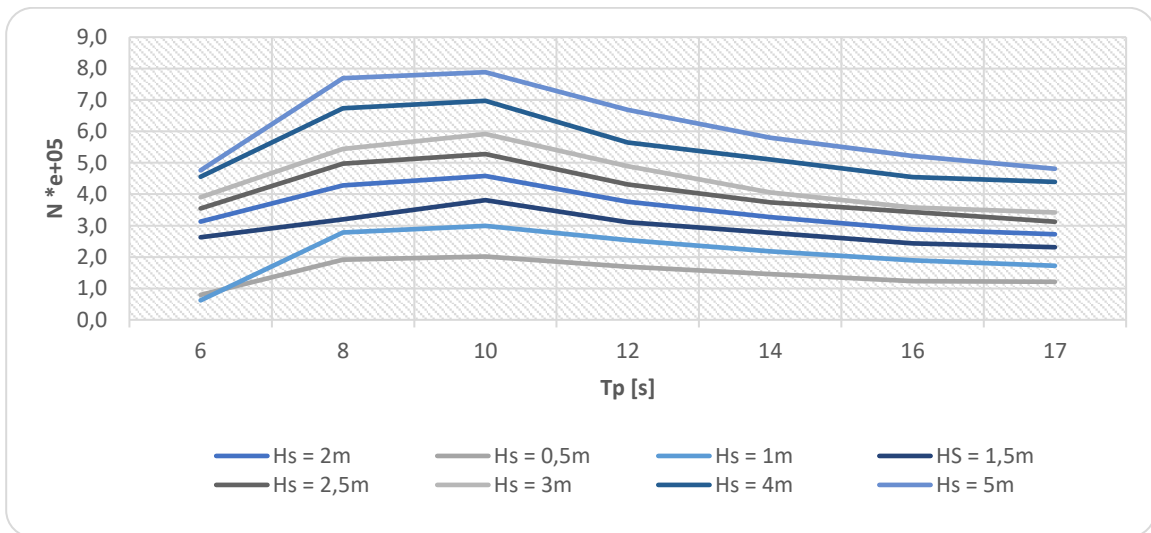**Figure B.0.9:** RMS: Max total force in top bumper global X-direction. β = 30 deg.

Figure B.0.10: RMS: Max total force in top bumper global Y-direction. β = 30 deg.

Horizontal dampers results

Table B.0.34: Damper DX/DY sensitivity analyses raw data.

Hs	DAMPING [Ns/m]	8 FORCE STD [N] X*e5	Y*e5	8 REL. STD [m] X	Y	12 FORCE STD [N] X*e5	Y*e5	12 REL. STD [m] X	Y	17 FORCE STD [N] X*e5	Y*e5	17 REL. STD [m] X	Y
1	10	0,00002	0,00001	0,88840	0,04113	0,00002	0,00001	1,45000	0,00334	0,00002	0,00001	0,89090	0,09501
	100	0,00020	0,00010	0,91450	0,04113	0,00022	0,00123	1,13900	0,01663	0,00018	0,00010	0,88580	0,05137
	1000	0,00210	0,00112	1,00700	0,00368	0,00231	0,00126	1,12500	0,00405	0,00212	0,00122	1,03300	0,12230
	10000	0,01819	0,00965	0,94480	0,00364	0,02338	0,01288	1,17500	0,00757	0,02072	0,01187	1,08100	0,05688
	100000	0,14770	0,07624	0,55550	0,00352	0,16520	0,08796	0,70550	0,00355	0,13980	0,08292	0,57380	0,07586
	1000000	0,84720	0,42700	0,17630	0,00300	0,85120	0,44350	0,27740	0,00843	0,60020	0,42480	0,21820	0,02669
	10000000	1,52600	0,79400	0,06326	0,00244	1,32800	0,77110	0,14160	0,00220	1,15300	1,74000	0,15170	0,00896
	100000000	1,73400	1,29600	0,09017	0,00858	2,04800	2,52300	0,14750	0,01738	4,14900	8,39500	0,13450	0,02712
2	10	0,00003	0,00002	1,87400	0,01274	0,00004	0,00002	1,78900	0,01496	0,00004	0,00002	2,33600	0,46240
	100	0,00036	0,00020	1,92300	0,01301	0,00038	0,00022	1,87500	0,02541	0,00438	0,00027	2,33700	0,66490
	1000	0,00367	0,00213	2,03900	0,01267	0,00400	0,00242	2,33300	0,10430	0,00437	0,00268	2,30800	0,66780
	10000	0,03457	0,01965	1,75600	0,01729	0,03645	0,02149	1,92300	0,01309	0,03744	0,02332	2,03200	0,75740
	100000	0,24670	0,13380	1,07600	0,01408	0,28630	0,16120	1,23700	0,01075	0,27360	0,17600	1,20400	0,31570
	1000000	1,61700	0,83500	0,33860	0,01321	1,62600	0,87820	0,53010	0,01681	1,23900	0,95290	0,47930	0,10660
	10000000	2,96000	1,55500	0,17310	0,00948	2,54900	1,55000	0,21260	0,00909	2,37900	3,80600	0,28740	0,07620
	100000000	3,17400	2,42400	0,14290	0,00177	4,03000	5,12100	0,36390	0,03355	7,94300	16,07000	0,24280	0,07280
3	10	0,00005	0,00003	2,43500	0,02310	0,00006	0,00000	3,11100	0,02114	0,00007	0,00005	3,75100	1,46600
	100	0,00049	0,00029	2,54400	0,03048	0,00061	0,00040	3,53700	0,01286	0,00074	0,00050	2,94100	1,78000
	1000	0,00509	0,00308	2,53800	0,01963	0,00567	0,00355	2,86500	0,01811	0,00732	0,00496	3,82400	1,43200
	10000	0,04580	0,27290	2,34300	0,01638	0,05744	0,03661	2,96000	0,04074	0,06681	0,04411	3,33600	0,84620
	100000	0,36830	0,20880	1,60000	0,01458	0,42260	0,25560	2,10600	0,06343	0,40890	0,28080	2,74300	0,68560
	1000000	2,39800	1,27500	0,59790	0,01234	2,38500	1,32400	0,75030	0,04343	1,86900	1,49500	0,65600	0,17990
	10000000	4,40200	2,33400	0,27650	0,00908	3,65400	2,30400	0,25530	0,01403	3,51400	5,69100	0,54070	0,12920
	100000000	4,64400	3,31000	0,14840	0,00322	5,35200	7,86800	0,38410	0,04138	11,88000	23,82000	0,30190	0,09647

Separat plots

In all figures below are standard deviation of max total force in damper pair presented with correlating relative motion in X/Y at reference point.
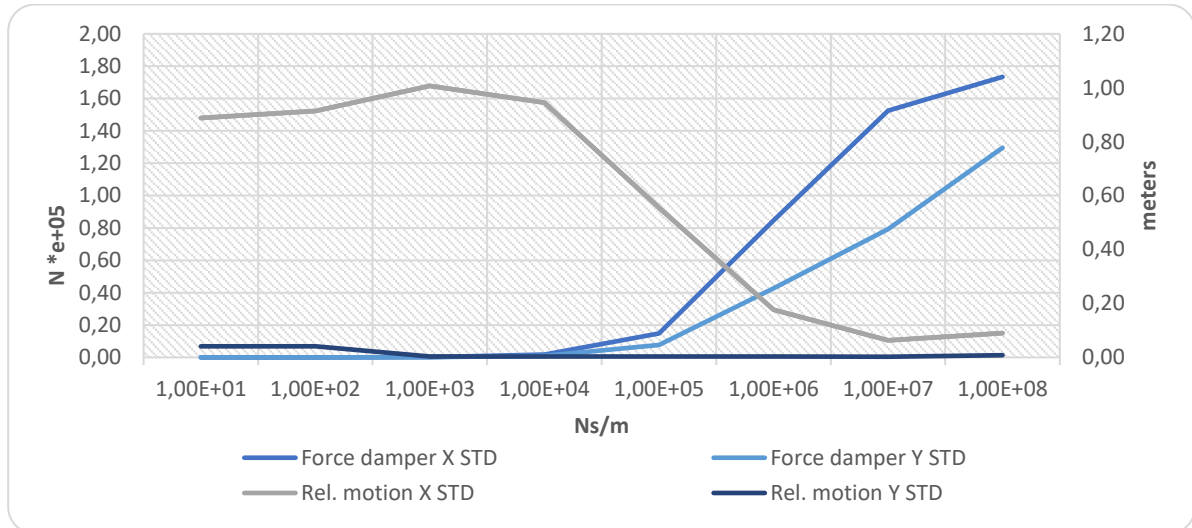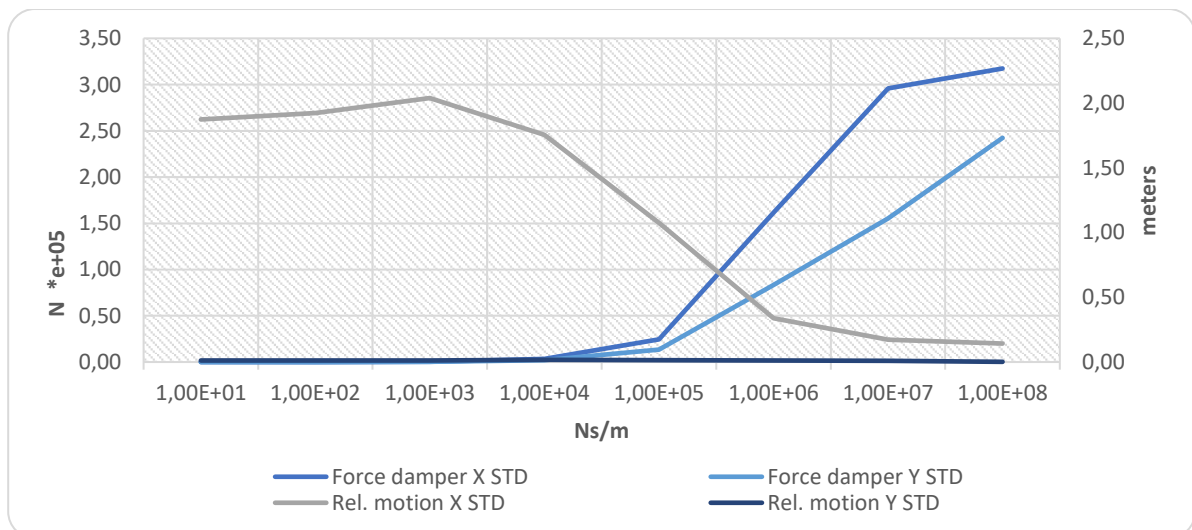

Figure B.0.11: STD: Hs = 1m, Tp = 8s.

Figure B.0.12: STD: Hs = 2m, Tp = 8s.
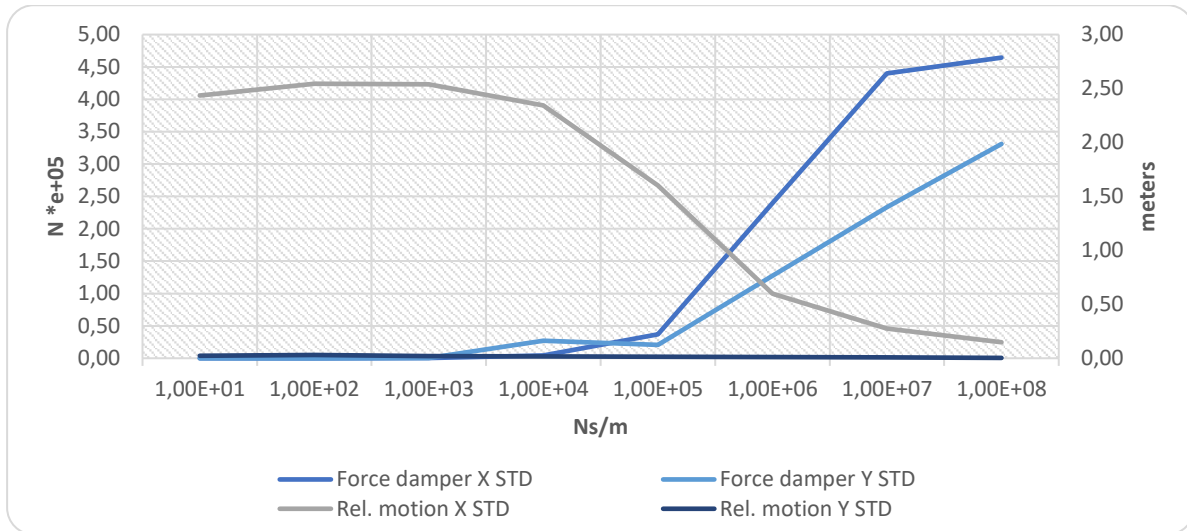
Figure B.0.13: STD: Hs = 3m, Tp = 8s.
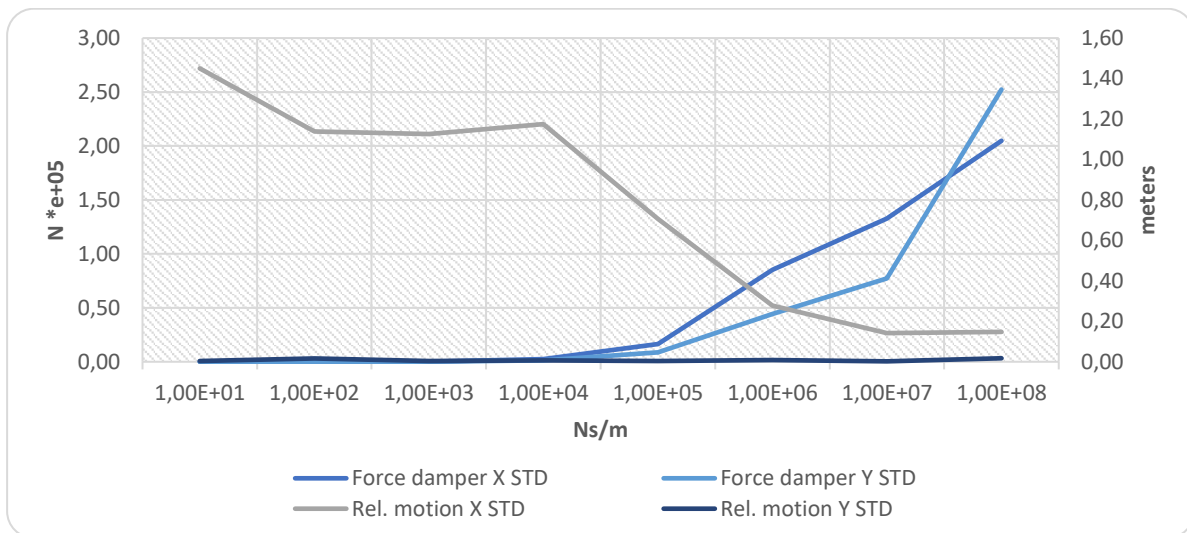
Figure B.0.14: STD: Hs = 1m, Tp = 12s.
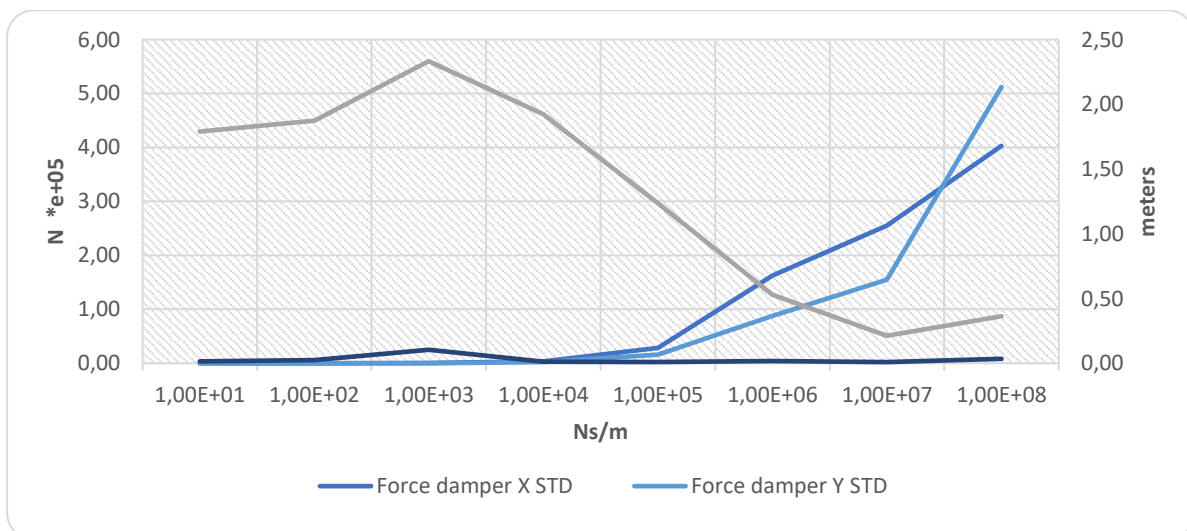
Figure B.0.15: STD: Hs = 2m, Tp = 12s.
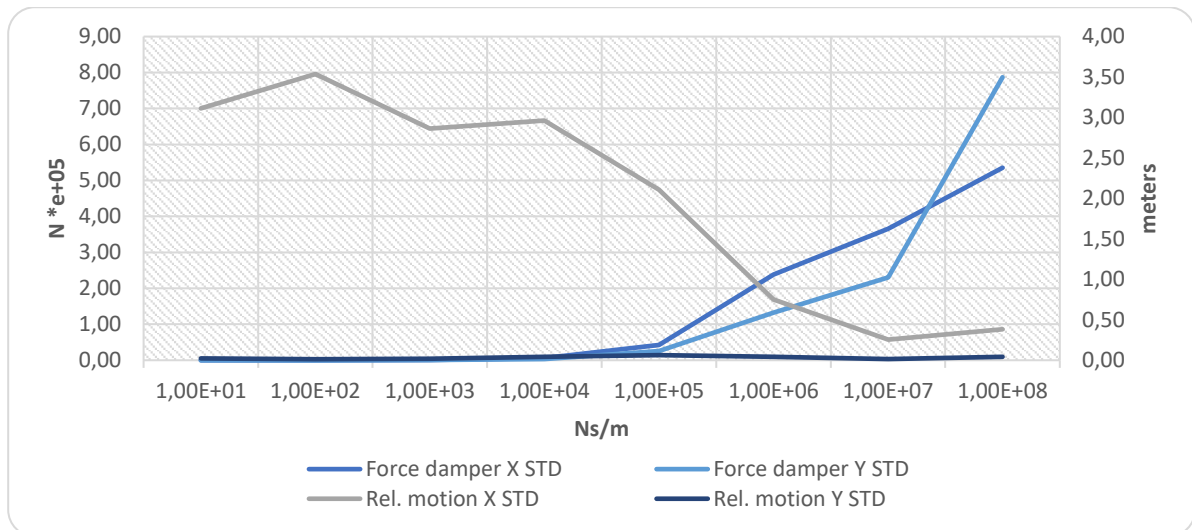
Figure B.0.16: STD: Hs = 3m, Tp = 12s.
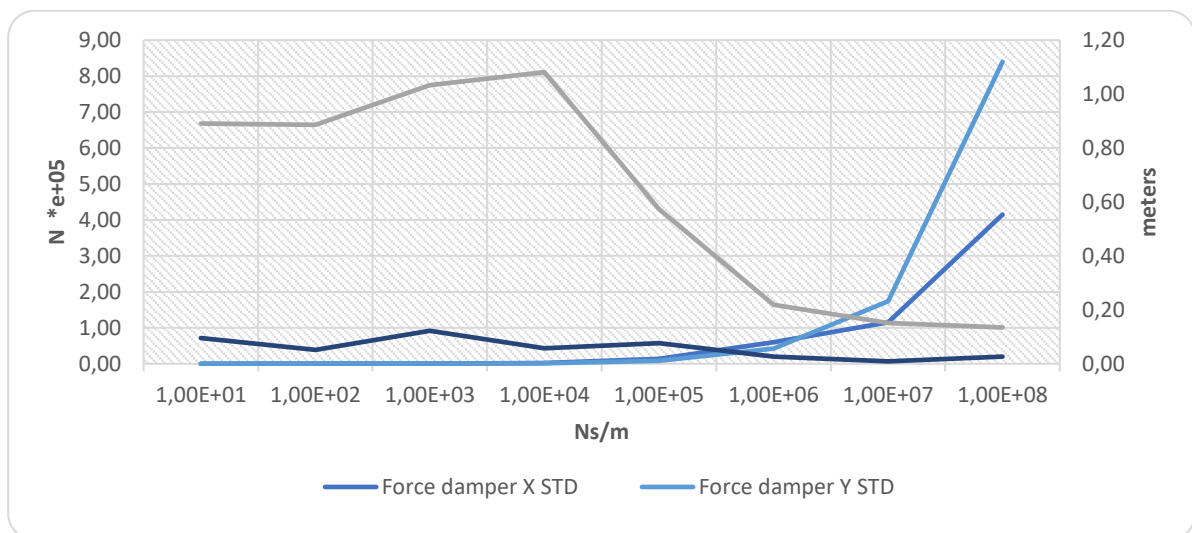
Figure B.0.17: STD: Hs = 1m, Tp = 17s.
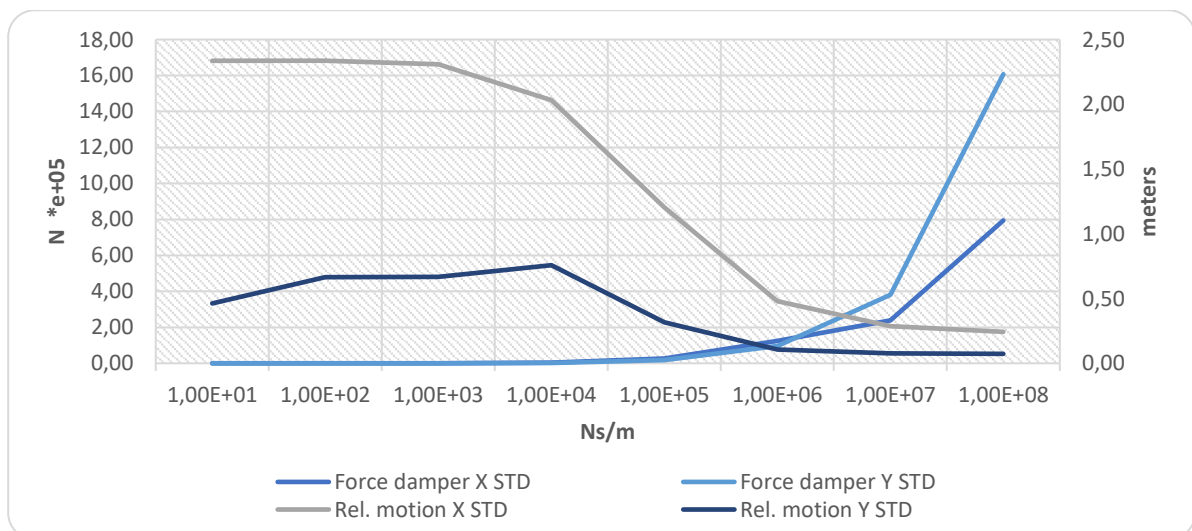
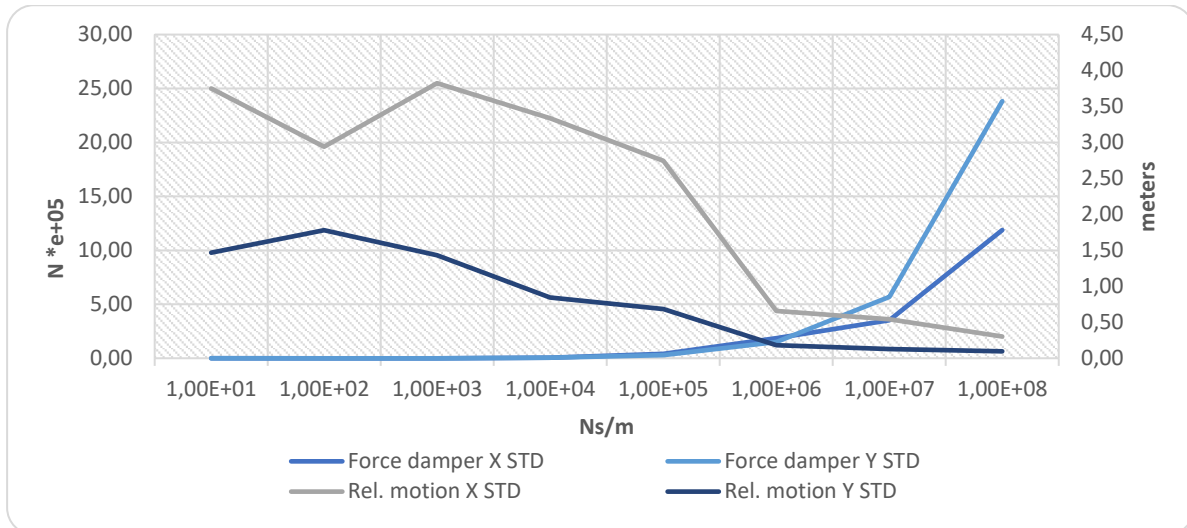**Figure B.0.18:** STD: Hs = 2m, Tp = 17s.

Figure B.0.19: STD: Hs = 3m, Tp = 17s.
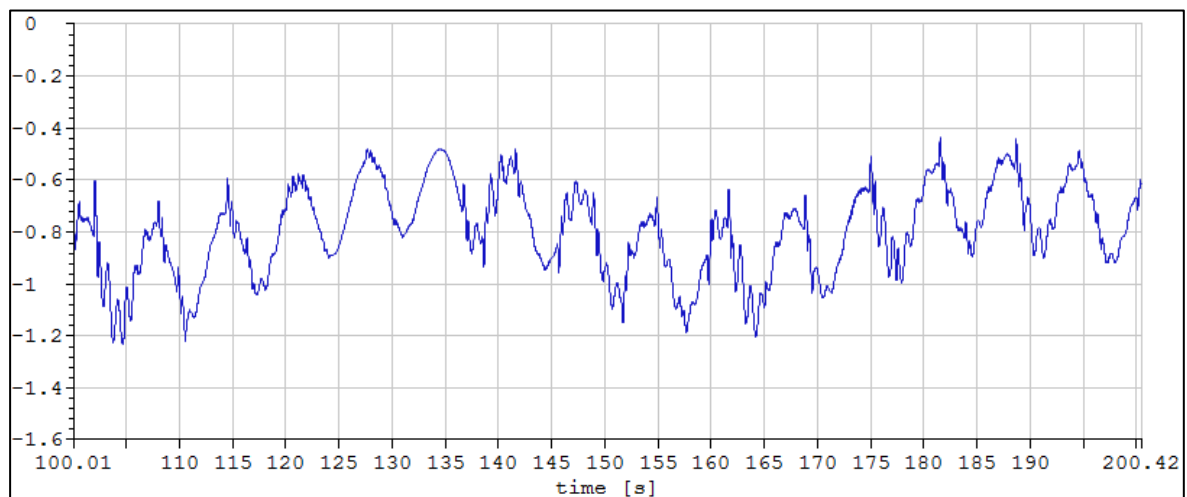
Damper max force in regular waves comparison

Figure B.0.20: Time history of radial reference error. Regular wave A = 1m, Tp = 6,66s. STD = 0,24m. Damping coefficient = 1,0e+07Ns/m.
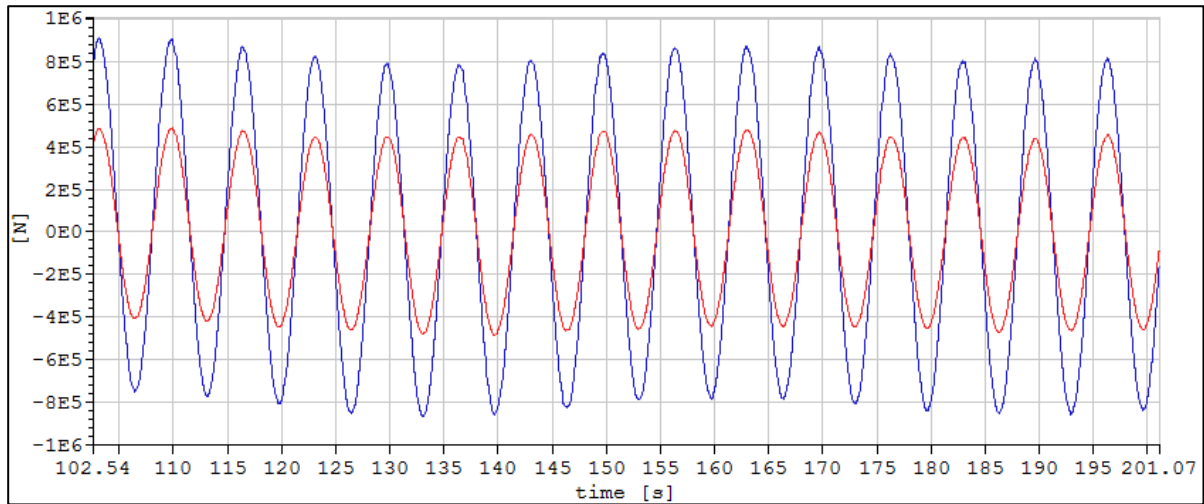
Figure B.0.21: Time history of max total force in dampers. Blue line repr. Damper X (STD = 5,9e+05N/mean = 2028N), red line repr. Damper Y (STD = 3,2e+05N/mean = 996N). Regular wave A = 1m, Tp = 6,66s. Damping coefficient = 1,0e+07Ns/m.